THE ROLE OF DMRT GENES DURING

NEUROGENESIS IN THE ZEBRAFISH FOREBRAIN

MARTIN GRAF

National University of Singapore

2012

THE ROLE OF DMRT GENES DURING NEUROGENESIS IN THE ZEBRAFISH FOREBRAIN

MARTIN GRAF

(*M. Sc. Biomedicine*, University of Würzburg)

A THESIS SUBMITTED FOR THE DEGREE OF

PHILOSOPHIAE DOCTOR (Ph.D)

DEPARTMENT OF BIOLOGICAL SCIENCES

NATIONAL UNIVERSITY OF SINGAPORE

2012

Declaration

I hereby declare that this thesis is my original work and it has been written by me in its entirety. I have duly acknowledged all the sources of information which have been used in the thesis.

This thesis has also not been submitted for any degree in any university previously.

_____

Martin Graf

August 2012

Table of contents

Acknowledgement

Publications

Haendeler, J., Mlynek, A., Büchner, N., Lukosz, M., **Graf, M.**, Güttler, C., Jakob, S., Farrokh, S., Kunze, K., Goy, C., Guardiola-Serrano, F., Schaal, H., Cortese-Krott, M, Deenen, R., Köhrer, K., Winkler, C., Altschmied, J. (2013). Two isoforms of Sister-of-Mammalian Grainyhead have opposing functions in endothelial cells and in vivo. Arteriosclerosis, Thrombosis and Vascular Biology. Under Revision.

Lim, J.W., Yao, S., **Graf, M**., Winkler, C., Yang, D.W. (2013). Structure-function analysis of full-length midkine reveals novel residues important for heparin-binding and zebrafish embryogenesis. Biochemistry Journal. Under Revision.

Graf, M., Teo, E.Q.W., Rajaei, F., Winkler, C. (2013). Dmrt5 controls neurogenesis in telencephalon and olfactory placode through different mechanisms. Manuscript in preparation.

Conference contributions

10th International Conference on Zebrafish Development and Genetics, June 20- 24, 2012, Madison, USA:

Poster: *Dmrt5* controls neuronal specification and differentiation in distinct regions of the developing zebrafish forebrain; **Graf, M.**, Teo Qi-Wen, E., Rajaei, F., Winkler, C.

Arteriosclerosis, Thrombosis and Vascular Biology 2012 Scientific Sessions; April 18-20, 2012, Chicago, USA:

Poster abstract contribution: The Janus-faced transcription factor sister-of-mammalian grainyhead: 2 isoforms with opposing effects in endothelial cells and in vivo; Mlynek, A., Lukosz, M., Köhrer, K., Deenen, R., Jakob, S., Güttler, C., **Graf, M.**, Winkler, C., Haendeler, J., Altschmied, J.

15th Biological Science Graduate Congress, December 15-17, 2010, Kuala-Lumpur, Malaysia:

Poster: A strategy to knock-out *dmrt3* by a zinc finger nuclease approach in zebrafish; **Graf, M.,** Rajaei, F., Gilligan, P.C., Winkler C.

Singapore Zebrafish Symposium 2010, November 08, 2010, Singapore, Singapore:

Poster: A strategy to knock-out *dmrt3* by a zinc finger nuclease approach in zebrafish; **Graf, M.,** Rajaei, F., Gilligan, P.C., Winkler C.

14th Biological Science Graduate Congress, December 10-12, 2009, Bangkok, Thailand:

Poster: A strategy to knock-out *dmrt3* by a zinc finger nuclease approach in zebrafish; **Graf, M.,** Rajaei, F., Gilligan, P.C., Winkler C.

Summary

Dmrt genes encode zinc finger transcription factors with important roles in sexual development as well as cell fate decisions in non-gonadal tissues. In zebrafish, two *dmrt* genes are expressed in overlapping domains of the early developing forebrain. *Dmrt3* is expressed in the olfactory placodes and dorsal telencephalic regions. *Dmrt5* is expressed in the telencephalon, olfactory placodes and the pituitary, as well as the ventral midbrain. I addressed the function of *dmrt* genes during forebrain formation in zebrafish by using knock-down and knock-out approaches.

Morpholino mediated gene knock-down of *dmrt3* did not influence neurogenesis as expression of *neurogenin* was not affected suggesting a possible functional redundancy with the co-expressed *dmrt5*. In contrast, knock-down of *dmrt5* revealed a crucial role during forebrain development by controlling neuronal differentiation and specification. In the dorsal telencephalon, *dmrt5* knock-down resulted in the inhibition of differentiation and prolonged maintenance of early neuronal stem cell populations. Consequently, morphants developed a smaller telencephalon. In addition, *dmrt5* was found to be involved in the development of the olfactory system. Morphants exhibited increased apoptosis of undifferentiated olfactory stem and/or progenitor cells and lacked proneural gene expression. This led to smaller noses and olfactory bulbs with reduced numbers of sensory neurons in *dmrt5* morphants. Finally, also the pituitary, preoptic area and ventral midbrain were affected. These brain structures also displayed reduced neuronal differentiation and specification that eventually resulted in the lack of distinct neuro-endocrine cell populations such as corticotropic and *gnrh2* expressing gonadotropic cells. The data obtained in this study show that a knock-down of *dmrt5* affects neurogenesis in a tissue-dependent fashion independent of *dmrt3*. *dmrt5* is a critical regulator of neuronal differentiation in the fore- and midbrain and of particular importance for the development of the telencephalon, olfactory system and the neuro-endocrine system. In parallel, I was able to knock-out *dmrt3* in zebrafish by introducing frameshift mutations of variable length into the *dmrt3* locus using zinc finger nucleases. These *dmrt3* mutants provide an important tool for future studies on the effect of a homozygous *dmrt3* knock-out on brain development.

List of Figures

List of Tables

List of Abbreviations

3'	3 prime end of nucleic acid	*gfap*	glial fibrillary acidic protein
3-AT	3-amino-triazole	**GFP**	green fluorescent protein
5'	5 prime end of nucleic acid	*gnrh*	gonadotrophin-releasing hormone
Δ	deletion	*gsu-α*	glycoprotein alpha
°	degree	**h**	hours
A	adenosine	*her*	Hairy/E(spl)-related genes
aa	amino acid	*Hes*	hairy and Enhancer of split [E(spl)] genes
ATP	adenosine triphosphate	**His-hisB**	Histidine-Histidine synthetase (Imidazoleglycerol-phosphate dehydratase)
avpl	arginine vasopressin-like		
bHLH	basic Helix-Loop-Helix	**hpf**	hours post fertilization
blbp	brain lipid binding protein	**IGF**	Insulin-like growth factor
BMP	Bone morphogenic protein	*krox20*	krueppel-like zinc finger protein 20
bp	base pair	**LB**	Lysogeny Broth
BrdU	Bromodeoxyuridine	*lh*	luteinizing hormone
BSA	bovine serum albumine	**M**	Mol
C	Celsius	*mab3*	male aberrant-3
C2H2	2-Cystein-2-Histidine zinc finger domain	**MHB**	midbrain-hindbrain boundary
cDNA	copy desoxyribonucleinacid	**Milli-Q**	deionized water
ChIP	Chromatin-Immuno-Precipitation	**min**	minutes
coe2	Col/Olf-1/EBF transcription factor 2	**μg**	microgram
conc.	concentration	**μl**	microliter
crh	corticotropin-releasing hormone	**μM**	microMol
C$_t$	C-terminus	**mg**	milligram
dbx1a	developing brain homeobox 1a	**ml**	milliliter
DIG	Digoxigenin	**mM**	milliMol
DM	doublesex and mab3 domain	**Mo**	Morpholino oligonucleotide
dmrt	doublesex and mab3 related transcription factor	**MO**	Morphant
DMSO	Dimethylsulfatoxide	**mod**	module
dmy	Y-chromosome specific DM domain gene	**mRNA**	messenger mRNA
DNA	deoxyribonucleic acid	**n**	number of samples
dNTP	deoxynucleosidtriphosphate	**NBT**	Nitro blue tetrazolium
dpf	days post fertilisation	**NCID**	notch intracellular domain
dsx	doublesex	**ng**	nanogram
dt	dorsal telencephalon	**NHEJ**	non-homologous end joining
EDTA	Ethylenediaminetetraacetic Acid	**nl**	nanoliter
fezf2	forebrain embryonic zinc finger 2	**NPO**	neurosecretory preoptic area
FGF	Fibroblast growth factor	**N$_t$**	N-terminus
FLU	Fluorescein	**oe**	olfactory epithelium
Fok-DD	Fok-endonuclease domain II	*otp*	orthopedia homolog
FokI	Flavobacterium okeanokoites I	**OSN**	Olfactory sensory neurons
Fok-RR	Fok-endonuclease domain I	*oxtl*	oxytocin-like
fsh	follicle stimulating hormone	*pax6*	paired homeobox gene 6
gDNA	genomic DNA	**pB1H2Ω2**	zinc finger expression vector

PBS	phosphate buffered saline		*sst1.1*	somatostatin
PBST	phosphate buffered saline + 0.1% Tween 20		**TAE**	Tris-Acetate-EDTA
PBSTT	PBST+ 0.1% TritonX 100		*th*	tyrosine hydroxylase
PCR	polymerase chain reaction		*trh*	thyrotropin releasing hormone
PFA	Paraformaldehyde		**TS**	target site
pH3	phosphorylated Histone 3		*tsh-β*	thyroid stimulating hormone, beta subunit
pH3U3	zinc finger target site vector		**TUNEL**	TdT-mediated dUTP-biotin nick end labeling
pit	pituitary		**U**	unit
pitx3	paired-like homeodomain transcription factor 3		**V**	Volt
PO	preoptic area		**v/v**	percentage volume in a total volume
pomc	proopiomelanocortin		**vmb**	ventral midbrain
pou50	pit1-oct1-Unc86 domain gene 50		**vz**	ventricular zone
prl	prolactin		**w/v**	weight per volume
pyrF	orotidine 5-phosphate decarboxylase		**WISH**	whole mount *in-situ* hybridization
RFLP	restriction fragment length polymorphism		**Wnt**	Wingless - Int
RNA	ribonucleic acid		**wt**	wild type
ropZ	DNA-directed RNA polymerase subunit omega		*Xdmrt4*	Xenopus dmrt4
rpm	revolutions per minute		*zash*	zebrafish achaete-scute homologue
sec	seconds		**ZFD**	zinc finger domain (part of ZFP)
shh	sonic hedgehog		**ZFM**	zinc finger module (part of ZFD)
sim1a	simple-minded homolog 1a		**ZFN**	zinc finger nuclease
sox	SRY-related HMG-box		**ZFP**	zinc finger protein (contains several ZFD)
SSC	sodium chloride/ sodium citrat		**zif268**	mouse zinc finger 268
SSCT	SSC+ Tween-20		*zli*	zona limitans intrathalamica

* In the context of this thesis, expression of several hormone encoding genes were analysed. Therefore, abbreviations that are used in this list for hormone names are defining the hormone encoding *gene* and not the peptide.

1. Introduction:

1.1 *Dmrt* genes

Dmrt genes encode for <u>d</u>ouble<u>s</u>ex and <u>mab3</u> <u>r</u>elated <u>t</u>ranscription factors that are crucial for sexual development (Zarkower, 2001; Hong *et al.*, 2007). Dmrt transcription factors are characterized by the presence of a DNA-binding DM domain (Fig. 1a), which was first described in *doublesex* (*D. melanogaster*) and *mab3* (*C. elegans*) (Shen *et al.*, 1988; Bownes, 1994). The DM domain is an uncommon zinc finger domain with two conserved intertwined zinc binding motifs at the N-terminus and a non-conserved C-terminal tail. The function of the tail is to mediate DNA binding whereas zinc is necessary for proper protein folding. DM-domain transcription factors bind into the minor groove of DNA leaving the opportunity for other transcription factors to bind to the major groove of DNA (Narendra *et al.*, 2002; Huang *et al.*, 2005; Murphy *et al.*, 2007).

DM-domain containing transcription factors are conserved within sex-developing pathways at rather downstream positions throughout different phyla, with the exception of *dmrt1bY*/*DMY* in medaka (Fig. 1b). They are expressed in primordial germ cells and in distinct cell populations of the gonads. Their gonadal expression regulates sex determination (Matsuda *et al.*, 2002) or sex differentiation (Raymond *et al.*, 2000; Guo *et al.*, 2005; Kim *et al.*, 2007). Remarkably, it seems that DM-transcription factors are conserved within sex-developmental pathways while no strict conservation can be found upstream of *dmrt* genes. This suggests that DM-containing transcription factors are the ancient conserved basis whereas the non-conserved variable upstream parts of sex determining pathways evolved independently within different phyla (Matson *et al.*, 2012). This hypothesis is furthermore supported by the partial interchangeability of *dmrt* genes between different species, e.g. a *mab3* deficiency in *C. elegans* can be rescued by expression of male specific *Drosophila dsx* (Raymond *et al.*, 1998). However, target genes of conserved DM transcription factors are still largely unknown and need to be revealed.

A)
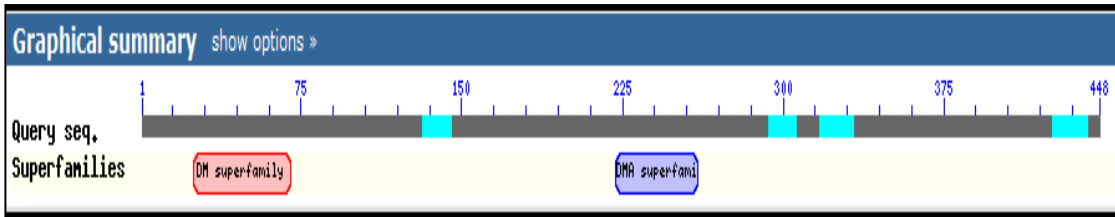
Fig. 1 Overall structure of Dmrt proteins, and their conserved position within sex-developmental pathways: A) Simplified scheme of the structure of DM-domain (red box) containing transcription factors. Besides the DM-domain at the N-terminus of the protein, the C-terminal end contains a DMA domain (blue box) that is believed to mediate protein-protein interactions. The overview was generated using NCBI structure prediction programs (http://www.ncbi.nlm.nih.gov/Structure/cdd/cdd.shtml) C) *Dmrt* genes encode transcription factors that are crucial during sex development. At least one member of this family was found to be involved in sex developmental pathways that are conserved from *C. elegans* (left) to mammals (right). Figure C kindly provided by C. Winkler.
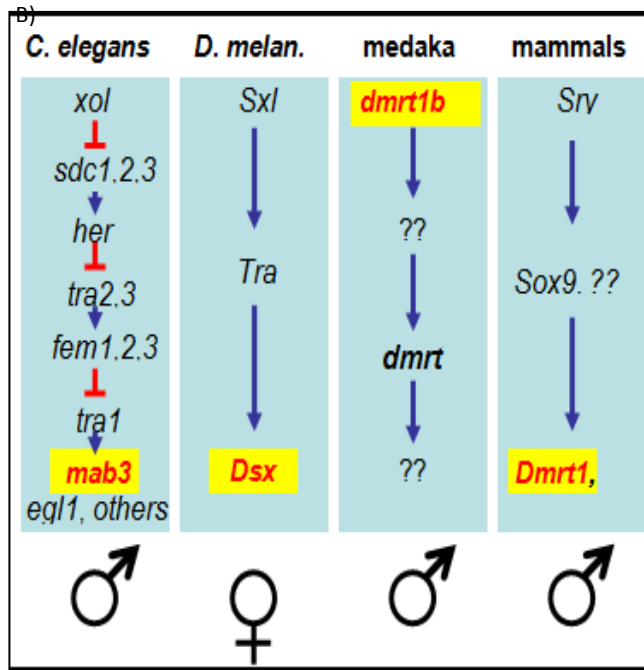
Zebrafish expresses at least five different *dmrt* genes (ZFIN database). An overview about the homologues of zebrafish Dmrt transcription factors are summarized as a phyllogenetic tree in Guo et al., 2004 (Guo *et al.*, 2004). As transcription factors important for sexual development, *dmrt* genes are expressed early in the differentiating gonad as well as in the adult gonad (Winkler *et al.*, 2004). Besides gonadal expression, *dmrt* genes are also expressed in restricted patterns in non-gonadal tissues, such as the presomitic mesoderm (Meng *et al.*, 1999; Saude *et al.*, 2005; Sato *et al.*, 2010) and the nervous system (Guo *et al.*, 2004; Gennet *et al.*, 2010; Yoshizawa *et al.*, 2011). Zebrafish *dmrt2* is expressed in the presomitic mesoderm as well as in somites and is involved in the regulation of somitogenesis, myogenesis, establishing left-right symmetry and positioning of organs (Meng *et al.*, 1999; Saude *et al.*, 2005; Sato *et al.*, 2010). Besides this, it is known from other *dmrt* genes that they are expressed in distinct regions of the developing nervous system, where they are involved in neuronal specification and differentiation.

1. 2 *Dmrt* genes and their role during neuronal development

It is known from different vertebrate models that several *dmrt* genes are expressed in the developing central nervous system (Guo *et al.*, 2004; Gennet *et al.*, 2010; Yoshizawa *et al.*, 2011) besides their gonadal expression at later stages.

In *Xenopus*, *Xdmrt4* expression starts in the anterior neural ridge and gets restricted to the olfactory placodes and the dorsal telencephalon at later stages. Its role during forebrain neurogenesis was demonstrated in *Xdmrt4* morphants and mutants (Huang *et al.*, 2005). Xdmrt4 regulates neurogenesis in the olfactory placode by acting as a transcriptional activator of the important proneural gene *neurogenin*. In *Xdmrt4* morphants, *neurogenin* expression was down-regulated and olfactory placode development was severely impaired. As a consequence of failed neuronal differentiation, neuro-ectodermal stem cells of the olfactory placodes developed with a non-neural ectodermal cell fate instead of forming neural tissues (Huang *et al.*, 2005).

In chicken and mouse embryos, *Dmrt5* is expressed in the olfactory bulb, the dorsal telencephalon and the ventral midbrain (Gennet *et al.*, 2010). *Dmrt5* over-expression in the naïve chicken neuroeptihelium led to the suppression of ventrolateral neuroepithelial cell fates and the up-regulation of ventromedial marker genes. As a consequence of the ectopic *Dmrt5* expression, neuroepithelial progenitor cells adopted medial midbrain cell fates. In addition, Gennet *et al.* (2010) showed that the overexpression of *dmrt5* in neuralized embryonic stem cells can be used to induce elevated numbers of dopaminergic cells that are formed from ventral midbrain progenitor cells. These data suggest that Dmrt5 may act on early neuroepithelial cells by regulating midbrain progenitor specification and differentiation towards a dopaminergic cell fate.

In zebrafish embryos, *dmrt3* is expressed in the forebrain, olfactory placode and a subset of spinal cord interneurons. Its expression within these tissues starts between 14 hours post fertilization (hpf) to 20 hpf and ceases after 55 hpf (Rajaei, PhD Thesis 2012). To analyse the role of Dmrt3 in zebrafish, loss-of-function studies using antisense morpholinos were

performed. It was shown that Dmrt3 regulates specification and differentiation of distinct interneuron populations from P_0 progenitor cells in the spinal cord of zebrafish embryos. Dmrt3 is required for the expression of a crucial determinant of spinal cord interneuron formation. In *dmrt3* morphants, the expression of this fate determinant was reduced, which resulted in reduced numbers of spinal cord interneurons (Rajaei, PhD Thesis 2012)

Additionally, *dmrt5* is also expressed in the developing central nervous system of the zebrafish (Guo *et al.*, 2004; Yoshizawa *et al.*, 2011). *Dmrt5* expression starts in the developing anterior neural ridge and gets restricted to the olfactory epithelium, the telencephalon and the ventral midbrain at 24 hpf. It was shown in a recent study using zebrafish *dmrt5* mutants that *her6* expression is ectopically up-regulated in the dorsal telencephalon. Her6 is a transcriptional repressor of *neurogenin* and prevents neuronal differentiation. As a consequence of the ectopic *her6* up-regulation, *dmrt5* mutants were characterized by neuronal differentiation defects in the dorsal telencephalon (Yoshizawa *et al.*, 2011). Zebrafish Dmrt5 regulates neuronal differentiation in the dorsal telencephalon in a relatively similar fashion like it was described for *Xdmrt4* in *Xenopus*. Moreover, since zebrafish do not have a *dmrt4* gene, it seems that the Xdmrt4 function was taken over by Dmrt5 in zebrafish.

These studies performed in various model organisms showed that the interference with DM-transcription factor expression affects the formation of parts of the central nervous system from earliest neural stem cells as well as from more differentiated and committed neuronal progenitor cells. Therefore, it seems that several *dmrt* genes have conserved bi-functional roles during development: a) at late stages in gonads, where they regulate sex differentiation; and b) at early stages in the central nervous system, where they regulate neurogenesis from *dmrt* expressing neuronal stem- or progenitor cells to differentiated neurons. However, the underlying mechanisms of how *dmrt* genes regulate neurogenesis are still poorly understood and need to be further evaluated.

1.3 Neurogenesis

During the development of the central nervous system, neuronal stem and/or progenitor cells give rise to differentiated neurons. The generation of mitotically inactive, but differentiated neurons from undifferentiated stem cells takes place in a step-wise manner and is called neurogenesis. The key components of neurogenesis are conserved between different phyla and will be discussed below.

The very first step of neural development is the induction of a neural cell fate in the neuroectoderm. The neuroectoderm is formed during gastrulation and contains neuroepithelial stem cells with the potential to form epidermal as well as neural cells. The "default-mode" model of neural induction suggests that neuroepithelial cells develop into neural stem cells by default unless this neural cell fate is suppressed by Bmp signalling (Hemmati-Brivanlou *et al.*, 1997; Reversade *et al.*, 2005; Reversade *et al.*, 2005). However, recent data suggest that the "default-mode" model needs to be revised and is more complex as Wnt, Fgf, Igf and even Bmp signalling itself are involved in early neuroepithelial cell fate decisions (Hemmati-Brivanlou and Melton, 1997; Bally-Cuif *et al.*, 2003; Stern, 2005).

1.3.1 Early neural stem cells and radial glia

Neuralizing signalling pathways initiate the expression of neural specifiers in bipotential neuroepithelial cells which promote the commitment of these cells towards a neural fate. Among the very early expressed neural markers are *sox1* and *sox2* (Collignon *et al.*, 1996; Mizuseki *et al.*, 1998; Pevny *et al.*, 1998; Graham *et al.*, 2003), *her6* (the zebrafish homologue of mouse *Hes1)* (Ishibashi *et al.*, 1994; Pasini *et al.*, 2001; Hatakeyama *et al.*, 2004; Scholpp *et al.*, 2009) and *pax6* (Krauss *et al.*, 1991; Amirthalingam *et al.*, 1995). After their initial commitment towards a neural fate, early neuralized neuroepithelial cells are proliferating to increase the pool of neural stem cells. During this initial proliferative phase, neural stem cells divide mostly symmetrically and give rise to two proliferative neuroepithelial daughter cells with the potential to form either glial or neuronal tissues (Rakic, 1995). However, asymmetric cell division were also described for early neural stem cell

populations giving rise to neural stem cells and early neuron populations that are used as a primary framework to guide further cell movements of later born neurons (Kimmel *et al.*, 1991; Alexandre *et al.*, 2010). After a phase of proliferation, early neural stem cells gradually change to another neural stem cell population with slightly different character. This gradual change from early to late derived neural stem cells is accompanied by a change of cell morphology from typical cylindrical neuroepithelial to bipolar shaped cells with long fibers and an oval nucleus (Rakic, 1972; Noctor *et al.*, 2001; Noctor *et al.*, 2002; Liour *et al.*, 2003; Pellegrini *et al.*, 2007). Based on their morphological features the later derived neural stem cell population will be further referred to as 'radial glia cells'. Besides the morphological change, it is more common for radial glia cells to divide asymmetrically and give rise to different daughter cells, which can be committed neuronal progenitor cells with a determined neuronal fate and limited mitotically capacity as well as neurons, glia or glial progenitors (Fishell *et al.*, 2003). Another difference between early stem cells and radial glia cells is that only radial glia cells are expressing marker genes such as *glial fibrillary acidic protein: gfap* (Levitt *et al.*, 1980), *monoclonal antibody radial cell 2: RC2* (Misson *et al.*, 1988) and *brain lipid binding protein*: *blbp* (Feng *et al.*, 1994). Therefore, it is possible to distinguish both cell populations based on their marker gene expression (Takizawa *et al.*, 2001; Hatakeyama *et al.*, 2004). However, it is also noteworthy to mention that radial glia populations are very heterogeneous and distinct groups of neural stem cells may express different combinations of radial glia markers (Marz *et al.*, 2010).

1.3.2 *Her/Hes* genes

It has been shown in different animal models that the maintenance of neural stem and progenitor cells is of great importance for the development of the central nervous system. One group of genes that supports neural stem cell maintenance is the group of *hairy-* and *enhancer of split* genes (Geling *et al.*, 2003; Itoh *et al.*, 2003), which were first described in *Drosophila*. The zebrafish and mice orthologous are called *her* and *Hes,* respectively. *her/Hes* genes encode for helix-loop-helix (HLH) transcriptional repressors that are important for the

maintenance of neural stem cell populations. The stem cell maintaining activity of Hes/Her proteins is achieved by antagonizing either the expression or the function of proneural basic helix-loop-helix (bHLH) genes and gene products, which are known to promote neuronal specification and differentiation (Akazawa *et al.*, 1992; Sasai *et al.*, 1992; Takke *et al.*, 1999; Bae *et al.*, 2005). It has been shown that the absence of *her/Hes* gene expression contributes to severe neuro-developmental defects due to the precocious up-regulation of proneural genes and the premature differentiation of neural stem cells towards neurons (Ishibashi *et al.*, 1995; Geling *et al.*, 2003; Hatakeyama *et al.*, 2004). Furthermore, it was also found that the set of expressed *her/Hes* genes differ between early neural and radial glia stem cells. In mice, early stem cells are expressing *Hes1* (zebrafish homologue: *her6*) and *Hes3 (her3)* but are negative for radial glia markers, while *Hes1* and *Hes5 (her15)* expressing cells are also positive for radial glia markers (Hatakeyama *et al.*, 2004). This illustrates that neuroepithelial cells can be distinguished from radial glia cells based on the sets of expressed *her/Hes* genes. At later stages of neural development, *her/Hes* gene expression is down-regulated and proneural gene expression is no longer suppressed. As a consequence, neural stem cells start to express proneural genes and neuronal specification and differentiation takes place (Skeath *et al.*, 1992; Blader *et al.*, 1997; Kim *et al.*, 1997; Kim *et al.*, 1997; Guillemot, 1999).

1.3.3 Notch signalling

Neural stem cells are changing gradually. For the development of the full neuronal diversity, it is essential to maintain some of the neural stem cells until later when stem cell characteristics change (Ishibashi *et al.*, 1995; Hirata *et al.*, 2001; Nieto *et al.*, 2001; Ohtsuka *et al.*, 2001; Geling *et al.*, 2003). Therefore, it is required to prevent that all neural progenitor cells are differentiating at the same time. This is achieved via "lateral inhibition", which is mediated by Delta-Notch signalling between different neural stem cells (Greenwald *et al.*, 1992; Yoon *et al.*, 2008). Notch is a transmembrane protein that is activated upon binding of its ligand Delta. At initial states, *delta* and *notch* expression is comparable in cells of the stem cell cluster (Fig. 2a/a'). At later stages, stochastic effects are generating slightly different

delta expression levels between different cells (Fig. 2b/2b'). As a consequence, these cells incorporate more Delta protein into their cell membrane. The increased binding of Delta to Notch molecules on neighbouring cells results in the cleavage of the Notch intracellular domain (NICD). The NICD translocates into the nucleus, where it binds to transcriptional co-factors. These NICD-co-factor complexes then induce increased *her/Hes* gene expression (Bertrand *et al.*, 2002; Cau *et al.*, 2009; Fortini, 2009). As previously described, the expression of *her/Hes* genes results in the suppression of proneural gene expression, and thus prevents premature neuronal differentiation in neighbouring cells (Fig. 2c/2c'). Lateral inhibition was described to act at a population level in early neuroepithelial cells to hamper the development to more fate-limited neuronal progenitor cells (Mizutani *et al.*, 2007), as well as at a single cell level in asymmetric dividing radial glia cells where lateral inhibition regulates the fates of the two daughter cells (Dong *et al.*, 2012). While the Notch-signalling active cells remain mitotically active, the Notch-signalling negative daughter cell gives rise to neurons (Dong *et al.*, 2012). Therefore, lateral inhibition is crucial for the correct timing of neural stem cell differentiation and the generation of the full neuronal diversity. Consequentially, mutations that result in the absence of Delta-Notch signalling contribute to reduced numbers of radial glia cells, increased numbers of early-born neurons and the absence of later-born neurons (Ishibashi *et al.*, 1995; Itoh *et al.*, 2003; Yoon *et al.*, 2008). Contrary, the persistent expression of *her/Hes* genes in neural stem cells and the lack of proneural gene expression produce increased numbers of normally late-born glia at the expense of neurons (Nieto *et al.*, 2001).

1.3.4 Proneural genes

A second essential group of genes involved in neurogenesis are proneural bHLH genes. Similar to *her/Hes* genes, proneural bHLH transcription factors govern neurogenesis at different hierarchical levels but with opposing effects to *her/Hes* genes. At early stages, proneural gene expression is induced by neuralizing signaling pathways in neuro-ectodermal stem cells at low levels, which defines prospective neural tissues. *Her/Hes* transcriptional

repressors restrict proneural gene expression and help to pre-pattern the forming central nervous system (Hirata *et al.*, 2001; Geling *et al.*, 2004). Pre-patterning becomes especially important during the development of organizers within the nervous system. Organizers, such as the mid-diencephalic organizer or the midbrain-hindbrain boundary, are structures that have patterning activity on surrounding tissues and do not develop to neurons. The ectopic expression of proneural genes in presumptive organizers leads to a loss of these structures and central nervous system patterning is heavily disturbed (Geling *et al.*, 2004; Ninkovic *et al.*, 2005; Baek *et al.*, 2006). Therefore, a persistently high expression of *Hes/her* genes is required to restrict proneural gene expression to defined proneural fields. At later stages, proneural genes are involved in neuronal specification and differentiation of progenitor cells. Paradoxically, proneural gene activity in the differentiating progenitor cells blocks proneural gene activity in neighbouring cell. This is mediated via an increased *delta* expression in differentiating cells, which enhances Notch signals in adjacent cells and fosters the suppression of proneural gene activity in surrounding neuronal progenitor cells (Fig. 2) (Lee, 1997; Bertrand *et al.*, 2002). This allows that only particular subsets of neurons differentiate at a distinct time point, while other progenitor cells are maintained in their stem cell niche (Cau and Blader, 2009; Fortini, 2009). Once single progenitor cells are determined to differentiate, they exit the cell cycle and start to express a second set of bHLH transcription factors that are particularly important for the maturation of these newborn neurons, for example the bHLH transcription factor *neuroD* (Korzh *et al.*, 1998).
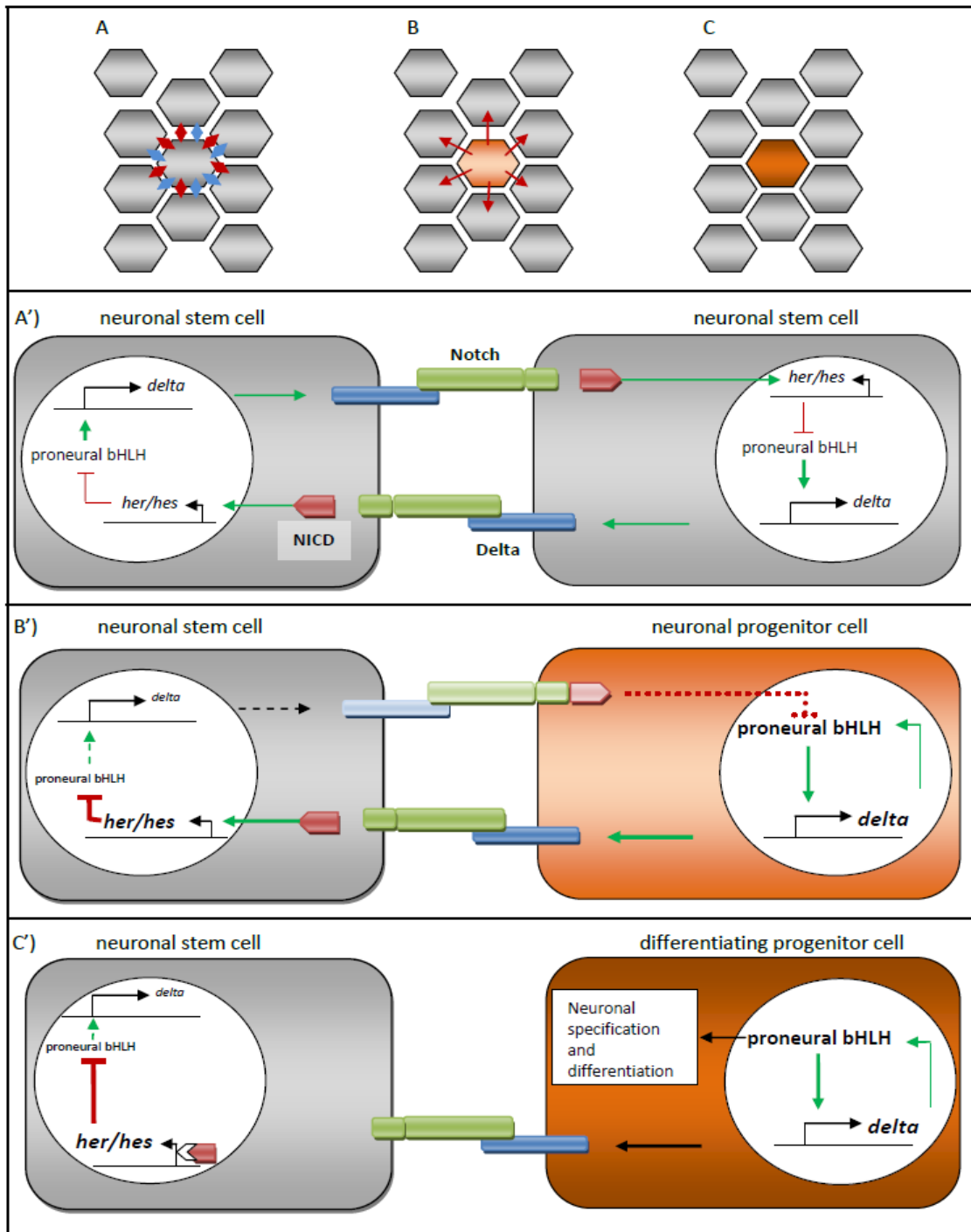
Fig. 2 Lateral inhibition and neuronal differentiation: A/A') In radial glia cell clusters (grey), all cells express approximately identical levels of *delta* (blue) and *notch* (green/red). The binding of Delta to Notch, leads to the proteolytic cleavage of the intracellular domain of notch (NICD: red) on neighbouring cells. The NICD translocates to the nucleus and initiates *her/Hes* expression, which leads to the block of proneural gene expression and a down-regulation of *delta* expression. Since *her/Hes* mRNA and proteins are extremely unstable, suppression of *delta* expression persists only over a short time period before it gets up-regulated again (Kageyama *et al.*, 2008; Shimojo *et al.*, 2008). As all cells stimulate each other via the Delta-Notch signalling, cells in the whole radial glia cluster (red and blue double arrows in A) maintain each other in an undifferentiated state. B/B') Upon the initiation of neural differentiation, proneural gene expression increases the expression of *delta* (bold) in the differentiating

radial glia cells (orange). As a consequence, Notch signalling is increased in the neighbouring radial glia cells (red arrows in B), which also leads to a reduced expression of *delta* in these cells. C/C') Positive feedback loop between Delta and proneural gene products result in a further up-regulation of both and cells start to differentiate (brown). Adopted from (Alberts *et al.*, 2002)

It is noteworthy that studies in mice and zebrafish have shown that the expression of some of the *her/Hes* genes are initiated by Notch independent pathways before neuronal differentiation and specification can take place. It was shown in zebrafish that *her5* expression is independent of Notch and probably initiated by local cues (Geling *et al.*, 2003; Geling *et al.*, 2004). Morpholino mediated knock-down of *her5* resulted in the ectopic expression of the proneural genes *neurogenin* and *coe2* and the loss of the MHB organizer structures (Geling *et al.*, 2004). The zebrafish studies were complemented with results obtained in mice. Hatakeyama *et al.,* 2004 described that *Hes1/Hes3* positive neuro-ectodermal stem cells are Notch independent and *delta*-negative (Fig. 3-2), while later formed radial glia cells expressing *Hes1/Hes5* and are also positive for *Delta* expression (Kageyama *et al.*, 2008). Both papers indicated the multifunctional roles of *her* genes at different levels of neurogenesis i.e. a) at very early stages, where they act as pre-patterning factors defining prospective proneural competence fields (Fig. 3-2 to 3-3) and b) to select single progenitor cells for neuronal differentiation after proneural fields are determined (Fig. 3-3 and 3-4).
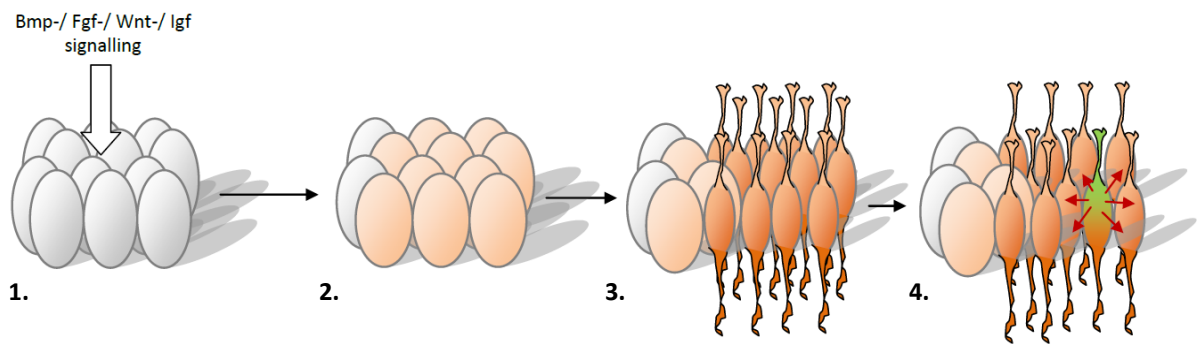
Neuralization		Pre-patterning		Neuro-differentiation	
Color	**Cell-type**	**Color**		**Color**	
(grey) → (orange)	undefined neuroectoderm / defined neuroepithel cells (early neuronal stem cells)	(orange) → (radial)	defined neuroepithel cells (early neuronal stem cells) / Radial glia: undifferentiated	(radial) → (green)	Radial glia: undifferentiated / differentiating radial glia

Signaling \ Cell type	(grey cell)	(orange cell)	(radial glia undiff.)	(radial glia green)
Neural specifiers	---	**+** (sox2/ pax6)	---	---
Early her genes	---	**+** (hes1 (her6)/ her5)	---	---
Notch signaling	---	---	**+** (delta/ hes5 (her4)	**+**
Lateral inhibition	---	---	---	**+** (notch/ delta/ her + proneural genes)

Fig. 3 Overview over early neuronal development and involved marker genes: 1. During gastrulation undefined neuroectodermal cells are receiving multiple signal input from several neural inducing pathways. The combination of the received signals determines the future fate of the bipotential cells either to neural or epidermal cell fates. 2. Cells that were receiving neuronal signals are switching on further neural inducing gene expression such as *sox2*. These very early neural stem cells are expressing notch-insensitive *her/Hes* genes, which helps to determine proneural fields and the position of future organizers. 3. Once the prepatterning of neuronal fields is accomplished, early neural stem cells in these fields gradually change their morphology and character to radial glia stem cells. Radial glia populations are maintained via Delta-Notch signaling until later stages and the expressed *her* genes are Notch-dependent. 4. Radial glia divides asymmetrically and gives rise to neurons. Lateral inhibition prevents the synchronous differentiation of neighbouring radial glia cells and maintains radial glia cells in their stem cell niche till later time points.

In summary, the development of differentiated neurons from neuroectodermal stem cells is regulated in a tightly controlled spatio-temporal manner. Hes/Her and proneural basic helix-loop-helix transcription factors are playing essential roles during this process, mainly via mediating opposing effects. While Hes/Her proteins usually block neuronal development and maintaining neuronal stem cell characteristics, proneural bHLH proteins promote neuronal determination, specification and differentiation. The correct balance of neuronal promoting and blocking bHLH factors is the key to a normal neuro-development and perturbations in that balance very often results in an impaired development of the nervous system.

1. 4 Zinc finger domains

Recently developed techniques allow a targeted knocking-out of specific genes of interest in zebrafish. One of these techniques is making use of zinc finger nucleases (ZFN), which are fusion proteins of multiple zinc finger domains with a DNA cutting endonuclease.

Zinc finger domains (ZFD) are DNA binding protein domains that can be commonly found in DNA interacting transcription factors (Brayer *et al.*, 2008). More than 20 different groups of ZFD are described and one common characteristic between them is the formation of zinc-ion stabilizing structures (Matthews *et al.*, 2002; Krishna *et al.*, 2003).

The most common group of ZFD are called C2H2 zinc fingers since the essential zinc ion is bound by two Histidine and two Cysteine residues within the domain (Fig. 4a). The biological importance of this particular group of ZFD is reflected by the high percentage of C2H2 ZFD containing proteins within the eukaryotic proteome. Almost 3% of the human proteome and 2% of the zebrafish proteome contain proteins with a C2H2 domain (Kersey *et al.*, 2005).

C2H2 ZFDs are approximately 30 amino acids long and form two N-terminal β-sheets and one C-terminal located α-helix. The zinc binding amino acid residues can be found in the two β-sheets as well as within the α-helix (Fig. 4b). The DNA-binding is mediated by seven amino acids at the N-terminal end of the α-helix, especially amino acid residues -1, 2, 3 and 6 (Elrod-Erickson *et al.*, 1996). These amino acid residues are mediating the binding to a

specific nucleotide triplet within DNA. The binding to longer DNA target sequences are mediated by assemblies of multiple ZFDs. In zinc finger nucleases, the ZFDs are linked to the next domain via a five amino acid long linker. The connection of different ZFDs to one larger assembled zinc finger protein may influence the binding of single modules to their target sequence. The reason for this is that distinct ZFD can bind to their particular nucleotide triplet as well as to single nucleotides in the neighbouring triplet (red connection, Fig. 4b). This interaction may influence the sterical binding of adjacent domains and shows that the modular context is very important for the binding affinity of an assembled ZFP even if single ZFD are binding to their target triplet *per se*.
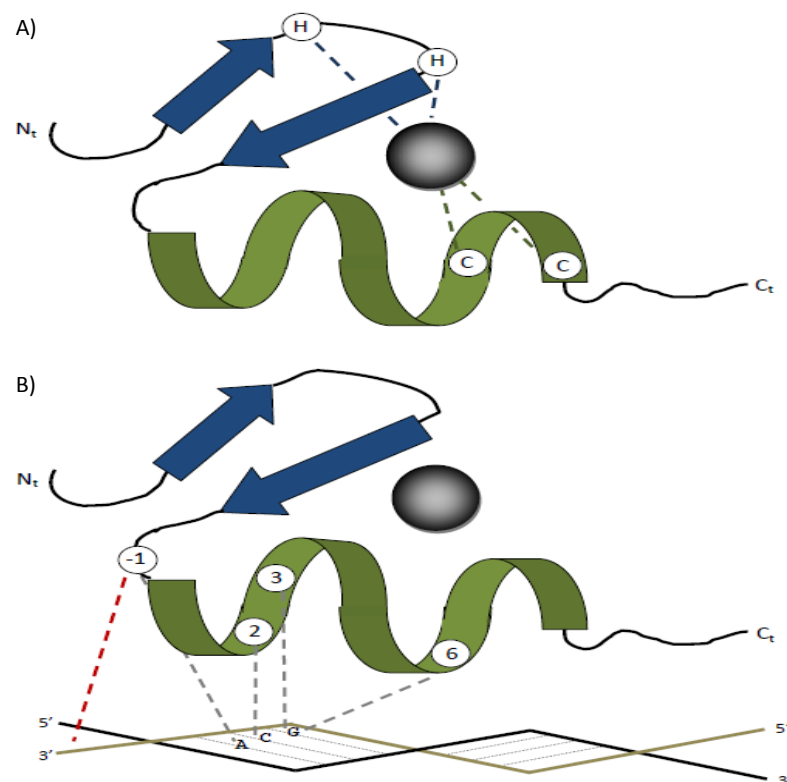
Fig. 4 Structure of C2H2 zinc finger domains and their binding to distinct nucleotide triplets: C2H2 zinc finger domains contain approx. 30 amino acid residues. A) The zinc ion (black circle) is bound by two Histidine (H) residues within the β-sheets (blue arrows) and two Cysteine (C) residues in the α-helix (green helix). B) The DNA binding is mediated by seven amino acids at the N-terminal end of the α-Helix. Especially the amino acid residues at helix positions -1, 2, 3 and 6 are important for mediating the binding to a particular nucleotide triplet (grey connection) within the DNA. Note that one ZFD may also interact with nucleotides in neighbouring triplets (red connection). This can influence the binding of adjacent ZFD when assembled in ZFP. N_t= N-terminus; C_t= C-terminus. Image adapted from Brayer and Segal, 2008.

The fact that the specificity of DNA-binding is only mediated by a maximum of seven amino acids within one module makes it feasible to customize the DNA-binding motif in a way that it binds to any target triplet. Furthermore, by linking different engineered modules with each other, it is theoretically possible to generate ZF proteins that bind to any desired nucleotide target sequence. The customizability of ZFDs and their ability to form larger DNA-binding assemblies makes zinc finger proteins a bio-molecular tool that can be used to modify DNA when fused to endonuclease domains.

1.5 Zinc finger nucleases

Zinc finger nucleases (ZFN) are artificially designed fusion proteins of multiple ZFDs fused to the endonuclease domain of the restriction nuclease FokI. This fusion protein unites the specific DNA-binding ability of the ZFDs with the unspecific nuclease activity of the restriction enzyme FokI. The zinc fingers are used to target the restriction enzyme to a specific site within the genome whereas FokI induces DNA double strand breaks (Bibikova *et al.*, 2001; Cathomen *et al.*, 2008). The endonuclease activity of the FokI domain gets only activated as a dimer (Smith *et al.*, 2000) and therefore it is necessary to use a second ZFN that binds specifically at a target site 5 to 7 bp up- or down-stream of the first ZFN binding site. To generate a knock-out of a gene, thus both ZFNs have to bind to their target sites since only then the two nuclease domains will be in close spatial proximity and the endonucleases become active. The DNA cut will be introduced in the 5 to 7 bp long spacer flanked by the two target sites. One target site contains 3 to 4 triplets. Since two binding sites are used, the overall length of the target site contains 18 bp which is long enough to determine a unique binding site (probability $= 1/6.87 \times 10^{10}$) within the zebrafish genome (zebrafish genome: 1.56×10^{9} base pairs according to Ensemble.org).

To reduce the chance of unspecific off-target cleavages outside the determined target site even further, two different endonuclease domains with modified dimerization interfaces are used. This modification prevents the homodimerization of one ZFN with itself and therefore unspecific cleavage at other target sites where the right and the left binding site are identical.

The two used endonuclease domains are therefore called FokI-RR and FokI-DD reflecting the amino acid residue change within their dimerization interface (Meng *et al.*, 2008).

1.6 ZFN knock-outs in zebrafish

One of the first successful knock-out that was described in zebrafish was performed by Doyon *et al.*, 2008. The *no tail* as well as the *golden* gene were knocked-out with 4-domain ZFNs. Embryos into which ZFN encoding mRNA was injected showed an obvious phenotype and the knock-out efficiency of the method was between 20 to 30%. Furthermore, knock-outs of these genes were verified by sequencing the targeted sites and insertions as well as deletions could be identified around the spacer region. In addition, it was possible to identify founder fish that inherited these gene modifications to the next generation. This proof-of-concept experiment showed that a ZFN mediated knock-out, as it was already described for *X. laevis* (Bibikova *et al.*, 2001) as well as *D. melanogaster* (Bibikova *et al.*, 2002), was now also available for *D. rerio* (Doyon *et al.*, 2008).

1.7 Aim of this project

Dmrt genes are essential regulators of sexual developmental pathways that are conserved across different animal phyla. In addition, several members of the *dmrt* family are also expressed in the central nervous system of vertebrates. Zebrafish *dmrt3* is expressed in the olfactory placode, the dorsal telencephalon and a distinct subset of spinal cord interneuron progenitors. In the spinal cord, it regulates the specification and differentiation of V_0 interneurons (Rajaei, PhD Thesis 2012). The function of *dmrt3* in the olfactory bulb and the dorsal telencephalon are unknown so far but its described role during spinal cord progenitor differentiation suggests that *dmrt3* may have a similar role during neurogenesis in these forebrain regions. In *Xenopus*, it was previously shown that XDmrt4 regulates cell differentiation in the olfactory placode via the positive regulation of proneural gene expression (Huang *et al.*, 2005). It was shown that mammalian Dmrt5 promotes dopaminergic neuron formation when over-expressed in neuralized embryonic stem cell cultures (Gennet *et al.*, 2010). In addition, it has been reported that Dmrt5 is an important regulator of neuronal

differentiation in the dorsal telencephalon of zebrafish (Yoshizawa *et al.*, 2011). From these studies it seems that *dmrt* genes may have a second important role during neuronal development in vertebrates besides controlling sexual development. Importantly, however, the underlying mechanisms regulating vertebrate neurogenesis are still poorly understood.

The aim of this study was to analyse the function of zebrafish *dmrt3* and *dmrt5* during forebrain development and to gain insights into the underlying regulatory mechanisms. Of particular interest was the question, whether in regions with overlapping expression both genes govern neuronal development in a gene-specific or alternatively a fully or partially redundant manner. To answer these questions, I knocked-down both genes using antisense morpholino techniques and evaluated if *dmrt* morphants showed neurogenesis defects. These morpholino studies revealed various roles of Dmrt5 during neurogenesis in multiple brain regions. These data extend data recently published by Yoshizawa *et al.* (2011), and provide further insight into their proposed model of Dmrt5 function for the development of the dorsal telencephalon. Aim of my thesis also was to address processes in the other fore- and midbrain regions where *dmrt5* is expressed during neurogenesis and to analyze whether Dmrt5 is crucial for neuronal differentiation in these distinct brain regions.

In addition, since the knock-down of *dmrt3* by antisense morpholino injection was not sufficient to interfere with *dmrt3* function during forebrain development, loss-of-function mutant zebrafish were generated using a targeted zinc finger nuclease approach.

2. Methods

This chapter describes the used methods while a completed list of all used Materials such as oligos, plasmids, chemicals and equipment can be found in the Appendix A2.

2.1 Fish husbandry

Zebrafish were kept in the fish facility of the Department of Biological Sciences, NUS under a 14 h light/10 h dark cycle. Water quality, photoperiod and temperature were kept constant and controlled daily. To produce eggs, mature fish were set up pair wise in separate mating tanks. On the next morning, mating was induced by removing the spacer between male and female. Eggs and embryos were collected and raised in 1x Danieau's solution at 28°C until they developed to the required stage. Staging was done according to Kimmel (Kimmel *et al.*, 1995). To suppress pigmentation, embryos were treated with 1-phenyl 2-thiourea (PTU, Sigma) at a final concentration of 0.003% after embryos reached gastrulation stage. All experiments were performed in accordance with approved NUS IACUC protocols no 082/10.

2.2 Fixation of embryos and adult tissues

Zebrafish embryos were fixed at the desired stage with 4% w/v paraformaldehyd (PFA)/phosphate buffer saline (PBS) solution for further analysis. If required, embryos were manually dechorionized using watchmaker forceps before they were fixed. Incubation of embryos in PFA was done overnight, if not mentioned otherwise (modified for immunostaining protocols: chapter 2.6). Following the fixation step, embryos were washed three times for 5 min and subsequently stored in 100% methanol at -20°C.

2.3 Gene knock-down by Morpholino injections

Morpholino stock solutions were prepared by resuspending lyophilized morpholino to a final concentration of 25 mg/ml. This stock was further diluted in Milli-Q water to morpholino working solutions with the desired concentration of the morpholino. Before use, working solutions were heated up to 65°C before they were shortly incubated on ice and loaded into

glass capillaries. Glass capillaries (Harvard Apparatus) were prepared with a needle puller (Narishige). The exact sequences of used morpholinos can be found in the table below.

Table 1: Used morpholinos and their sequences

Name of morpholino	5' to 3' sequence	Reference
dmrt3 splice up	TGAGAAAGCGGTTACCTTGCGGTGT	Flora Rajaei; PhD thesis 2012
dmrt3 splice down	TCACTTAGGTCTGGAAAACACACAC	Flora Rajaei; PhD thesis 2012
dmrt3 mismatch	TCAGTTAGCTCTGCAAAAGACAGAC	Flora Rajaei; PhD thesis 2012
dmrt5 splice up	AACGTTTCTACTTACCAGAGTTTGA	This study
dmrt5 splice down	TTTGATTCTCCTGGAATAGATTTGT	This study
dmrt5 scrambled (referred to as control morpholino)	GATTCGTCAGCTTTATTGATTTGTA	This study
her6 morpholino	TATCGGCAGGCATCTTCTCTGGGAA	Pasini *et al.*, 2004
p53 morpholino	GCGCCATTGCTTTGCAAGAATTG	Robu *et al.*, 2007

Morpholino working solutions were injected into the yolk of 1-cell stage embryos using an Eppendorf microinjector by means of applied air pressure. The injected droplet volume was around 0.5 to 1 nl per embryo. Injected embryos were transferred and kept in 1x Danieau's solution at 28°C. Unfertilized and death eggs were discarded 6 hpf. Survival rates and, if present, alterations of morphological features were noted once daily.

2.4 Molecular biology procedures

2.4.1 RNA isolation

Zebrafish RNA was isolated using Qiagen's RNAeasy kit. The isolation of RNA was done according to the manufacturer's manual. In short, 25 embryos were transferred into a 1.5 ml Eppendorf tube and manually homogenized in 350 µl RLT/β-Mercaptoethanol using a pestle. The homogenized embryos were well mixed with 70% ethanol and subsequently transferred onto RNA affinity columns. The columns were centrifuged to separate cell debris from column-bound RNA. Next, the filter material was washed several times with washing buffer

and the RNA was eventually eluted using RNAse free water. To remove traces of genomic DNA, the RNA was incubated for 30 minutes with 1 µl of DNAseI (Fermentas) at 37°C. The DNAse treated RNA was further purified with the RNeasy kit according to the RNA clean-up protocol. Briefly, RNA was mixed with RLT buffer and 100% ethanol and the mix was transferred onto RNA affinity columns. The columns were washed several times with washing buffer RW and RPE. Following that, the RNA was eluted from the columns with 100 µl of RNAse free water.

2.4.2 Phenol-Chloroform clean up

To separate RNA from protein contamination, an acidic phenol-chloroform clean up was performed. For that, the eluted RNA was mixed with 100 µl phenol-chloroform, pH5.3 (Amresco) and 50 µl 1:1 chloroform/isoamylalcohol mix (Merck). The tubes were vortexed and centrifuged at full speed for 5 min. After the centrifugation, two phases were visible and the RNA-containing upper phase was transferred to a new tube and mixed with Chloroform in a 1:1 ratio. The mixture was vortexed and subsequently centrifuged for 5 min. Two phases were formed and the aqueous RNA containing phase was transferred into a new 1.5 ml reaction tube.

2.4.3 Sodium-acetate and ethanol precipitation

To increase the concentration of the isolated RNA, the eluate was precipitated overnight at -20°C with 1/10 volume 3 M NaAc, pH 5.3 (Sigma) and 2.5x volume of 100% ethanol. On the next day, the precipitated RNA was pelleted by centrifugation at full speed in a cooled table top centrifuge (45 min, Sorvall) and the supernatant was discarded. The RNA pellet was washed with 1 ml of 70% ethanol and the centrifugation step was repeated. Supernatant was discarded and the pellet was air dried and dissolved in 20 µl Milli-Q water. Finally, the RNA was quantified using a nano-drop photo spectrometer (WPA), and RNA aliquots were stored at -80°C.

2.4.4 Reverse transcription

To synthesize cDNA, "RevertAid first strand cDNA kit" (Fermentas) was used. 2 µg of total RNA was mixed with 2 µl of random hexamer primer (0.2 µg/µl), heated up to 70°C and cooled down to room temperature to anneal primers to their target sites. In the next step, reaction buffer, dNTPs and RNAse inhibitor (20 units) was added to the RNA. The reaction mixture was split into two separate reactions, one with reverse transcriptase (200 units) and the second without reverse transcriptase. The reaction without the reverse transcriptase was used as a negative control for testing for contamination with genomic DNA. Both reactions were incubated at 42°C for 1 hour. Reactions were stopped by heat inactivation of reverse transcriptase at 70°C. The synthesized cDNA was stored at -20°C and used as a PCR template for further reactions.

2.4.5 Semi-quantitative PCR/ splice assay

This protocol was used to evaluate the efficiency of the used *dmrt* splice-blocking morpholinos and based on a semi-quantitative PCR protocol (table 2).

Table 2: Semi-quantitative PCR protocol

Reagent	Volume/Amount	Final conc.	Temperature	Time	Cycles
cDNA	0.2 µl	-	98°C	40 sec	
10 mM Primer forw.	2.5 µl	0.5 mM	98°C	10 sec	
10 mM Primer rev.	2.5 µl	0.5 mM	60°C	10 sec	35 cycles
10 mM dNTPs	1 µl	0.2 mM	72°C	20 to 45 sec	
100% DMSO	1.5 µl	3%	72°C	10 min	
5x HF buffer	10 µl	1x			
Phusion polymerase	0.5 µl	0.5 U	Standard protocol for Phusion- PCR. The annealing temp. was 60°C unless stated otherwise.		
Milli-Q water	up to 50 µl				

First, the relative amounts of cDNA from control and *dmrt5* morpholino injected embryos were determined based on the expression of housekeeping gene *gapdh* (Sequence: Appendix A.2). Next, normalized amounts of cDNAs were used and splice test PCRs were set up and performed as stated in table 2 in a Veriti or Biometra thermocycler. Used primers were binding in exon sequences flanking the introns of *dmrt5* or *fezf2* (primer sequences are given

in Appendix A2). Correctly spliced transcripts and intron-retaining transcripts could be separated according to their size by means of gel electrophesis. The relative amount of amplified PCR products were measured based on the intensity of PCR bands on the gel using ImageJ. The splice blocking efficiencies were calculated based on these intensity value differences between controls and *dmrt5* morphants. A summarizing flow chart of this method is shown in figure 5.
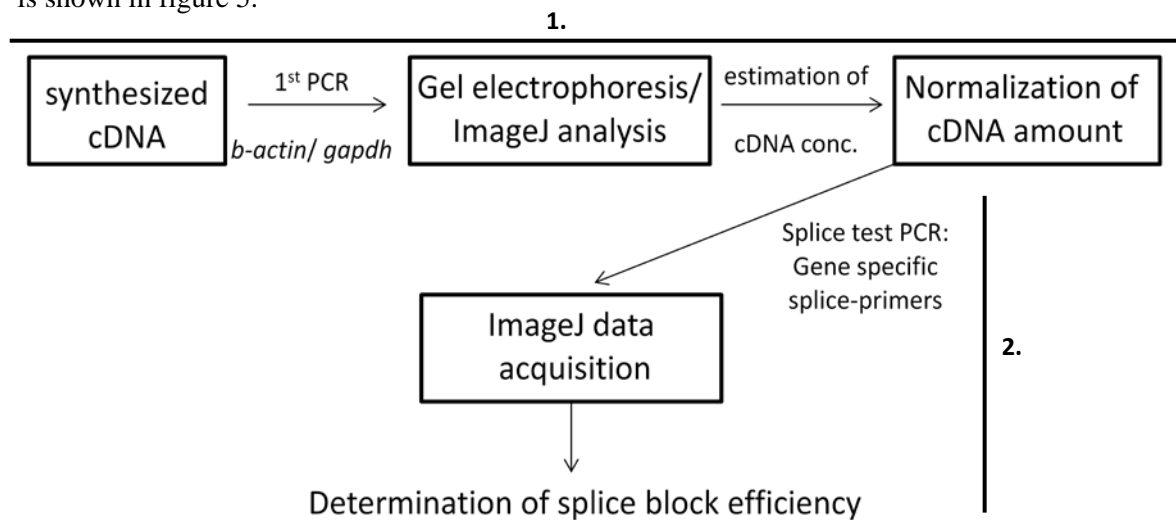
Fig. 5 Flow chart semi-quantitative PCR: The chart above summarizes the steps that are required to determine the splice blocking efficiencies of used morpholinos. 1) Normalization of cDNA amounts based on the expression of housekeeping genes, and 2) Determination of the splice blocking efficiency, based on the amplification of gene specific spliced- and intron-retaining transcripts.

2.4.6 Amplification of gene specific cDNA templates

To amplify DNA templates for riboprobe or mRNA preparations, 0.2- 1 µl of stock cDNA was mixed with the reagents according to table 2. To minimize the chance of sequence errors by amplification, proof-reading "Phusion" polymerase (Finnzymes) was used. PCR products were analysed on a 1% TAE gel and isolated with a gel extraction kit (2.4.8).

2.4.7 Separation of PCR products by gel electrophoresis

1% agarose gels were prepared by dissolving 1 g of agarose (1st Base) in 100 ml of 1x TAE (50x TAE: 242 g Tris Base, 57.1 ml Glacial Acetic Acid,100 ml 0.5 M EDTA) buffer. 5 µl of 20000x concentrated Sybr-safe DNA stain (Invitrogen) was added to the agarose gels and diluted to a 1x working concentration. Agarose was casted into gel trays (Bio Rad) and

solidified agarose gels were loaded with DNA or RNA samples and DNA/RNA ladders (Fermentas). Before loading the samples into the agarose wells, reaction products were mixed with loading dye (Fermentas) at a 10:1 ratio. Gel electrophoresis was performed at a constant voltage of 90V using a Bio RAD power pac for 30 to 60 min. DNA/RNA bands were visualized and documented using a G: box gel documentation system (Syngene). Fragments of interest were cut out with sterile lancet blades and isolated using a Promega gel extraction kit.

2.4.8 Isolation of DNA from agarose gels

DNA bands were visualized with a UV-transilluminator (WISD) and fragments of correct size were cut out from the gel. The DNA was isolated from gel fragments with a "Wizard® SV Gel and PCR Clean-Up" kit (Promega) according to the manufacturer's instructions. After the extraction of DNA from gel fragments, DNA was quantified measuring the absorbance at 260nm using a photo-spectrometer (WPA).

2.4.9 Cloning of PCR fragments flanked by restriction sites

2.4.9.1 Amplification, clean-up and digestion of PCR products and plasmids

Column-purified PCR products that contained unique flanking restriction sites were digested with appropriate restriction enzymes and reactions were set up according to table 3. Around 1 µg of DNA per 20 µl reaction volume was used. The used restriction enzymes were purchased from Fermentas or NEB and reaction conditions were optimized using the recommended restriction buffer.

Table 3: DNA digestion reaction set up

Reagent	Volume/Amount	Final concentration
DNA	1 µg	
Restriction enzyme	1 µl	10 U/rxn
Restriction buffer	2 µl	1x
BSA (optional)	0.02 µl	1x
Milli-Q water	Add to 20 µl	

Digests were incubated for at least 2 hours at 37°C. The digestion reactions were stopped by heat-inactivating the enzymes at 65°C or 80°C. In parallel to insert digestions, plasmid

vectors of interest were linearized with the same restriction enzymes as the inserts using an identical reaction set up.

2.4.9.2 Phosphorylation and dephosphorylation of PCR fragments and linearized vectors

To increase the ligation efficiency and prevent religation of digested plasmids, phosphorylation of insert and dephosphorylation of plasmids were done according to the manufacturer's protocols. For the phosphorylation of inserts, T4 polynucleotide kinase (T4 PNK, Fermentas) was used. For dephosphorylation of linearized plasmids, shrimp alkaline phosphatase (SAP, Fermentas) was used. ATP and enzyme were added directly to the heat inactivated digestion reactions.

Table 4: Phosphorylation and dephosphorylation set up

T4 PNK reaction		SAP reaction	
Reagent	Amount	Reagent	Amount
Linear ds DNA	1-20 pmol of 5'-termini	Linear DNA (~3 kb plasmid)	1 μg (~1 pmol termini)
10 mM ATP	1/10 of final volume, 1 mM	Shrimp Alkaline Phosphatase	1 μl (1 U) per pmol of 5' termini
T4 Polynucleotide Kinase	1 μl (10 U) per pmol 5' termini		

Reactions were carried out for 30 to 60 min at 37°C and subsequently purified using phenol-chloroform protocol similar to the previously mentioned protocol (see 2.4.2). The difference to the first protocol is that the phenol-chloroform solution had an increased pH of 8. Following the clean-up, the DNA was precipitated as described in 2.4.3.

2.4.9.3 Ligation reaction

Precipitated inserts and linearized vectors were mixed together in a molecular ration of 3:1. T4 ligase buffer (NEB) was added to a final concentration of 1x, 1 μl of T4 ligase (NEB) was added and the reaction was topped up to a final volume of 20 μl with water. Ligation reactions were performed at 16°C overnight.

2.4.10 Subcloning of riboprobe templates

For *in-situ* probe production, pDrive (Qiagen), pJet (Fermentas) or TOPO-blunt end ligation kits (Invitrogen) were used. For amplicons generated with Taq-polymerase, the pDrive vector was used. For blunt end PCR products generated with Phusion polymerase, either pJet or TOPO blunt end vectors were used. Purified amplicons were added to the plasmids in a molecular ratio of 3:1 and reaction mixtures were set up according to the kit instructions. The reaction was incubated at room temperature (RT) for 1 hour and subsequently transformed into chemical competent DH5α cells.

2.4.11 Transformation of plasmids into bacteria

Ligation reactions were stored on ice for 5 minutes before 1-5 µl of the reaction were transferred and mixed with 100 µl of chemical competent *E.coli,* strain DH-5α. Bacteria were incubated for 30 min on ice before they were exposed to a 42°C pulse over 35 sec. After the heat shock, 250 µl of LB-media were added to the bacteria and they were incubated for 1 h in a thermo shaker (Infor). After that, bacteria were plated out on LB-agarose plates. LB-agarose plates contained either 50 mg/l Kanamycin or 100 mg/l Ampicillin, depending on the used plasmids. LB-plates were incubated at 37°C for 12-16 h until single bacterial colonies became visible.

2.4.12 Colony-test PCR

Single bacterial colonies were tested for the presence of the desired plasmid by colony-test PCR. Either a set of gene-specific primers, two insert flanking vector-specific primers (M13 rev/forw or Sp6/T7) or a combination of vector-specific and gene-specific primer were used during the PCR. Bacterial colonies were directly used as templates for the PCR reaction and mixed with reagents as stated in table 5. Before the bacterial colony was mixed with the PCR reagents, the bacteria were transferred onto the surface of a fresh LB-plate (with the respective antibiotic). Growing bacteria contained the same plasmid as the PCR-tested sample and were used a plasmid stock for later applications.

Table 5: Colony-test PCR reaction protocol

Reagent	Volume/Amount	Final conc.		Temperature	Time	Cycles
Bacterial template	- one colony			95°C	10 min	
10 mM Primer forw.	1 µl	0.5 mM		95°C	30 sec	
10 mM Primer rev.	1 µl	0.5 mM		58°C	30 sec	35 cycles
10 mM dNTPs	0.5 µl	0.25 mM		72°C	30 -60 sec	
25 mM MgCl$_2$	1 µl	1.25 mM		72°C	3 min	
10x Taq reaction buffer with (NH$_4$)$_2$SO$_4$	2 µl	1x				
Taq polymerase	0.5 µl	2.5 U/rxn				
Milli-Q water	Up to 20 µl					

PCR products were analysed on a 1% TAE gel by means of gel electrophoresis and positively tested colonies were transferred from the safety plate into 2- 5 ml of fresh LB medium (Becton Dickinson). Cultures were incubated overnight at 37°C under vigorous shaking at 225 rpm (Infors).

2.4.13 Isolation of plasmid DNA and preparation of bacterial glycerol stocks

Plasmids from overnight cultures were isolated using "Promega Wizard plus DNA purification kits" according to the supplier's manual. Overnight cultures were centrifuged and bacteria were pelleted and separated from the media. The bacteria were lysed and the lysates were transferred to the provided DNA affinity columns. The columns were spun and washed several times before the plasmids were eluted with Tris-EDTA (TE) buffer or Milli-Q water. In parallel to the isolation of bacterial plasmid DNA, 0.8 ml of overnight culture was mixed with 0.6 ml 100% glycerol (AppliChem), vortexed for 30 sec and stored at -80°C. Bacterial glycerol stocks can be stored long-term and were used, if plasmid propagation was necessary.

2.4.14 Sequencing reaction

To confirm the identity of isolated plasmids or amplified PCR products, sequencing reactions were carried out using a BigDye Terminator v3.1 Cycle Sequencing Kit (Applied Biosystems). 50 to 200 ng of purified DNA were mixed with 1 µl 10x BigDye buffer, 2 µl BigDye reaction mix, 1 µl of the appropriate sequencing primer and topped up to 10 µl with

Milli-Q water. Sequencing reactions were performed in a PCR machine and reaction settings are stated below.

Temperature	Time	Cycle number
96ºC	1 min	
96ºC	15 sec	25 cycles, annealing temperature primer dependent
50ºC	10 sec	
60ºC	4 min	

After the reaction, sequencing products were precipitated according to protocol 2.4.3 and the pelleted DNA was air dried for 10 min at room temperature. Sequencing products were electrophoretically separated in a Abi3130x1 sequencer (Applied Biosystems) and resulting chromatograms were analysed using BioEdit v7.0.5.2

2.4.15 mRNA synthesis

To produce capped mRNA for zebrafish injections, 1-2 µg of linearized plasmid DNA was mixed with mMESSAGE *mMACHINE* Kit (Ambion) reagents as described in table 7. After 2 h of incubation at 37°C, 1 µl of DNAse (Fermentas) was added to the reaction mix and incubated for another 30 min.

Reagent	Volume/Amount	Final concentration
linearized plasmid	1 µg	
10x reaction buffer (either T7 or SP6)	2 µl	1x
2x NTP/CAP solution	10 µl	1x
SP6 or T7 RNA polymerase	2 µl	
RNAse free water	Ad to 20 µl	

Proper polyadenylation is required for efficient translation and increased stability of the synthesized mRNA. To ensure correct polyadenylation, plasmid-internal polyadenylation sites were used. However, for some of the used plasmids it was not possible to linearize the plasmid 3' of the poly-A signal without digesting the mRNA encoding sequence. Hence, poly-A tails were added to transcribed mRNAs during an additional polyadenylation reaction step using E-PAP (Ambion). After the DNAse digest of DNA template in *in-vitro*

transcription reactions, the transcribed RNA was mixed with the following components according to the manual's instruction.

Table 8: Poly-A tailing reaction mixture

Reagent	Volume/Amount	Final concentration
mRNA	10 µl	
E-PAP	2 µl	4 U/rxn
5x reaction buffer	10 µl	1x
10 mM ATP solution	5 µl	1 mM
25 mM MnCl$_2$	5 µl	2.5 mM
Milli-Q water	ad to 50 µl	

The reagents were gently mixed and incubated at 37°C for 30 min. The efficiency of the polyadenylation reaction was evaluated by analysing untreated mRNA (after *in-vitro* transcription) next to treated mRNA (with poly-A tail) on a gel. A size shift of around 150 to 300bp was indicative for successful addition of multiple A's to the 3' end of mRNA. After polyadenylation reactions, mRNAs were purified using the phenol-chloroform protocol (2.4.3). In addition and following the phenol-chloroform clean up, mRNAs were further purified using Qiagen's RNeasy kits according to the manufacturer's manual. The quality and size of purified mRNA was evaluated on a 1% TAE gels by means of gel electrophoresis. If single, clear RNA bands could be visualized on agarose gels, mRNAs were stored at -80°C.

2.4.16 Riboprobe production

To produce probes for in-situ hybridization, 1-2 µg of linearized plasmid DNA was mixed with the reagents as listed in table 9 and incubated at 37°C for 2 h. After that, 1 µl of DNAse (Fermentas) was added to the reaction mix and incubated for another 30 min.

Table 9: In-vitro transcription set up for RNA antisense probe production

Reagent	Volume/Amount	Final concentration
linearized plasmid	1 µg	
10x transcription buffer	2 µl	1x
10x DIG/Fluorescein labelled dNTPs	2 µl	1x
RiboLock RNAse Inhibitor	0.5 µl	20 U/rxn
RNA polymerase (Sp6 or T7)	1 µl	20 U/rxn
RNAse free water	Ad to 20 µl	

After heat inactivating the reactions at 65°C, riboprobes were cleaned-up using an RNeasy kit (Qiagen) and eluted in 25 µl RNase free water. 1 µl of riboprobe was qualitatively analysed by gel electrophoresis, while the other 24 µl were mixed with 76 µl of Hybridization mix (recipe in table 14) and stored at -20°C.

2.4.17 Isolation of genomic DNA (gDNA) from zebrafish embryos

To isolate gDNA from zebrafish, a protocol described by Meeker was used (Meeker *et al.*, 2007). Embryos or isolated adult fin tissues were transferred to 50 µl of 50 mM NaOH (Merck) and incubated at 95°C until tissues were completely dissolved. After that, the pH of the solutions was neutralized with 1/10 volume of 1 M Tris-HCl while samples were kept on ice. Before genomic DNA was used for subsequent PCR reactions, tubes were centrifuged at full speed in a table top centrifuge for 1 min to separate cell debris from gDNA. The isolated gDNA was stored at -20°C.

2.5 Custom-made synthesis of Dmrt3 zinc finger nucleases (ZFN)

To generate zinc finger proteins that bind and cut the zebrafish genomic *dmrt3* locus, I used the well characterized zinc finger 268 (zif268) as framework zinc finger (Wolfe *et al.*, 1999). The three DNA binding domains (ZFD) of zif268 had to be modified in such a way that they bound to the *dmrt3* locus. This was done via PCR mutagenesis using degenerated ZFD primers. Resulting new binding capacities of the zinc finger proteins (ZFP) were evaluated using a bacterial one-hybrid system (Meng *et al.*, 2006) and most suitable ZFD were selected to be fused with the endonuclease domain of FokI.

2.5.1 Determination of degenerated primer sequences for zinc finger module synthesis

Suitable target ZFN binding sites were determined using ZiFit (http://zifit.partners.org/ZiFiT/ChoiceMenu.aspx) and the ZFPserach tool (http://pgfe.umassmed.edu/ZFPsearch.html). Potential target sites were blasted against the zebrafish genome to exclude possible off-target sites. The ZFPsearch also suggested

sequences for degenerated primers, which were used for PCR mutagenesis of zif268. The list of used primers and plasmids can be found in the Appendix A2.

2.5.2 Selecting customized zinc finger proteins

The template zinc finger was customized using degenerated primers as explained in 2.5.3. In this section, I will describe how *dmrt3* binding ZF proteins were selected from a library of randomized ZF proteins.

To identify binding from non-binding ZF proteins, a previously described bacterial-one-hybrid screening assay was used (Meng and Wolfe, 2006; Noyes *et al.*, 2008). In short, the bacterial strain *USO hisB- pyrF- rpoZ-* (Addgene: 18049) was double transformed with customized zinc finger expression plasmids pB1H2ω2 (Addgene: 18045) as well as a *dmrt3* target site vector pH3U3 (Addgene: 18046). The expression vector encodes for a DNA-binding zinc finger protein with an N-terminally fused *E. coli* RNA-polymerase. The used target site vector contains a potential ZFP binding site located upstream of the promoter region of a gene encoding a Histidine synthetase. The bacterial strain *USO hisB- pyrF- rpoZ-* is characterized by the disability to grow on media lacking Histidine (NM-media). In double transformed bacteria, binding of the RNA-polymerase to the promoter region of the Histidine-synthesizing enzyme as mediated by the binding of the ZFP to its target site, resulted in the expression of the enzyme and the ability of bacteria to survive the selection. If only one out of the three zinc finger modules failed to bind to their target sites, no Histidine synthetase was expressed and the bacteria died. Hence, it was possible to select binding from non-binding ZFPs by this bacterial one-hybrid assay.
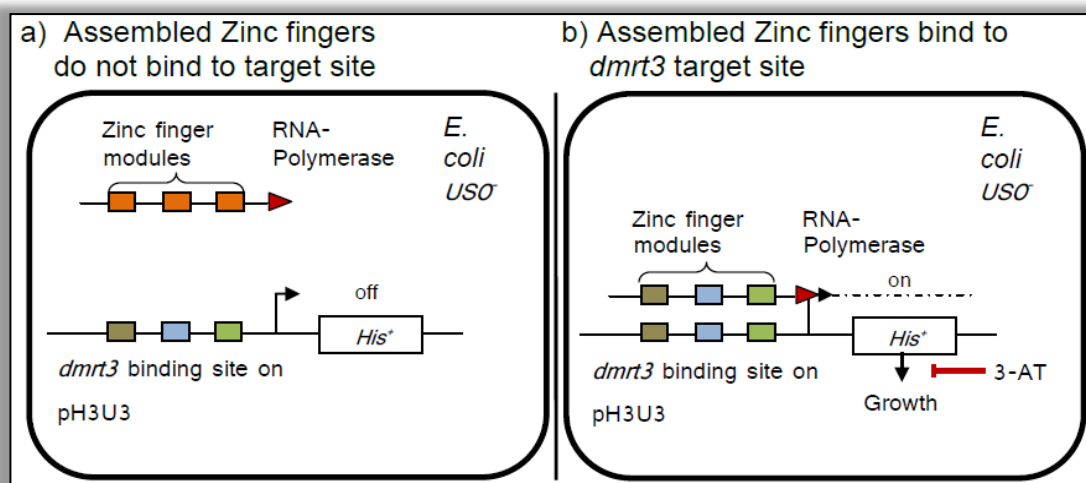
Fig. 6 Zinc finger module selection strategy: *US0⁻ bacteria were double transformed with the customized target site vector pH3U3 and the zinc finger expression vector pB1H2. The expressed zinc finger (coloured boxes and black line) is N-terminally fused to a RNA-polymerase (red triangle). Double transformed bacteria were plated out on NM-media without Histidine. a) In the case that the customized zinc finger assembly does not bind to the* dmrt3 *binding site, the bacteria are not able to grow. b) In case, the customized zinc finger polymerase binds to the* dmrt3 *target site (colour matched), expression of the Histidine-synthesizing enzyme is induced and bacteria are able to survive the selection process. 3-AT is added to the media to distinguish the binding efficiencies of different zinc finger assemblies.*

Additionally, 3-amino-triazole (3-AT; Sigma) was added to the media. 3-AT is a competitive inhibitor of the His-synthesizing enzyme and may block bacterial grow if too little enzyme is produced. Since the amount of His-synthetase is correlating to the quality of binding of the ZFP to its target site, an increasing concentration gradient of 3-AT can be used to distinguish low from high affine ZFPs.

Table 10: Required solutions and medium recipes for the bacterial one-hybrid selection

10x M9 Salt for NM medium	Total volume: 500 ml	Final concentration
Na₂HPO₄	30 g	422 mM
KH₂PO₄	15 g	220 mM
NaCl	2.5 g	85 mM
NH₄Cl	5 g	167 mM
Milli-Q water	Add to 500 ml	
Amino acid solutions for NM medium	Total volume 100 ml	Final concentration
Solution I (200x): Phe, Lys, Arg dissolve to 100 ml water	0.99 g, 1.1 g, 2.5 g	0.99%, 1.1%, 2.5% w/v
Solution II (200x): Gly, Val, Ala, Trp dissolve to 100 ml water	0.2 g, 0.7 g, 0.84 g, 0.41g	0.2%, 0.7%, 0.84%, 0.41% w/v
Solution III (200X): Thr, Ser, Pro, Asn dissolve to 100 ml water	0.71g, 8.4 g, 4.6 g, 0.96 g	0.71%, 8.4%, 4.6%, 0.96% w/v
Solution IV (200X):	1.04 g, 14.6 g	1.04%, 14.6% w/v

First make up 9.1 ml 36.5% HCl, add 80 ml water, then dissolve Asp, Gln to 100 ml water		
Solution V (200X): Dissolve K.Glu in 80 ml water, then add Tyr + 4 g NaOH pellets, add water to 100 ml	18.7 g, 0.36 g	18.7%, 0.36% w/v
Solution VI (200X): Ile, Leu dissolve to 100 ml water	0.79 g, 0.77 g	0.79%, 0.77%
Mix all 6 solutions equally which results in an 33x amino acid master mix		

2x NM medium/NM selection plates	Total volume 500 ml	Final concentration
Milli-Q water	418 ml	
10x M9 salt	100 ml	2x
20% Glucose	20 ml	80 mg/ml
20 mM adenine HCl	10 ml	400 µM
33x amino acid mix	30 ml	2x
1 M MgSO$_4$	1 ml	2 mM
10 mg/ml Thiamine	1 ml	20 µg/ml
10 mM ZnSO$_4$	1 ml	40 µM
100 mM CaCl$_2$	1 ml	200 µm
20 mM Uracil	10 ml	400 µm
Filter sterilize and add 1 ml of 100 mg/ml Ampicillin, 1 ml of 50 mg/ml Kanamycin and 100 µl of 100 mM IPTG; mix 250 ml of the medium with 3% bacto- agar to get 1x NM selection plates (add 3-AT as desired: 0- 60 mM)		

2.5.3 Customization of the zinc fingers as well as their target sites

Degenerated primers and a PCR mutagenesis protocol were used to change the coding sequences of single ZFD from template zif268. Reaction reagents were mixed according to table 11.

Table 11: Degenerated primer mediated PCR mutagenesis protocol for ZFD customization

Reagent	Volume/Amount	Final conc.	Temperature	Time	Cycles
pB1H2Ω2-zif268	1 µl	100 ng	98°C	40 sec	
10 mM Primer forw.	2.5 µl	0.5 mM	98°C	10 sec	
10 mM Primer rev.	2.5 µl	0.5 mM	65°C	10 sec	35 cycles
10 mM dNTPs	1 µl	0.2 mM	72°C	20 sec	
100% DMSO	1.5 µl	3% v/v	72°C	10 min	
5x HF buffer	10 µl	1x			
Phusion polymerase	0.5 µl	0.5 U/rxn			
Milli-Q water	up to 50 µl				

As a result of PCR mutagenesis, pools of ZF proteins that differ at a particular ZFD were generated. Consequently, their binding properties towards the desired target site differed as

well. Depending on the module, that had to be modified, different primer combinations were used (Table 12).

Table 12: Overview of primer combinations and annealing scheme to generate different zinc finger proteins

	Primer combination used to amplify specific ZFP encoding fragments		
	Pre-selection primers: Used to randomize ZFDs		Post-selection primer combinations: Used to isolate fragments that encode for *dmrt3* sequence binding ZFD after the selection
	Customized fragment	Annealed with backbone fragment	Selected fragment
Module 1	p_mod1_Lib x reverse primer VI	OligoI	Oligo1 x Mod1_rev
Module 2	p_mod2_Lib x reverse primer VI	Oligo1 x Mod1_rev	Oligo1 x Mod2_rev
Module 3	p_mod3_Lib x reverse primer VI	Oligo1 x Mod2_rev	Oligo1 x reverse primer VI
Overview of the location of used primers			

For better clarity, the protocol for one exemplary selection round will be described in more detail here. The primers used to customize **mod**ule **1** of the **5'** binding zinc finger protein were designated as **5p_mod1_lib primer**. These degenerated primers were used in combination with reverse primerVI that binds at the end of the coding sequence. The amplicons generated in this PCR encode for zinc finger proteins with an **unselected ZFD** (**Lib**) 1 in combination with the two standard zif268 (Fig. 7 a). The resulting PCR products were lacking a required 5' KpnI restriction site for subsequent cloning into ZFP expression

vector pB1H2Ω2. Therefore, it was necessary to anneal the ZFD encoding amplicons with OligoI that contained an internal KpnI restriction site (Fig. 7 b).
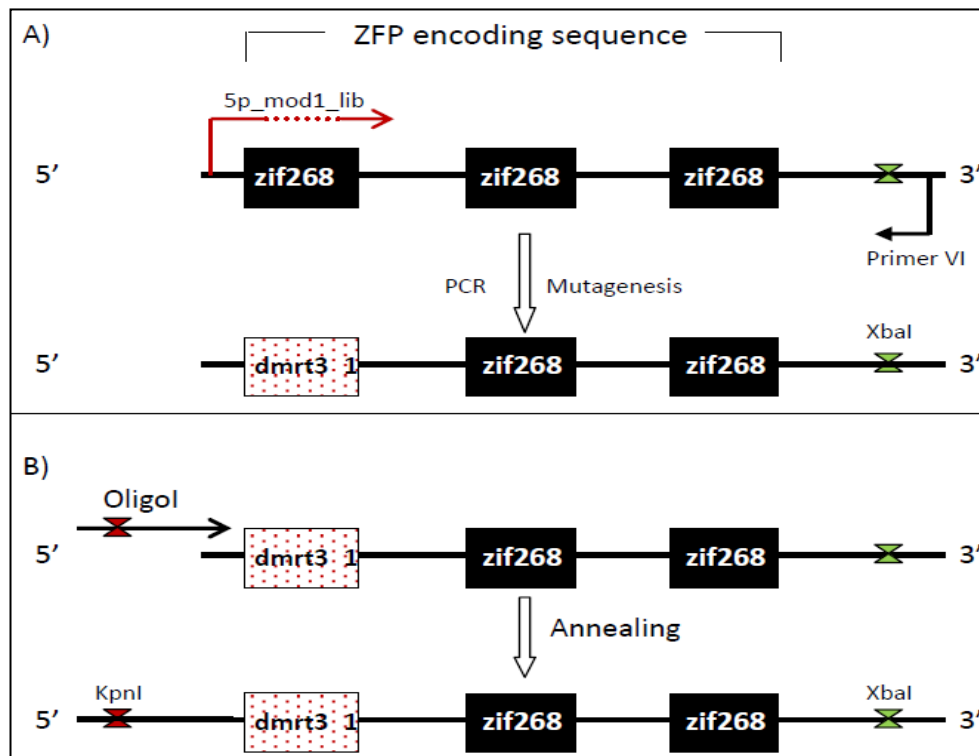
Figure 7 PCR mutagenesis and annealing for the first ZFD of the 5' ZFP: A) Degenerated primer mediated ZFD mutagenesis: The coding sequences for the first ZFD of template zinc finger 268 (black boxes) is getting customized using the degenerated primer for the 1st module of the 5' ZFP (red arrow) and reverse primer VI (black arrow). After the PCR, the first module is highly randomized but yet unselected (red box). B) Annealing of PCR mutagenesis amplicons from A) with OligoI: Since PCR products from the first round were missing the required KpnI restriction site (red label), the ZFD assembly had to be annealed with OligoI (black arrow with red label).

For the annealing of different modules, a combined annealing and amplification protocol was used. Reagents were added into the reaction tube at a particular time point. During the first part of the reaction, sequences encoding for different modules (for example OligoI and module 1) were added to reaction buffer, MgCl$_2$ and water. The reaction was heated up to melt the module-encoding double strand DNA and cooled down slowly to facilitate annealing of different modules. During the second phase, dNTPs and polymerase were added to elongate single stranded sequences of the annealed DNA hybrids. The PCR amplification was initiated during the last phase of the protocol after forward primer OligoI and reverse primerVI were added to the reaction.

45

Temperature	Time	Cycles/ comments	Added reagent/ Comments		Reagent	Volume/ Amount	Final conc.
95°C	3 min	/	**Amplicons of different modules**: Encoding module fragments (ratio: 1:1:1) 10x Taq reaction buffer Milli-Q water, MgCl$_2$		ZFD amplicons	X µl	1:1:1 Module ratio
95°C to 35°C	60 min	-1°C/min	**Annealing of modules**		10x Taq reaction buffer	10 µl	1x
72°C	20 min	/	**Elongation of gaps in annealed fragments:** Phusion-polymerase dNTPs		10 mM OligoI	2.5 µl	0.5 mM
95°C	3 min				10 mM PrimerVI	2.5 µl	0.5 mM
95°C	30 sec				10 mM dNTPs	1 µl	0.2 mM
65°C	30 sec	35 cycles	**PCR to amplify whole ZFP encoding DNA sequences:** OligoI and primerVI		25 mM MgCl$_2$	2 µl	1 mM
72°C	25 sec				Taq Polymerase	1 µl	1U
72°C	10 min				Milli-Q water	Up to 50 µl	
4°C	-						

After the PCR, the ZFP encoding fragments were digested with KpnI and XbaI and analysed on a 2% TAE gel. Digested fragments were 108bp shorter than the undigested 412bp long fragments and were isolated from the gel. Purified fragments were cloned into KpnI/XbaI digested pB1H2Ω2 vectors and resulting plasmids were encoding for a new, randomized zinc finger. Plasmids were subsequently transformed into USO hisB- pyrF- rpoZ- bacteria harbouring the corresponding target site plasmids, and selections were done as described previously (see chapter 2.5.2).

2.5.3.1 Sequential selection method

After each round of selection, the surviving bacteria were collected and their zinc finger encoding plasmids were isolated and pooled. The selected library pools were used as a template for the next round of ZFD customization. For this, target site binding domains were isolated and annealed with unselected, randomized modules of the next zinc finger domain. These procedures were repeated until all three modules were customized. Parallel to the customization of the standard zinc finger, it was necessary to modify the corresponding target site in three steps accordingly. This altered the original zif268 target site step by step into the desired *dmrt3* binding site (Fig. 8 a). Alterations of target site plasmids were done step-wise

by PCR based mutagenesis with primers (see Appendix A2) that bound to the target site and changed it to the desired *dmrt3* target site sequence. After amplification of customized target site fragments, fragments were purified and digested with restriction enzymes. In parallel, the target site vector pH3U3 was cut with the corresponding enzymes and subsequently ligated with the customized ZFP target site fragments. The sequential selection took the modular context of already selected binding modules into account. The context-sensitivity of this method ensures that final selected ZFD assemblies interact well with each other, which increases the chances of the binding to the *dmrt3* loci. On the other hand, the disadvantage of this sequential selection was that it was very time-consuming. One selection round had to be finished first before the next selection round could be started.

2.5.3.2 Modular assembly method

Due to the time-intensive sequential selection, a modular assembly approach was undertaken in parallel for the 3p binding ZFP. Selection processes for all three ZFP modules were done in parallel in a zif268 context. In addition, only one out of three nucleotide triplets had to be changed to generate corresponding target site plasmids. The modular assembly approach was much faster but less context sensitive than the sequential selection method. The overview schemes below (Fig.8) illustrate the basic principles of both selection methods.
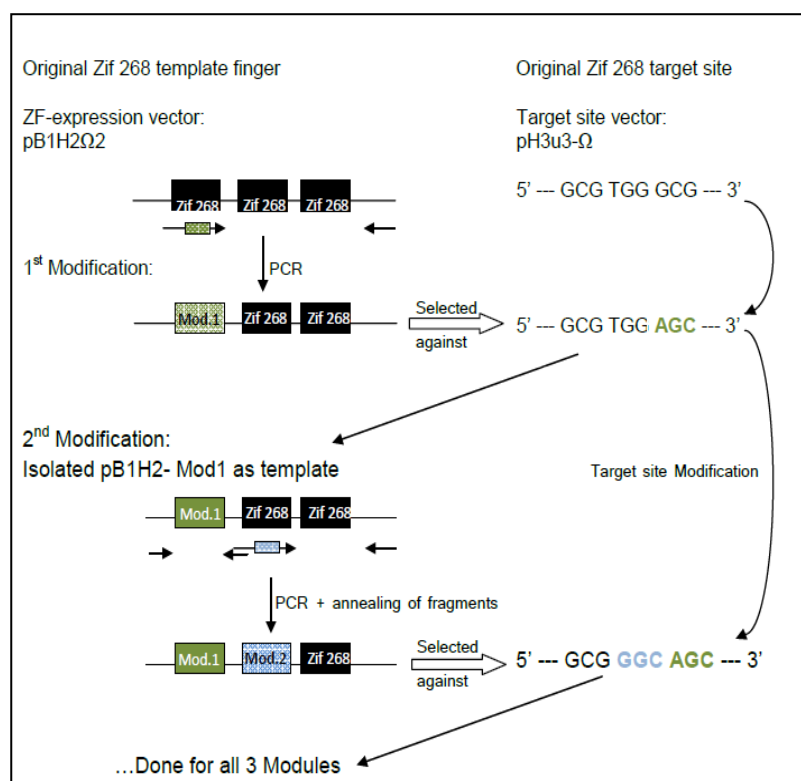
Fig. 8 A) Sequential selection and B) modular assembly: A) Zinc finger 268 was used as a template that was PCR customized using degenerated primers (arrows with coloured boxes). Generated sequences encoded for one unselected but randomized finger (patterned box) and two zinc finger 268 modules (black boxes). This zinc finger was selected against a 9 bp long target site containing the first three nucleotides of the *dmrt3*-site (coloured AGC). Plasmids encoding for zinc finger proteins that contained *dmrt3*-triplet binding modules (coloured boxes) were isolated and used as templates for the next selection step.
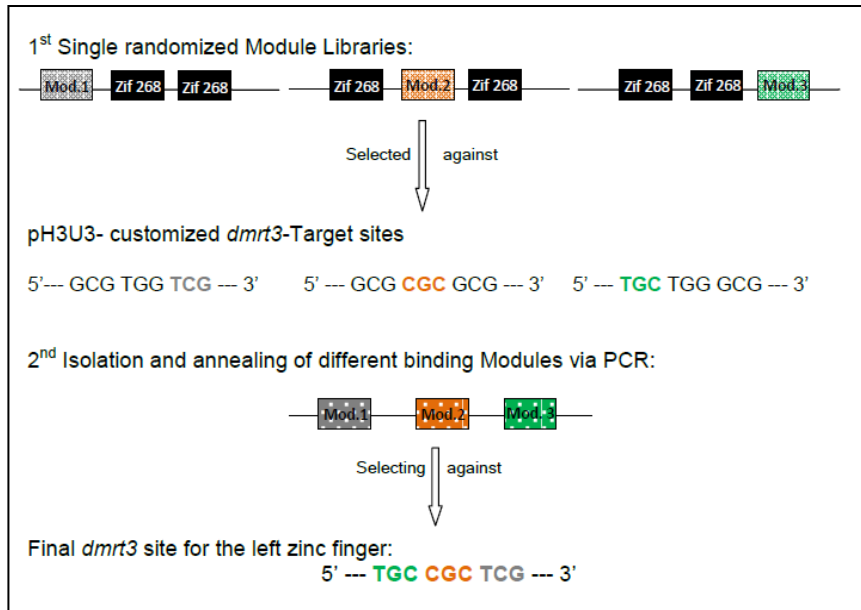
B) Modular assembly: 1) Selections of customized ZFD's were done in parallel for all three modules. 2) After all 3 modules were tested, modules of binding zinc finger proteins were isolated and annealed to each other. A final selection round was required to identify whole *dmrt3*-target site binding proteins. This selection method was less *dmrt3*-context sensitive, since selection took place in a zif268 environment.

After three rounds of ZFD modification and selection, single bacterial colonies that survived high 3-AT concentrations were picked and plasmids encoding ZF proteins were isolated. The DNA encoding the ZFD was sequenced and unique ZF protein plasmids were identified. To compare and evaluate binding affinities of these particular ZF proteins towards the complete *dmrt3* target sequence, a comparative binding assay was performed. Equal amounts of unique ZF protein encoding plasmid were transformed into electro-competent cells harbouring a pH3U3-*dmrt3* target site, spread out side by side and incubated on 3-AT plates. This allowed comparison and identification of the best *dmrt3* target site-binding ZF proteins.

2.5.4 Generation of plasmids encoding ZFN that bind to the *dmrt3* locus

After the final isolation step, DNA sequences encoding high-affine ZF proteins were amplified using a primer combination of OligoI (KpnI) and primer X (BamHI). Next, ZF protein encoding amplicons and FokI expression vectors (Addgene: 18754/18755) were digested with KpnI and BamHI, purified and ligated with each other using a T4 quick ligation kit (Roche). Ligated plasmids were transformed into chemically competent cells and the presence of ZFN encoding plasmids was verified via colony test PCR and sequencing.

2.5.5 Production of ZFN mRNA

To produce ZFN encoding mRNA, ZFN plasmids were linearized with NotI (Fermentas) and mRNA was synthesised using the mMESSAGE *mMACHINE* Kit SP6. *In-vitro* transcribed mRNA was purified as described in chapter 2.4.15 and injected into one-cell stage zebrafish embryos.

In addition, to the ZFN produced by modular and sequential assembly as described above, customized ZFN targeting the *dmrt3*-locus were obtained from ToolGene. These plasmids were linearized using XbaI, and the mMESSAGE *mMACHINE* Kit T7 was used for *in-vitro* transcription of ZFN encoding mRNAs. XbaI cuts the plasmids in front of the poly-A signal. Hence, it was necessary to add an additional poly-A tail to the transcripts. A poly-A tailing reaction was performed as described in 2.4.12. Transcripts were analysed on a 1% agarose gel to confirm the efficiency of the tailing reaction and successfully treated transcripts were purified and injected into one-cell stage embryos.

2.5.6 Analysis of ZFN activity

To test if the ZFN mRNA caused any frameshift mutation within the *dmrt3* loci in injected zebrafish embryos, gDNA from pooled as well as single embryos was isolated. Using a primer combination that flanks the potential target site (Appendix A2: ZFN screening primers), *dmrt3* amplicons were generated, gel purified and applied to a diagnostic restriction digest. PCR amplified *dmrt3* fragments contained both ZFN binding sites as well as the spacer region. The spacer region for the self-assembled ZFNs included an MspA1I restriction site while the spacer region of the ToolGene made ZFNs contained a CviAII restriction site. If the ZFN cut within the *dmrt3* loci, non-homologues repair mechanisms introduce insertions and deletions in the spacer region between both ZFN binding sites. The presence of a restriction fragment length polymorphism (RFLP) introduced by the ZFN rendered the *dmrt3* amplicon indigestible for MspAI or CviAII. Therefore, the occurrence of undigested *dmrt3* fragments on TAE gels was indicative for the presence of site-directed active ZFNs (fig. 9).
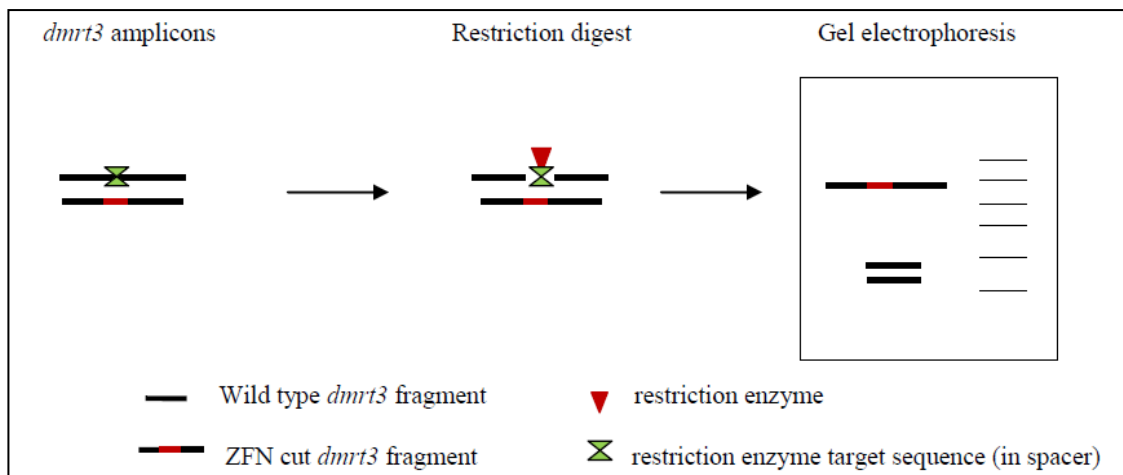
Fig. 9 Schematic overview of RFLP assay: Wild type or ZFN injected embryo gDNA served as a template to amplify *dmrt3* encoding fragments. The PCR amplicons contained a unique restriction site (green label) that was flanked by the ZFN binding sequences. In case the ZFN did not cut the *dmrt3* locus, the PCR product was digested and bands with a smaller size than the PCR amplicon became visible on the gel. In case the ZFN introduced a frameshift (red mark), the unique restriction site was destroyed, which rendered the *dmrt3* amplicon indigestible for the restriction enzyme (red triangle). As a result, the *dmrt3* amplicon remained undigested after the incubation with the restriction enzyme.

Single embryos that showed a RFLP in comparison to control embryos were further analysed by sequencing of the *dmrt3* locus. For that, undigested *dmrt3* amplicons were isolated, cloned into TOPO-blunt vectors and sequenced with vector specific primers, such as M13 reverse.

In addition to MspAI, I also analysed the *dmrt3* amplicons using a T7 endonuclease assay. T7 endonuclease recognizes and cuts double stranded DNA that contained secondary structures caused by a mismatch alignment of different DNA species. If ZFNs introduced frameshift mutations into the *dmrt3* loci, gDNA isolated from these injected embryos yield different gDNA species. These different gDNA species were used as templates to PCR amplify the *dmrt3* sequence. In a next step, *dmrt3* amplicons were denatured at 95°C for 10 min. The melted DNA was then cooled down slowly (-1°C/min) to allow re-annealing of *dmrt3* encoding fragments. The presence of different *dmrt3* sequences will result in homo- as well as heteroduplex variants of the *dmrt3* amplicon. Re-annealed fragments were applied to T7 endonuclease digests in 1x T7 endonuclease buffer and analysed on TAE gels. If the analysed embryo contained *dmrt3* mutations, secondary structures in heteroduplex amplicons were recognized and digested by the endonuclease, and smaller fragments in addition to the

undigested *dmrt3* homoduplex became visible on the TAE gel. An overview about this technique is illustrated in figure 10.
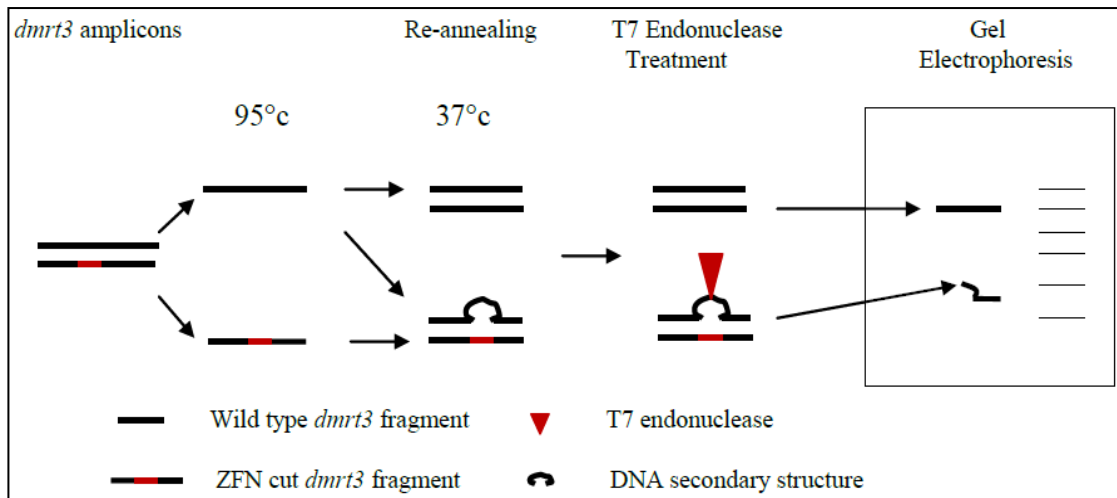
Fig. 10 Schematic overview of T7 endonuclease assay: gDNA from control and *dmrt3* ZFN mRNA injected embryos were isolated and used as a template to amplify *dmrt3* PCR fragments. If the *dmrt3* fragment contained frameshift mutations (red label), the length of these fragments were different from wild type fragments. Next, the PCR reactions were heated up to 95°C and cooled down slowly to anneal frameshift fragments with unaltered *dmrt3* amplicons. If two different fragments re-annealed with each other, a hetero-duplex formed that contained loop structures due to different fragment lengths. Finally, re-annealed PCR products were treated with T7 endonuclease (red triangle), which recognizes and cleaves double stranded DNA-loop structures and smaller fragments would have been become visible on analytical agarose gels. Smaller fragments than the undigested *dmrt3* amplicon indicated *dmrt3* frameshift mutations.

If digested fragments were detectable after T7 endonuclease digest, amplicons from affected embryos were sequenced and analysed for frameshift mutations.

To identify potential founders at later stages, gDNA were isolated from fin clips (see 2.4.17) and applied to RFLP analysis using CviAII. To confirm frameshift mutations, undigested *dmrt3* amplicons were isolated from the gel, cloned and sequenced. Positively tested fish were kept separately until fish were sexually matured. *Dmrt3* mosaic mutants were in-crossed with each other and progenies were analysed for a complete 100% RFLP indicating homozygosity of the *dmrt3* mutant locus.

2.6 Staining protocols and imaging

2.6.1 RNA whole mount *in-situ* hybridization (WISH)

For analysis of gene expression patterns, DIG or Fluorescein-labelled WISH probes were synthesized as described above. Depending on the concentration of the probe, probe stock solutions were diluted with hybridization mix to 1:50 - 1:200 working solutions.

Zebrafish embryos were raised to the desired stage and fixed for at least 2 h in 4% PFA. The PFA was exchanged and 100% methanol was added. Embryos were stored at -20°C for at least overnight and on the next day. Embryos were rehydrated using a descending methanol series of 75%, 50% and 25% in phosphate buffered saline with tween (PBST) and each incubation step lasted 5 min. After hydration, the embryos were washed twice in PBST before embryonic structures were permeabilized with proteinase K (1.25 µl proteinase K/5 ml PBST; Fermentas). The concentration and incubation time of the permeabilization step was stage-dependent. Proteinase K activity was stopped by adding 1x glycine (AppliChem) and embryos were rinsed twice with PBST. Next, embryos were fixed in 4% PFA for at least 20 min. The PFA was removed and the samples were washed thoroughly with PBST (5x 5 min). To block unspecific binding sites, PBST was exchanged with hybridization mix and incubated for at least 1 h at 65°C. After this pre-hybridization step, the hybridization mix was exchanged with probe solution and samples were incubated at 65°C overnight. On the next day, probes were removed and samples were washed twice with 2x SSCT/50% formamide, followed by one 2x SSCT and two 0.2x SSCT washing steps. All SSCT washing steps were performed at 65°C and lasted 30 min. After the last washing step, unspecific antibody binding sites were blocked by adding 5% sheep serum (Sigma)/PBST and incubating the samples for 1 h at room temperature. After this, the blocking solution was discarded and replaced by alkaline phosphatase conjugated anti-DIG/ fluorescein antibodies (Roche). The zebrafish were incubated for at least 2 h at room temperature before antibodies were removed and samples were washed thoroughly with PBST (6x 20 min). Before transcripts were visualized with NBT staining solution, embryos were incubated twice in pre-staining buffer for 5 min. The

staining was stopped by adding PBST when samples showed a sufficient colouration and
stored in 4% PFA. Recipes and reagents used are listed below.

__Table 14: Whole mount in-situ hybridization reagents__

10x PBS solution	Total volume: 1 L	Final concentration
NaCl	58.44 g	1 M
KCl	1.45 g	19.5 mM
Na_2HPO_4	8.38 g	59 mM
KH_2PO_4	1.5 g	11 mM
Milli-Q	add to 1 L	
1x PBST	Total volume: 1 L	Final concentration
autoclaved 10x PBS	100 ml	1x
20% Tween 20	5 ml	0.1% v/v
Milli-Q	895 ml, filtered through 0.22µm polyethersulfone bottle filter (Nalgene)	
	Total volume: 10ml	Final concentration
50x Glycine	1 g/10 ml PBST	50x
1x Glycine	200 µl 50x Glycine/10 ml PBST	1x
Hybridization mix		
Formamide	25 ml	50% v/v
20x SSC	12.5 ml	5x
50 mg/ml Heparin	150 µl	150 µg/ml
Torula RNA	250 mg	5 mg/ml
20% Tween 20	250 µl	0.1% v/v
Milli-Q water	add to 50 ml	
2x SSCT buffer/50% Formamide:	Total volume: 50 ml	Final concentration
Formamide	25 ml	50% v/v
20xSSC	5 ml	2x
20% Tween20	250 µl	0.1% v/v
Milli-Q water	add to 50 ml	
2x SSCT buffer:	Total volume: 50 ml	Final concentration
20x SSC	5 ml	2x
20% Tween 20	250 µl	0.1% v/v
Milli-Q water	add to 50 ml	
0.2x SSCT buffer:	Total volume: 50 ml	Final concentration
20x SSC	0.5 ml	0.2x
20% Tween 20	250 µl	0.1% v/v
Milli-Q water	add to 50 ml	
Pre-staining buffer:	Total volume: 50 ml	Final concentration
5 M NaCl	1 ml	0.1 M

0.5 M MgCl$_2$	5 ml	0.05 M
1 M Tris-HCl, pH9.5	5 ml	0.1 M
20% Tween 20	250 µl	0.1% v/v
Milli-Q water	Add to 50 ml	
NBT staining solution:	Total volume: 10 ml	Final concentration
5 M NaCl	200 µl	0.1 M
1 M Tris-HCl, pH9.5	1 ml	0.1 M
20% Tween 20	50 µl	0.1% v/v
Milli-Q water	add to 10 ml	

2.6.2 Two-colour whole mount *in-situ* hybridization

The two-colour WISH is a modified version of the normal *in-situ* protocol. Instead of using only DIG-/or fluorescein-labelled probes, both probes are used together at the same time. The first steps until the antibody blocking step were the same like mentioned in the standard WISH protocol. The samples were then incubated with anti-fluorescein antibody at room temperature for at least 2 h. After the incubation step, samples were washed 6 times for 20 min. The primary staining followed to detect fluorescein-labelled transcripts. The samples were incubated two times for 5 min in equilibration buffer and stained in "Fast Red" solution until the expression patterns of transcripts were clearly detectable. Staining reactions were stopped by washing embryos three times for 5 min with PBST. For the second colour reaction, it was necessary to remove the bound anti-fluorescein antibodies. This was done by washing the embryos two times for 10 min in antibody removal solution. After antibodies were removed from the samples, they were washed four times for 5 min in PBST. The secondary stain was performed utilizing alkaline phosphatase conjugated anti-DIG antibody as described above.

Table 15: Additional reagents required for two colour whole mount in-situ hybridization

Equilibration buffer:	Total volume: 500 ml	Final concentration
Tris	6.057 g	0.1 M
20% Tween 20	2.5 ml	0.1% v/v
Adjust pH with 37% HCl to 8.2		
Milli-Q water	add to 500 ml, filter through 0.22µm polyethersulfone bottle filter	
Antibody removal solution:	Total volume: 50 ml	Final concentration
Glycine	3.75 g	0.1 M
20% Tween 20	2.5 ml	0.1% v/v

Adjust pH with 37% HCl to 2.2	
Milli-Q water	Add to 500 ml, filter through 0.22μm polyethersulfone bottle filter
Fast Red staining solution:	dissolve one Fast Red tablet (Roche) in 2 ml equilibration buffer and filter solution through 0.22μm syringe filter

2.6.3 Immunostaining

Immunostaining of specimen was done using fluorescense-labeled secondary antibodies. Embryos of the desired stage were fixed for 2 h in 4% PFA and stored at -20°C in methanol. Embryos were rehydrated using a descending methanol series of 75%, 50% and 25% methanol in PBST. Next, samples were washed and incubated in Milli-Q water for at least 1 h to increase tissue permeability. Unspecific antibody binding sites were blocked by incubating embryos in PBDT for at least 1 h. After that, the blocking solution was replaced by 500 µl of the diluted primary antibody in PBDT .The samples were incubated at 4°C overnight. On the next day, antibodies were removed and samples were washed at room temperature four times for 1 h with PBST with 0.1% TritonX-100 (PBSTT). Afterwards, PBDT diluted fluorescence-labeled secondary antibodies were added and specimens were incubated for at least overnight. On the next day, antibodies were removed and specimens were washed four times for 1 h in PBSTT. After removal of non-bound antibodies, samples were ready for analysis using a fluorescence microscope (Nikon). A list of used primary and secondary antibodies can be found in the appendix A2.

Table 16: Immunostaining reagents

PBDT solution:	Total volume: 25 ml	Final concentration
100% DMSO	250 µl	1% v/v
BSA	0.25 g	1% w/v
TritonX-100	125 µl	0.5% v/v
Sheep serum	625 µl	2.5% v/v
10x PBS	2.5 ml	1x
20% Tween 20	125 µl	0.1% v/v
Milli-Q water	add to 25 ml	
PBSTT:	Total volume: 1 l	Final concentration
10x PBS	100 ml	1x
100% Tritonx-100	1 ml	0.1% v/v
20% Tween 20	5 ml	0.1% v/v
Milli-Q water	894 ml, filter through 0.22 polyethersulfone bottle filter	

2.6.4 BrdU incorporation assay

To detect proliferating cells in S-phase, embryos were dechorionized and incubated in BrdU solution (10 mM BrdU/15% DMSO) on ice for 20 min. Following that, the BrdU solution was removed and embryos were rinsed several times with PBST before they were fixed in 4% PFA. Embryos were kept in PFA for 2 h before the embryos were washed three times for 5 min each with PBST. After the last washing step, 100% methanol was added and embryos were stored at -20°C. For staining, embryos were rehydrated using a descending methanol series followed by incubation in 2N HCl at 37°C for 1 h. After that, the normal immunostaining protocol was carried out as described before (2.6.3).

2.6.5 Sample preparation and image acquisition

PFA fixed and *in-situ* or immunostained embryos were washed three times for 5 min with PBST before they were transferred to 50% glycerol (AppliChem). Samples were kept in 50% glycerol for 10 min prior to transferring them into 100% glycerol. Image acquisition took place with embryos placed in 100% glycerol.

Pictures were acquired either at low magnification using a stereomicroscope (Nikon) or at high magnification using a Nikon Eclipse 90i compound microscope. The NIS element basic software (Nikon) was used for image acquisition. Recorded images were analysed, labelled and edited using Photoshop.

For confocal microscopy, stained samples were fixed in low melting agarose (1st Base) in glass bottom dishes and pictures were acquired on a confocal system LSM510 Meta (Zeiss). Recorded z-stacks were analysed with LSM Image Browser (Zeiss) and labelled and edited with Photoshop.

3. Results

Previous studies have shown that *dmrt* genes control various aspects of neuronal development, for example neurogenesis in the X*enopus* olfactory placode (*dmrt5*; Huang *et al.*, 2005) or spinal cord interneuron formation in zebrafish (*dmrt3;* Rajaei, PhD Thesis 2012). Aim of the present study was to reveal potential roles of *dmrt* genes during neurogenesis in the forebrain. For this, I focussed on the two *dmrt* genes, *dmrt3* and *dmrt5*, which are known to be expressed in embryonic forebrain regions. Gene knock-out and knock-down approaches were used to uncover their functions based on phenotype analysis. The first part of this section will describe results gained by the use of a *dmrt3* and *dmrt5* morpholino-based knock-down approach. The knock-down proved to be very efficient for *dmrt5* while the *dmrt3* knock-down had some limitations. Therefore, a second *dmrt3* loss-of-function approach was conducted. The last part of this section describes the generation of *dmrt3* zinc finger nucleases (ZFNs) and *dmrt3* knock-out zebrafish.

3.1 Spatio-temporal expression of *dmrt3* and *dmrt5* during forebrain neurogenesis

Earlier studies have shown that *dmrt3* is expressed in a subset of dorsal telencephalon and olfactory placode cells in zebrafish embryos (Li *et al.*, 2008). A study from Guo *et al.*, 2004 used real-time PCR to illustrate that *dmrt5* is expressed in embryonic brain tissue but failed to illustrate the detailed spatio-temporal *dmrt5* expression patterns. Furthermore, it is known from *Xenopus* that one member of the *Dmrt* gene family (*Xdmrt4*) regulates neurogenesis in the developing olfactory placode (Huang *et al.*, 2005). Taken together, the previously published data in combination with preliminary expression analysis of *dmrt3* and *dmrt5* suggested a potential role of both *dmrt* genes during zebrafish forebrain development. I therefore addressed the question if *dmrt3* and/or *dmrt5* are involved during forebrain neurogenesis.

Wild-type zebrafish embryos were collected and fixed at different embryonic stages to analyse the expression of *dmrt5* by RNA whole-mount hybridization. *Dmrt5* mRNA was untraceable in zebrafish embryos before and during shield and epiboly stages, but at bud-stage *dmrt5* expression became detectable as a u-shaped expression domain along the anterior

neural ridge (arrow, Fig. 11 c). Shortly thereafter, the expression of *dmrt5* expanded throughout the presumptive telencephalic field (Fig. 11). At the 14 somite stage, *dmrt5* expression was up-regulated in the forming telencephalic and diencephalic forebrain regions and was additionally expressed in the ventral midbrain. *Dmrt5* transcripts were detectable throughout the dorsal telencephalon, the telencephalic ventricular zones, olfactory epithelium, dorsal diencephalon, and as a stripe of cells ventrally to the olfactory epithelium (Fig 11 e) at 25 hpf. Weak forebrain staining was also detectable in a group of cells in the anterior and ventral forehead. Their position suggested that these are migrating pituitary cells (arrowhead, Fig. 11 e'). Expression in the aforementioned domains was maintained at 52 hpf albeit at a weaker level (Fig. 11 f-f"). Additionally, *dmrt*5 expression became restricted to the anterior pituitary domains (dashed area, Fig. 11 f"). The transcript levels of *dmrt5* were reduced in telencephalon and diencephalic forebrain regions at 74 hpf, while midbrain (asterisk, Fig. 11 g) and pituitary expression remained relatively strong (Fig. 11 g').
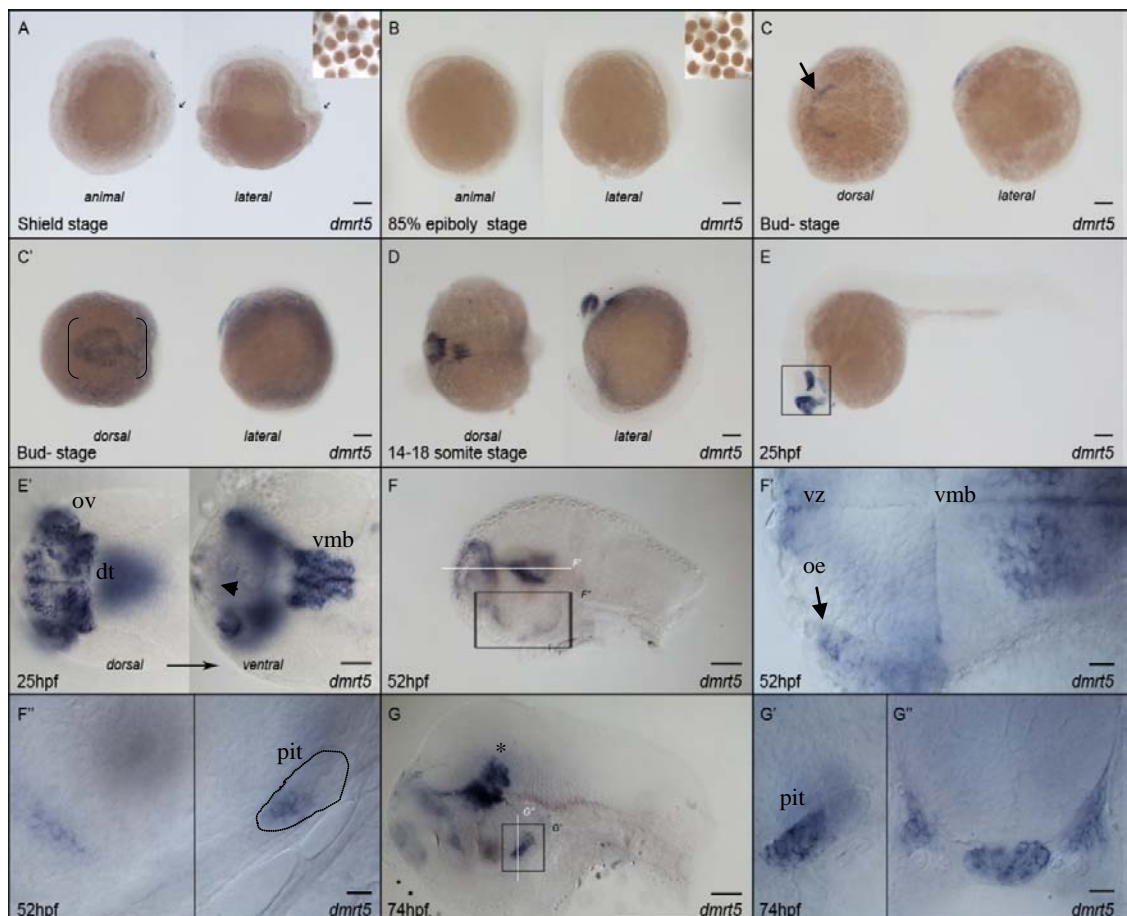
Fig. 11 Spatio-temporal expression pattern of dmrt5 until 74 hpf: Images taken at early stages. Images A to E are overview pictures of whole embryos. Embryos are shown from two views: A, B:

animal and lateral; C-D: dorsal and lateral. Pictures E' to G'' are images of embryonic head regions at different stages from dorsal, lateral or as cross section at higher magnifications. Embryonic stages are indicated in the lower left corner of each image. Used abbreviations: dorsal telencephalon (**dt**), ventral midbrain (**vmb**), olfactory epithelium (**oe**), pituitary (**pit**), ventricular zones (**vz**). Scale bars in A-E, F and G: 100 µm, E': 50 µm, F'/F'' and G'/G'': 20 µm.

To determine if *dmrt3* and *dmrt5* act in identical or separate brain compartments, expression patterns of *dmrt3* and *dmrt5* were compared by two colour-whole mount *in-situ* hybridization in 24 hpf embryos. It was found that both genes were expressed in overlapping domains of the dorsal telencephalon (arrow) and olfactory epithelium (arrowhead, Fig. 12 a''/b''). In figure 12 a, the red fluorescence signal from *dmrt5* expression domains were partially quenched by the NBT-staining of *dmrt3* positive cell populations in the dorsal telencephalon, resulting in a weaker *dmrt5* signal (indicated by the white arrow, Fig. 12 a'). Figure 12 b shows the overlapping expression domains of *dmrt3* and *dmrt5* in the olfactory epithelium (arrow head, Fig. 12 b/b') although the staining of *dmrt3* was very weak in this region. Thus, it is possible that *dmrt3* and *dmrt5* act redundantly and that a knock-out or knock-down of one gene could be functionally rescued by the other *dmrt* gene.
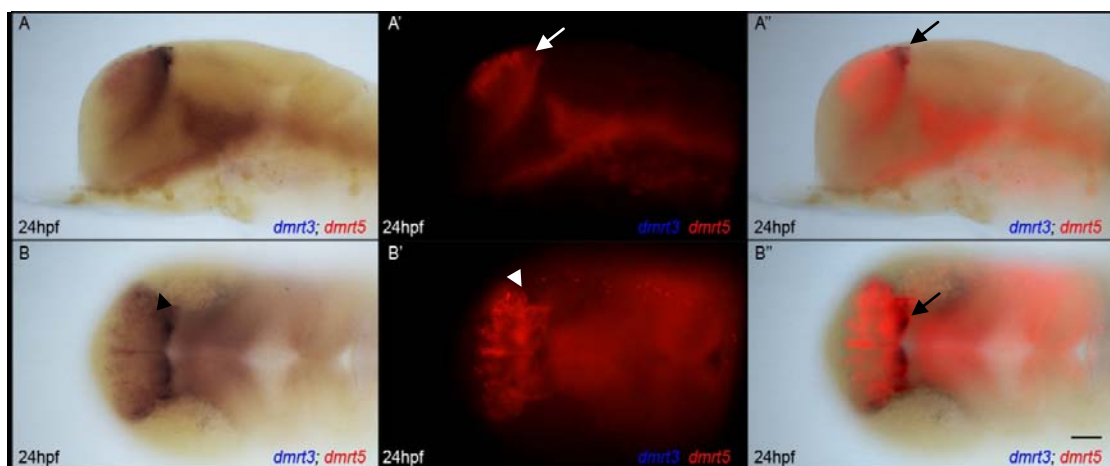
Fig. 12 Double in-situ dmrt3- dmrt5: Two colour *in-situ* hybridization of 24 hpf embryos for *dmrt3* in blue and *dmrt5* in red. Both genes are expressed in the dorsal-most parts of the lateral telencephalon close to the ventricular surface (arrow) and the olfactory epithelium (arrow head). A) lateral views, B) dorsal views of the same embryo as shown in A). Images were captured as A/B) bright field; A'/B') fluorescence and A''/B'') overlay pictures of bright field and fluorescence images to illustrate overlapping expression domains of *dmrt3* and *dmrt5*. Anterior left. Scale bar: 50 µm.

Noteworthy, the expression of *dmrt5* expands throughout the forebrain including the rest of the telencephalon and diencephalon and is additionally expressed in parts of the ventral midbrain. In contrast, *dmrt3* expression is restricted to the dorsal telencephalon and the

olfactory epithelium. This suggests that Dmrt5 has a broader area of biological activity than Dmrt3 and that it could influence a larger cell population during brain development. This hypothesis is also consistent with the observation that *dmrt5* expression starts earlier (bud stage; 10 hpf, Fig. 11 c) than *dmrt3* (around 14 hpf; Rajaei F., PhD Thesis 2012).

3.2 Design and analysis of *dmrt3* and *dmrt5* morpholinos

To analyse the role of Dmrt3 in the dorsal telencephalon and olfactory placode, *dmrt3* splice blocking morpholinos were used for gene knock-down and were previously characterized in our lab (Rajaei, PhD Thesis 2012). Used concentrations were 1.6 mg/ml to 3.125 mg/ml.

To investigate the function of Dmrt5 during zebrafish forebrain development, *dmrt5* splice site morpholinos were designed. These *dmrt5* splice-blocking morpholinos bind to the exon-intron boundaries of exon 1- intron 1 (*dmrt5* splice up) and intron 1- exon 2 (*dmrt5* splice down) (Fig. 13). In order to prevent nonspecific binding of *dmrt5* morpholinos to potential unspecific morpholino binding sites, morpholino sequences were blasted against zebrafish nucleotide database to reveal possible unspecific binding sites. No other 100% identical sequences were found other than *dmrt5*.

Fig. 13 Schematic overview of dmrt5 splice-block morpholinos and PCR primer binding sites: Both *dmrt5* splice –blocking morpholinos bind to the internal splice acceptor and donor sites within the *dmrt5* pre-mRNA. This binding results in a block of pre-mRNA splicing and the unspliced mRNA gets degraded. Hence, the injection of *dmrt5* morpholinos results in a loss-of function of Dmrt5 in zebrafish embryos. Different *dmrt5* mRNA species can be detected using intron-flanking PCR primers (arrows) to evaluate splice-block efficiencies.

For analysing the efficiency of the used splice blocking morpholinos, total RNAs from morpholino and control morpholino injected as well as wild type embryos were isolated and reverse transcribed into cDNA. The cDNA was used as PCR template and proper splicing of pre-mRNA was evaluated with *dmrt5* intron-flanking primers. This setting allowed the

detection of cDNA templates, generated from spliced or unspliced RNA (Fig. 14). Injection of single splice morpholinos at 12.5 mg/ml showed that the use of single splice site morpholinos was not sufficient to block *dmrt5* pre-mRNA splicing efficiently (block efficiency: 63% and 11%, Fig. 14, top, lanes: 3 and 4) as two bands with expected sizes for spliced and unspliced *dmrt5* mRNA were obtained. I therefore tested a combination of splice site morpholinos for injection. Splice efficiencies were determined for morpholino concentrations at 1.6 mg/ml and 3.125 mg/ml. Injections of 1.6 mg/ml *dmrt5* splice site morpholinos were not sufficient to block splicing of *dmrt5* pre-mRNA efficiently (78%, Fig. 14, top, lane: 2). At 3.125 mg/ml, *dmrt5* splice site morpholinos blocked pre-mRNA splicing with 97% efficiency. Only PCR fragments were amplified that represented unspliced *dmrt5* pre-mRNA fragments (Fig. 14, top, lane 1). These results show that the co-injection of two morpholinos in combination leads to synergy effects that block *dmrt5* pre-mRNA splicing efficiently at relatively low doses. A quantitative ImageJ analysis of obtained amplicon intensity is shown in Fig. 14 B.
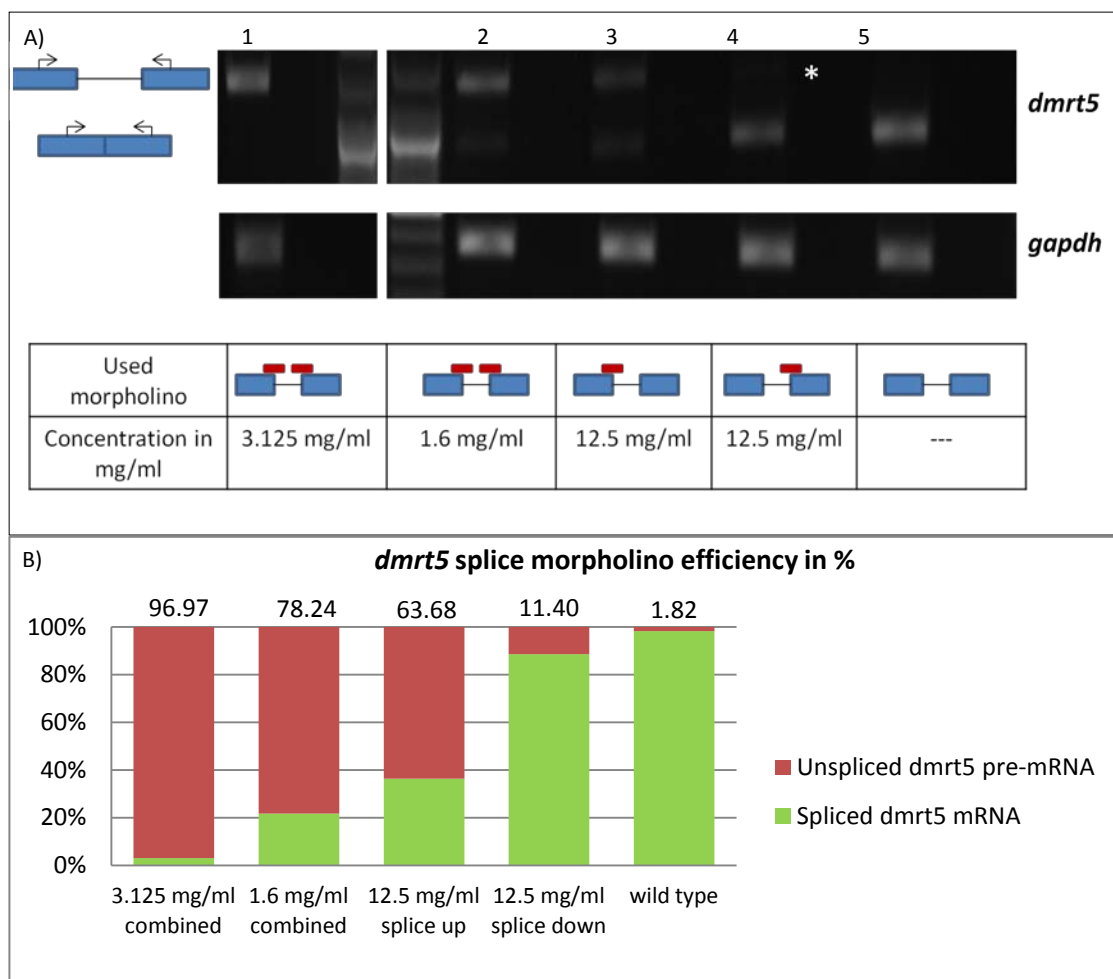
Fig. 14 Efficiency of dmrt5 splice blocking morpholinos: A) Top row: Semi-quantitative PCR to determine the ratio of unspliced to spliced *dmrt5* transcripts from embryos injected with different morpholinos. The used morpholino combinations and their concentrations are given below the gel picture. Lane 1 and 2: combined morpholino injections at 3.125 mg/ml (1) and 1.6 mg/ml (2). Lane 3 and 4: single morpholino injections with *dmrt5* splice up (3) and splice down (4) morpholino. Working solutions were both 12.5 mg/ml. The asterisk marks a weak band that represents unspliced *dmrt5* transcripts. Lane 5: uninjected control. Lower bands correspond to spliced *dmrt5* transcripts (922 bp) while upper bands correspond to unspliced *dmrt5* transcripts (1347 bp). Bottom row: Corresponding semi-quantitative PCR results for *gapdh* transcripts used as loading control. B) Quantitative data analysis of *dmrt5* morpholino splice assay using ImageJ. Splice efficiencies were calculated according to intensities of semi-quantitative PCR amplicons after they were normalized against the *gapdh* signal. The numbers above the columns indicate the percentage of unspliced product in relation to total *dmrt5* transcripts.

Both splice site morpholinos were injected in combination. A dose-response study was performed to determine the final morpholino concentration to be used throughout the entire course of the study to exclude possible nonspecific morphological defects. Indicators for nonspecific morpholino mediated effects were an overall altered morphology, delayed development and/or elevated apoptosis, especially in mid- and hindbrain regions. Combined injection of morpholino concentrations up to 3.125 mg/ml (each) did not alter the overall morphology or induce unspecific apoptosis, while morpholino concentration of 6.25 mg/ml or higher induced increased and nonspecific apoptosis in hindbrain regions (data not shown). Based on the high efficiency to block *dmrt5* pre-mRNA splicing and the compatibility with regards to overall morphology, I used injection of combined splice up and down morpholinos at 3.125 mg/ml throughout the course of this study.

Additionally, I was interested over what time periods *dmrt5* splice site morpholinos were active. Thus, wild type zebrafish embryos were injected with splice site morpholinos at 3.125 mg/ml and total RNAs were isolated at 24, 48, 74 and 102 hpf. The splice analysis was carried out as described above (Fig. 15). As shown before, the morpholinos were very efficient in blocking *dmrt5* pre-mRNA splicing during the first 24 hpf when only 8% of detected *dmrt5* transcripts were spliced (Fig. 15). This value increased during the next 50 hours to 51% before the amount of correctly spliced *dmrt5* products again dropped to 15% at 102 hpf. A possible explanation is that the morpholinos get degraded during earlier time

points resulting in an increase in the amount of spliced transcripts. However, after 74 hpf, *dmrt5* transcripts got endogenously down-regulated and the amount of morpholinos left (although less than at the beginning) were sufficient to block splicing of *dmrt5* transcripts effectively. These data suggest, that the injected amount of splice site morpholinos was sufficient to block *dmrt5* pre-mRNA splicing during the time window when the formation of the forebrain takes place.
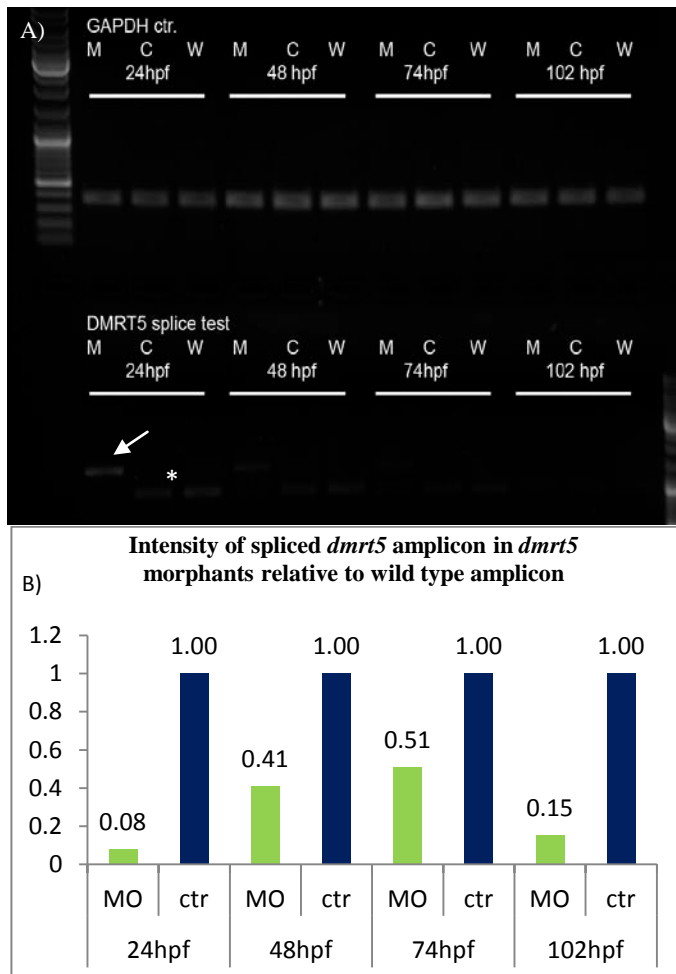
Fig. 15 Analysis of dmrt5 splice-block morpholino stability: Morpholino stability was analysed by scoring the efficiency of *dmrt5* knock-down. A) *dmrt5* mRNA splice assay: Top row: *gapdh* used as loading control for expression at indicated stages. Bottom: Splicing of *dmrt5* pre-mRNA was studied at 24 (lanes1-3), 48 (lanes4-6), 74 (lanes 7-9) and 102 hpf (lanes 10-12). mRNA isolated from: **M:** *dmrt5* morpholino injected, **C:** control morpholino injected, **W:** wild type embryos. Only *dmrt5* morpholino injected embryos showed a higher band, indicative for unspliced *dmrt5* pre-mRNA (arrow) products, while the controls showed only a lower band (*) indicative for the fully spliced *dmrt5* mRNA. Unspliced products: 1347bp, spliced products: 922b. B) Quantitative analysis of *dmrt5* splicing: Intensities of visualized *dmrt5* amplicons were measured using ImageJ and normalized to *gapdh* expression. Splicing of *dmrt5*was calculated in relation to wild type *dmrt5* amplicon intensities. *Dmrt5* pre-mRNA splicing was efficiently blocked at early stages (24 hpf). At 48 and 74 hpf, *dmrt5* pre-mRNA splicing was still impaired yet more spliced *dmrt5* mRNAs were detectable. At 102 hpf: endogenous *dmrt5* levels were very low and calculated variations reflective of experimental limitations.

It is worth mentioning that one of the less-similar BLAST hits was located in the pre-mRNA of *forebrain embryonic zinc finger 2* (*fezf2*) and shared 16/25 nucleotides with the upstream *dmrt5* splice morpholino target site. Moreover, the potential binding site in *fezf2* pre-mRNA was also an exon-intron boundary. Since *fezf2* plays a crucial role during embryonic forebrain

development and its expression overlaps with *dmrt5* expression, the correct splicing of *fezf2* was investigated. For that, I used the same splice assay technique as before but replaced *dmrt5* with *fezf2* primers. Both *fezf2* primers flanked the intron (81bp) of interest allowing us to determine if *fezf2* pre-mRNA was correctly spliced. As illustrated in figure 16, *fezf2* pre-mRNA was properly spliced since no unspliced *fezf2* pre-mRNA products were detected. To confirm the presence of *dmrt5* morpholinos, non-spliced *dmrt5* pre-mRNA was used as positive control.
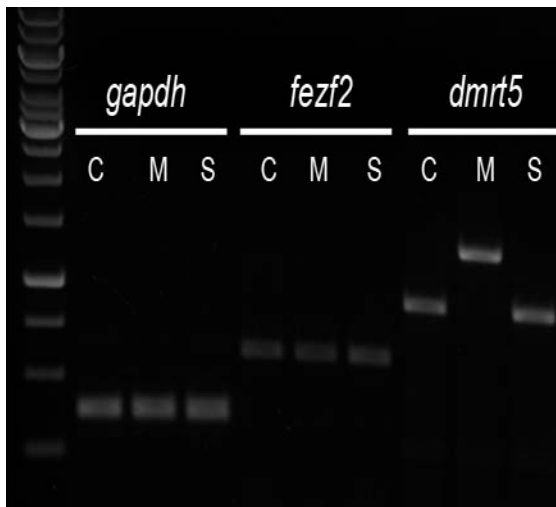
Fig. 16 Morpholino targets dmrt5 but not fezf2 splicing: Splice assays were performed as described before. Lane 1: DNA ladder. Lanes 2-4: loading control *gapdh*. Lanes 5-7: splice assay for *fezf2*. Lanes: 8-10: positive control: *dmrt5*. Only *dmrt5* pre-mRNA showed intron retention upon *dmrt5* morpholino injection, while *fezf2* pre-mRNA was correctly spliced and showed no unspliced transcripts. *fezf2* unspliced products: 705 bp, spliced products: 624 bp. *dmrt5* unspliced products: 1347 bp, spliced products: 922 bp. **M** = *dmrt5* morpholino injected, **S**= control morpholino injected, **C**= wild type embryos

3.3 Gene knock-down identifies roles of *dmrt* genes during forebrain neurogenesis

It was recently shown that the morpholino mediated knock-down of Xenopus *Xdmrt4* resulted in significant down-regulation of *neurogenin* expression in the olfactory placodes (Huang *et al.*, 2005). As a result of the down-regulation of *neurogenin*, *Xenopus* olfactory placode neurogenesis was impaired (Huang *et al.*, 2005). As both *dmrt3* and *dmrt5* are expressed in the zebrafish forebrain, I tested if a knock-down of *dmrt3* and/or *dmrt5* affects *neurogenin* expression in a similar manner in zebrafish. Hence, the embryonic forebrain expression of *neurogenin* was examined in a *dmrt3, dmrt5* and combined *dmrt* knock-down context. Due to concentration limitations in double- morpholino injections, concentrations no higher than 1.6 mg/ml per morpholino were used. Higher doses of *dmrt3* and *dmrt5* morpholino co-injection led to severe developmental delays and in embryonic malformations (data not shown).

Neurogenin expression domains in the forebrain were unaltered in *dmrt3* morphants upon injection of 1.6 mg/ml *dmrt3* splice morpholinos (22/24, Fig. 17 b). This shows that a knock-down of *dmrt3* does not recapitulate results from *Xenopus* studies. Since *dmrt3* expression overlaps completely with the expression domains of *dmrt5,* it is possible that the *dmrt3* knock-down was functionally compensated by Dmrt5. I therefore analysed the *neurogenin* expression pattern in *dmrt5* morphants injected with 1.6 mg/ml *dmrt5* splice morpholinos. 22 out of 26 analysed embryos showed a strong reduction in *neurogenin* expression in the following brain domains: dorsal telencephalon, preoptic area and ventral midbrain (1, 2 and 4b, Fig. 17 c). To test possible synergetic effects on the down-regulation of *neurogenin*, *dmrt3* and *dmrt5* double-morphants (1.6 mg/ml splice site morpholinos each) were analysed. The observed down-regulation of *neurogenin* completely recapitulated the *dmrt5* morphant phenotype (22/27) and showed no synergistic effects after knocking-down both *dmrt* genes (Fig. 17 d). In conclusion, a single knock-down of *dmrt5* was sufficient to reduce *neurogenin* transcription in the forebrain and *dmrt5* morpholino injected embryos displayed similar *neurogenin* expression patterns as double morphants. The knock-down at higher doses (3.125 mg/ml splice site morpholino) recapitulated these results (data not shown).
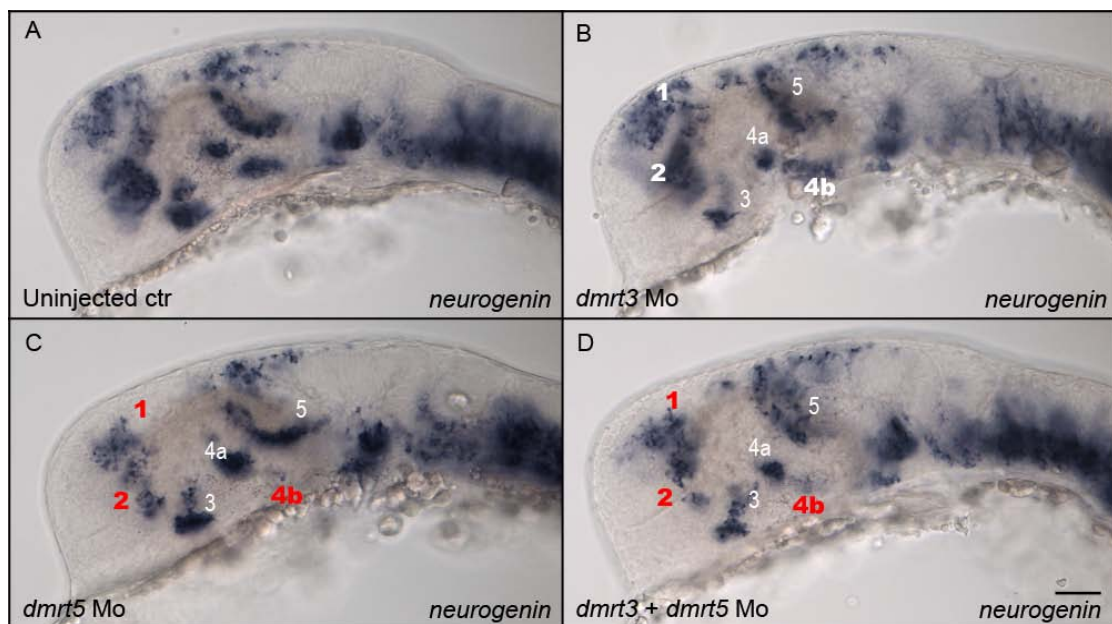
Fig. 17 Neurogenin expression is reduced in dmrt5 but not dmrt3 morphants: Comparison of *neurogenin* expression in forebrain domains after single and double knock-down of *dmrt* 3 and 5 at 24 hpf in lateral view of head regions. While *dmrt3* knock-down embryos showed no change in

neurogenin expression domains throughout the forebrain (B), the knock-down of *dmrt5* (C) resulted in reduced *neurogenin* expression in the dorsal telencephalon (1), the preoptic area (2) and the ventral midbrain (4b). Adjacent *neurogenin* expression domains remained unaffected (3, 4a and 5). *Dmrt3* and *dmrt 5* double morphants (D) recapitulated the reduced *neurogenin* expression as described in *dmrt5* morphants. Used morpholino concentrations were 1.6 mg/ml. Scale bars: 50 µm, letters in red indicate domains with reduced *neurogenin* expression.

The down-regulation of *neurogenin* was restricted to domains that were overlapping with *dmrt5* expression while non-overlapping *neurogenin* expression domains remained unaffected (Fig. 18). Thus, it seems that *dmrt5* and not *dmrt3,* is required for *neurogenin* expression in dorsal telencephalon, olfactory epithelium, preoptic area and ventral midbrain. In addition, when *dmrt5* was knocked-down using *dmrt5* morpholinos alone, the severity of *neurogenin* down-regulation correlated with the amount of unspliced *dmrt5* RNA. Embryos injected with 3.125 mg/ml splice-blocking morpholino showed a slightly stronger *neurogenin* down-regulation than embryos injected with 1.6 mg/ml (data not shown). Based on the fact that concentrations of 3.125 mg/ml *dmrt5* morpholino were sufficient to block *dmrt5* pre-mRNA splicing efficiently, this concentration was used for all following experiments.
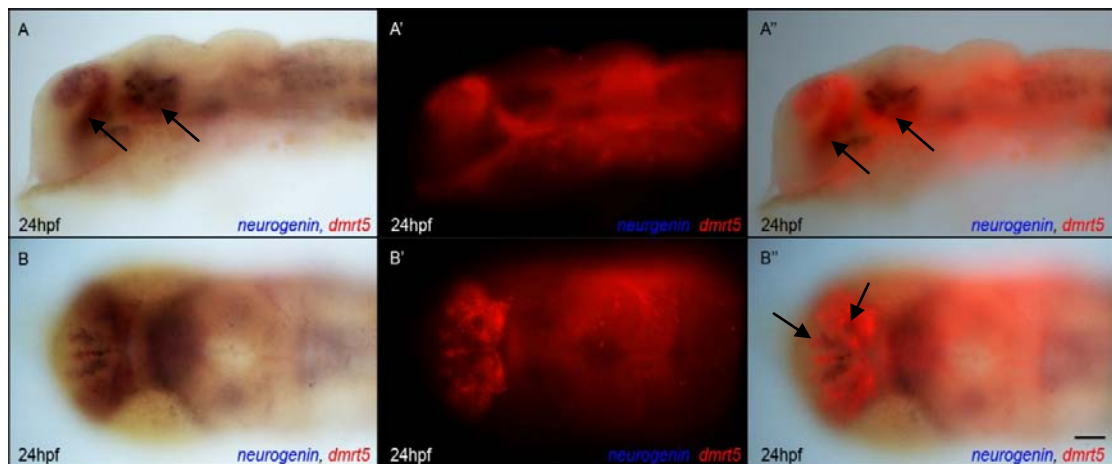
Fig. 18 Overlapping expression domains of dmrt5 and neurogenin at 24 hpf: *Dmrt5* expression domains are shown in red and *neurogenin* in blue. Arrows define overlapping expression domains of both genes A, A' and A": lateral bright field, fluorescence and overlay of both. B, B' and B": dorsal bright field, fluorescence and overlay of both. *Dmrt5* and *neurogenin* expression overlap in dorsal telencephalic, olfactory epithelium, preoptic area and ventral midbrain cell populations. Scale bar: 50 µm.

In order to delineate the epistatic relationship between *dmrt3* and *dmrt5,* the expression of *dmrt5* in *dmrt3* morphants and *vice versa* was analysed. The knock-down of *dmrt3* upon injection of 3.125 mg/ml splice morpholinos did neither increase nor reduce the expression of

dmrt5 (31/31) when compared to wild type (69/69) or *dmrt3* control morpholino injected embryos (43/43, Fig. 19 a-c). The injection of control morpholino was used to exclude the possibility that the observed phenotypes were due to unspecific effects of morpholino injection. On the contrary, knock-down of *dmrt5* upon injection of 3.125 mg/ml splice morpholinos resulted in a loss of telencephalic *dmrt3* transcription (59/59) when compared to wild type (57/57) and *dmrt5* control morpholino injected embryos (43/43, Fig. 19 d-f). Since *dmrt3* is expressed in a subset of *dmrt5* positive cells and is dependent on *dmrt5* expression, these results place *dmrt5* at a higher hierarchical level during forebrain development than *dmrt3*. Whether Dmrt5 regulates *dmrt3* directly at the transcriptional level or whether the down-regulation is a secondary effect due to neurogenesis defects remains unclear at the moment.
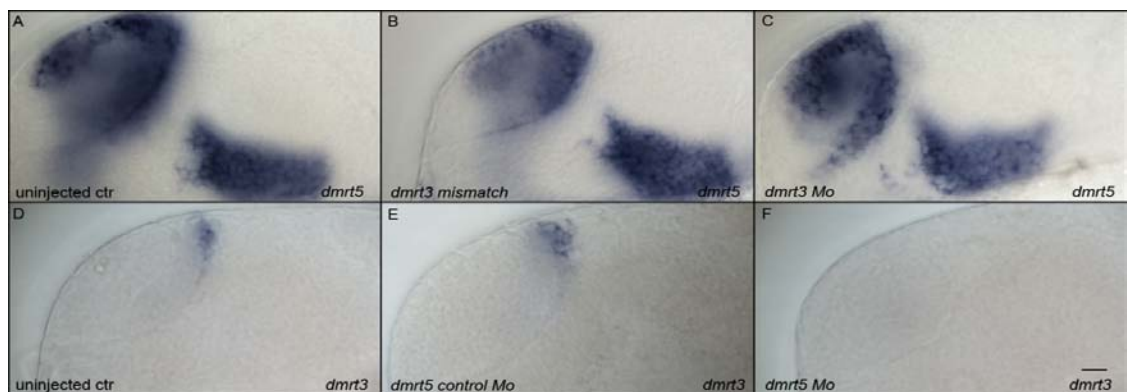
Fig. 19 Revealing epistatic hierarchies between dmrt3 and dmrt5: *Dmrt5 expression was analysed in dmrt3 morphants and vice versa. A-C: Examination of dmrt5 transcription after dmrt3 knock-down. No alterations were observed between controls (A/B) and dmrt3 morpholino injected embryos (C). D- F: Knock-down of dmrt5 in contrast resulted in a complete loss of dmrt3 expression while controls were unaffected. Used morpholinos are mentioned in the lower left-hand corner of each image. Lateral views, anterior to the left. Scale bar: 20 µm.*

Taken together, *dmrt3* is expressed in a small subset of *dmrt5* positive cells in the dorsal telencephalon and a *dmrt3* knock-down had no visible effect on *neurogenin* transcription. Moreover, its expression is dependent on *dmrt5* expression yet it is not known if *dmrt3* expression is regulated directly by Dmrt5 or if Dmrt5 regulates other processes that lead to *dmrt3* regulation. Moreover, my data show that *dmrt5* apparently has roles in multiple regions of the forebrain through the regulation of *neurogenin* expression. Therefore, follow-up studies were designed to further understand *dmrt5* and its role during embryonic brain development.

3.4 Role of *dmrt5* for dorsal telencephalon, olfactory region and pituitary development

The data obtained above revealed that a reduction of Dmrt5 altered *neurogenin* expression in the a) dorsal telencephalon, b) olfactory region, c) pituitary, d) preoptic area and e) ventral midbrain. Potential neurogenesis defects in these regions were scrutinized. Furthermore, the expression of genes known to be involved during neurogenesis was analysed to resolve the position of *dmrt5* in neuro-regulatory gene cascades. The following subsections elaborate on the differentially modulated gene expression patterns in wild type and *dmrt5* morphant embryos. The concentration of injected *dmrt5* splice site morpholinos was kept at 3.125 mg/ml unless stated otherwise. To focus on the main changes seen in morphants, images of control morpholino injected embryos are shown in the Appendix.

3.4.1 *Dmrt5* knock-down results in dorsal telencephalic differentiation defects

Firstly, expression of proneural genes other than *neurogenin* was analysed to determine if the transcriptional regulatory defects were only limited to *neurogenin* or if *dmrt5* morphants show a general effect on proneural gene expression. Expression of *neuroD*, *zash1a* and *zash1B* was analysed in the dorsal telencephalon (Fig. 20). *NeuroD* is expressed throughout the whole dorsal telencephalon (Fig. 20 c) while *zash1b* is only expressed in cell populations of the anterior telencephalon and lateral ventricle walls (Fig. 20 e). In *dmrt5* morphant embryos, *neurogenin* expression was strongly down-regulated in the dorsal telencephalon, yet the expression was not completely gone (20/20, Fig. 20 b). In contrast, *neuroD* (31/31; 29/29 in *dmrt5* morphants injected with a morpholino concentration of 1.6 mg/ml) and *zash1b* (37/41), expression was almost completely absent in the dorsal telencephalon of *dmrt5* morphants (Fig. 20 d/f). Additionally, although only weakly expressed in dorsal telencephalic regions of wild type embryos, I also observed a down-regulation of *zash1a* in *dmrt5* morphants (34/35) when compared to wild type embryos (data not shown). TUNEL staining was performed to determine if the lack of *neurogenin* expressing cells was due to increased apoptosis, however this was not the case as the embryos did not show elevated apoptosis in dorsal telencephalic regions at this stage (see page 78, Fig. 28). The observed phenotype was also not rescuable by

p53 morpholino co-injection, which confirms that the detected defects are specific for the *dmrt5* knock-down (data not shown).
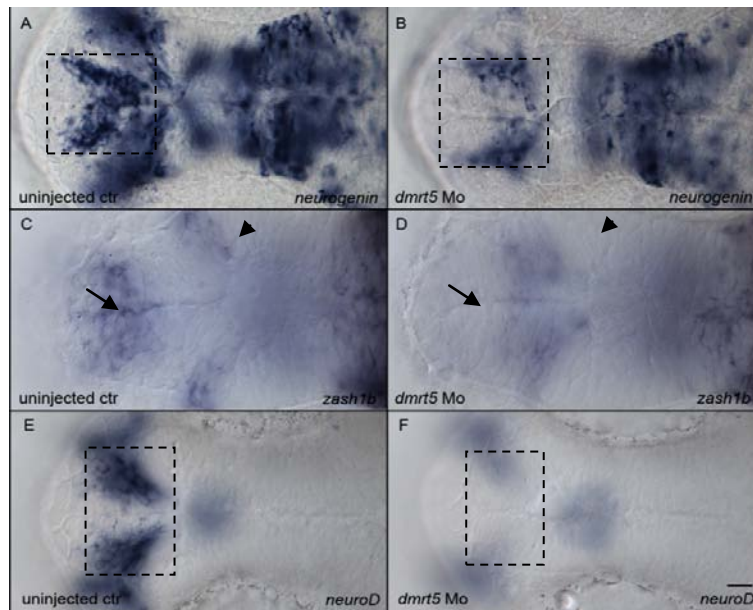
Fig. 20 Knock-down of dmrt5 leads to down-regulation of proneural genes zash1b and neuroD: Expression of *neurogenin* (A/B); *zash1b* (C/D) and *neuroD* (E/F) in the dorsal telencephalon of wild type and *dmrt5* morphants at 25 hpf. In wild type embryos (A/C/E), dominating proneural genes expressed in this area were *neurogenin* and *neuroD (*boxed areas*)*, while *zash1b* was expressed only in the anterior-most part of the telencephalon (arrow) and lateral ventricle walls (arrow head). All tested proneural genes were down-regulated in *dmrt5* morphants (B/D/F). Dorsal views, anterior to the left. Scale bar: 20 μm.

As the expression levels of several proneural genes were found to be down-regulated, neuronal differentiation and specification processes were evaluated through the expression pattern of the post-mitotic neuronal marker, HuC/D and telencephalic markers, *fezf2* and *pou50*. In wild type embryos, *fezf2* and *pou50* genes are expressed in a broad spectrum of neuronal cells as well as a subset of dorsal telencephalic neurons (black arrows, Fig. 21 c/e). These cell populations are believed to be post-mitotic since their expression domains overlap with HuC/D. In *dmrt5* morphants, HuC/D signals were reduced in all tested embryos (n= 5) when compared to wild type embryos (white brackets, Fig. 21). Additionally, *fezf2*$^{+}$ (20/20) and *pou50*$^{+}$ cell populations were absent in the dorsal telencephalon of *dmrt5* morphants (Fig. 21). The down-regulation of *fezf2* was not rescuable by co-injection with a p53 morpholino (37/37) indicating specificity of this defect, while *pou50* expression was not tested in *dmrt5/ p53* double morphants. These data show that *dmrt5* morphants portrayed an impaired neuronal differentiation defect in telencephalic neurons most likely caused by the lack of proneural gene expression.
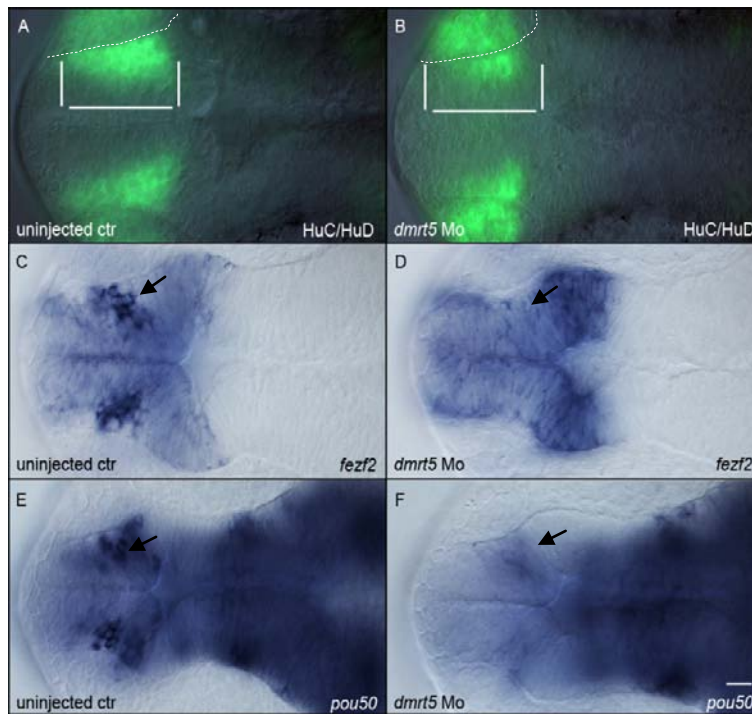
A/C/E: wild type embryos. B/D/F: *dmrt5* morphants. Presence of neuronal differentiation in wild type embryos as indicated by HuC/D signals in the dorsal telencephalon (A). The same white bracket as shown in A is superimposed in B to illustrate the lack of post-mitotic neurons in *dmrt5* morphants. Only a small population of cells within this post-mitotic cell cluster express *fezf2* or *pou50* indicating a loss of differentiated neurons (arrows, D/F). Dorsal views, anterior to the left side. Scale bar: 20 µm. Dashed line: boundary to olfactory epithelium.

Next, I tested the expression of *her* genes, to determine if Dmrt5 regulation of proneural gene expression occurs through direct or indirect means. The family of *her* genes encodes inhibitors of proneural gene transcription and consequently prevents neuronal differentiation. Therefore, telencephalic and diencephalic *her* gene expression was analysed to test for possible ectopic gene expression. In wild type embryos, the two *her* genes *her4.1* and *her15.1* are expressed around the ventricular surfaces in dorsal telencephalic regions (boxed areas, Fig. 22 c/e). In contrast to *her4* and *her15*, *her6* is not expressed in the dorsal telencephalon of wild type embryos (arrow, Fig. 22 a) and is only expressed in a small population of anterior telencephalon cells (asterisk, Fig. 22 a) and diencephalic expression domains. In *dmrt5* morphants on the other hand, endogenous expression of *her4.1* (39/40) and *her15.1* (85/94) were diminished. Interestingly however, the diencephalic *her6* expression domain extended into the dorsal telencephalon (44/45, p53 co-injection: 39/39). It is known that *her6* acts as transcriptional repressor of proneural genes (Scholpp *et al.*, 2009); hence its ectopic up-regulation can explain the previously described reduction of proneural gene expression. Consequently, neuronal differentiation processes are impaired and numbers of post-mitotic (HuC/D) and differentiated (*fezf2/pou50*) neurons are strongly reduced.
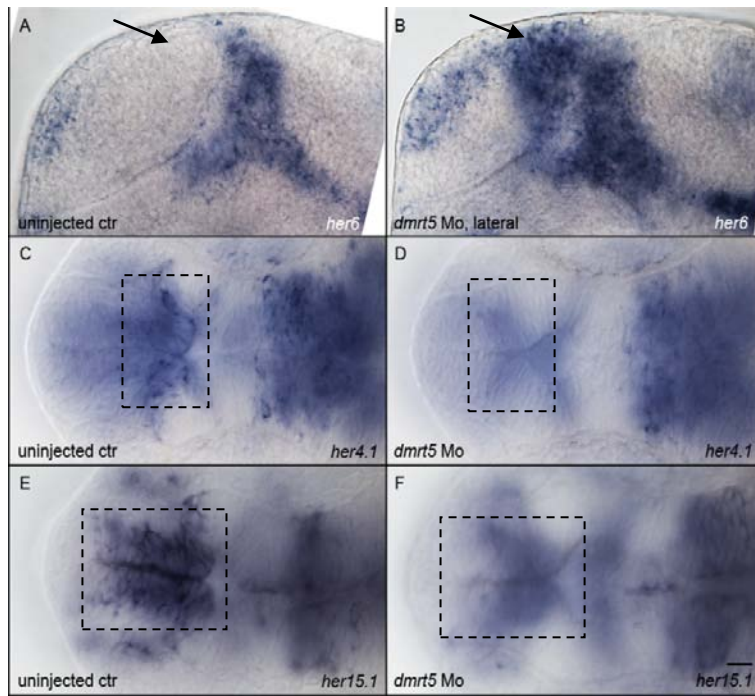
Fig. 22 The knock-down of dmrt5 affects her gene expression in the telencephalon: her genes *6, 4.1* and *15.1* displayed altered expression patterns upon *dmrt5* knock-down. *Her6* was ectopically expressed and expanded from its original diencephalic expression domain into the dorsal telencephalon (arrows, A/B). *Her* genes *4.1* and *15.1,* which are normally expressed in the dorsal telencephalon (boxed area), were strongly down-regulated in morphants compared to wild type embryos (C-F). A/B are lateral views while C-F are dorsal views. Anterior is to the left. Scale bar: 20 μm.

Given that *her* genes are upstream of proneural genes, up-regulation of *her6* explains the observed neuronal differentiation defects in the dorsal telencephalon of *dmrt5* morphants. Moreover, the observed expression changes of *her4.1* and *her15.1* can also be explained by the ectopic up-regulation of *her6*. *Her6* expression starts in the neuroectoderm and gets down-regulated to restricted expression domains, for example the mid-diencephalic boundary (Pasini *et al.*, 2001; Scholpp *et al.*, 2009). It seems that the down-regulation of *her6* is a pre-requisite for neuronal specification and differentiation and that the observed ectopic expression of *her6* is maintained from earlier stages. The findings in *dmrt5* morphants are in accordance with findings in mouse, where it has been shown that the *her6* homologue *Hes1* is earlier expressed than the *her4* homologue *Hes5* (Kageyama *et al.*, 2008). This supports the idea that different *her* genes may label different stem cell populations. The ectopic up-regulation of *her6* could indicate that early stem cell populations are maintained in their early state and fail to develop into more differentiated *her4/her15*[+] stem cell/progenitor populations.

3.4.2 The knock-down of *dmrt5* leads to the maintenance of very early neural stem cell populations

To test the possibility that the *dmrt5* knock-down influences neural stem cell development, I analysed expression of marker genes for different neural stem and progenitor populations. At first, the expression of *notch* genes was examined. Notch proteins are known to be positive regulators of *her* gene expression (Takke *et al.*, 1999; Hatakeyama *et al.*, 2004). Hence, possible alterations in endogenous *notch* expression could explain the observed transcriptional changes of *her* genes. Therefore, dorsal telencephalic expression of *notch3* was analysed in controls and morphants. In wild type embryos, *notch3* transcripts are detectable in cell populations restricted to the ventricular zone and ventricle wall and label putative radial glia populations (arrow, Fig. 23 a). *Notch3* expression overlaps completely with that of *her4* and *her15* (Fig. 22 c/e and Fig. 23 a). Both *her* genes are thought to be transcriptionally regulated by Notch3. This hypothesis is consistent with findings in *dmrt5* morphants, where *notch3* transcripts were absent from the dorsal telencephalon (37/40) as well as the expression of both *her4.1* and *her15.1* genes. The ectopic *her6* expression upon knock-down of *dmrt5* indicates that the underlying regulatory transcriptional mechanisms are independent from Notch signalling. This is in accordance with mouse data that showed that telencephalic expression of the homologue of *her6* (*Hes1*) is insensitive to Notch signalling (Hatakeyama *et al.*, 2004).

In addition, Notch-signalling has also been reported to be involved in radial glia maintenance (Yoon *et al.*, 2008; Chapouton *et al.*, 2010). Since a down-regulation of Notch-signalling components was observed, a reduced number of radial glia cells was expected. Thus, neural radial glia markers, *blbp* and *gfap* were investigated in wild type and *dmrt5* knocked-down embryos (Fig. 23). In wild type embryos, both markers are expressed in dorsal telencephalic cell populations and label probably distinct radial glia populations that also express *notch3, her4* and *her15 (*Fig. 22/23*)*. In contrast, in *dmrt5* morphants the radial glia markers, *gfap* (39/42) and *blbp* (72/74), were absent from the telencephalic ventricular zones (Fig. 23 f/h). This suggests that these radial glia populations were not formed in *dmrt5* morphants. It seems

that Dmrt5 is required for the formation of radial glia populations from very early neural stem cell populations and that the loss of Dmrt5 results in the prolonged maintenance of early neural stem cell populations.
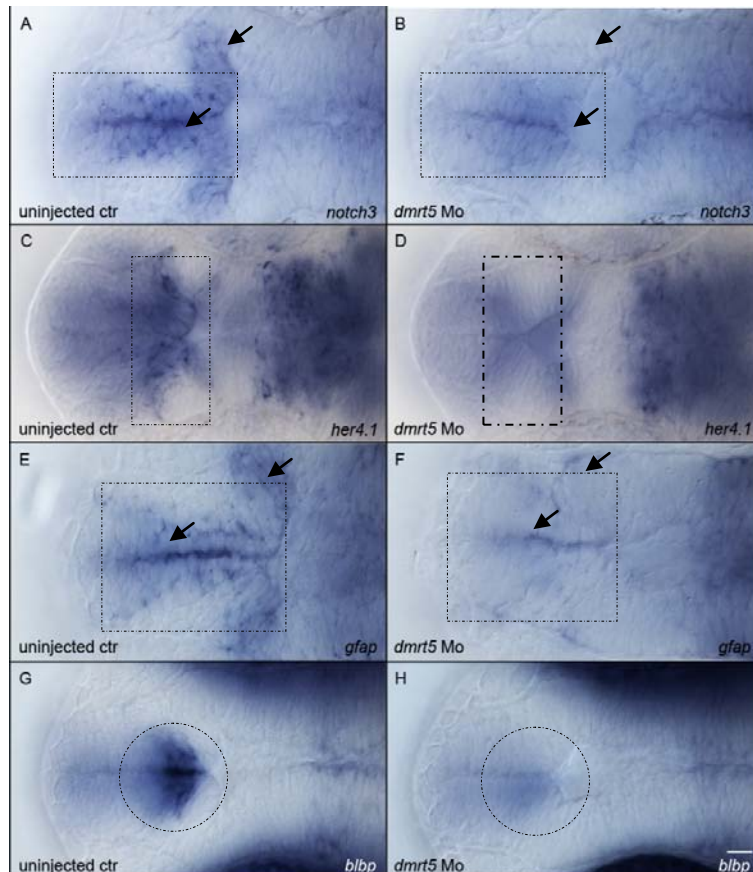
Fig. 23 Dmrt5 knock-down results in reduced radial glia pools: Expression analysis of *notch3* (A/B), *her4.1* (C/D), *gfap* (E/F) and *blbp* (G/H) expression. A/C/E and G: wild type embryos at 25 hpf. Images B/D/F and H show *dmrt5* morphants at the same stage. As a consequence of the *dmrt5* knock-down, radial glia populations are not formed and marker expression was missing. Morphants showed strongly reduced *notch3* (B), *her4.1* (boxed, D), *gfap* (F) and *blbp* (H) transcription. Dorsal views of 25 hpf embryos, anterior is to the left. Scale bar: 20 µm.

To address the question if the down-regulation of *dmrt5* leads to increased numbers of early neural stem cells, expression of early neural markers *sox2* and *pax6a* was analysed. In wild type embryos, both genes are expressed at low levels in few cells of the telencephalon (*pax6a*: out of focus; *sox2*: arrows, Fig. 24). Conversely, *dmrt5* morphants showed expanded *pax6a* expression from diencephalic domains into the dorsal telencephalon (30/30, Fig. 24) and the ectopic up-regulation of *sox2* expression (36/37, Fig. 24). The ectopic *sox2* and *pax6a* expression patterns overlapped completely with ectopic *her6* expression and supported the idea that early neural stem cell populations were maintained in *dmrt5* morphants. This suggests that Dmrt5 activity is required for the switch of early neural stem cells to neurogenic active *notch3$^+$/her4$^+$/blbp$^+$* or *gfap$^+$* radial glia cells. Without this switch, neuronal

differentiation processes are blocked and neither radial glia nor terminally differentiated neurons are formed.
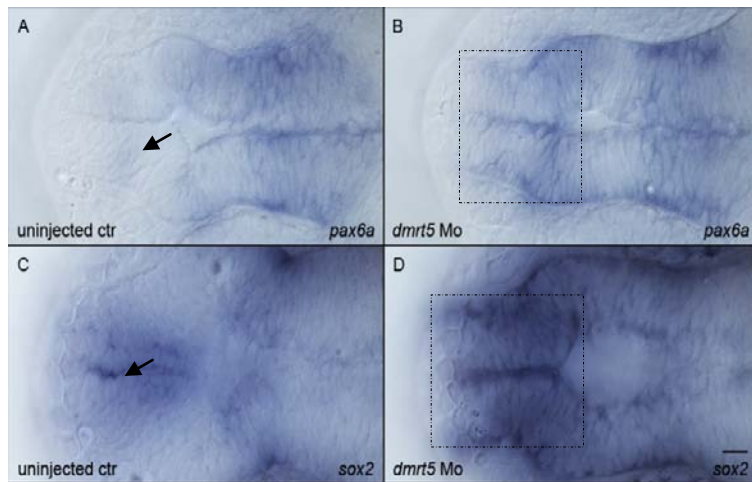
Fig. 24 Knock-down of dmrt5 results in ectopic pax6a and sox2 expression: Wild type embryos express only low levels of *pax6a* and *sox2* in dorsal telencephalic brain domains (arrows, A/C). *Dmrt5* morphants showed ectopic telencephalic up-regulation of both genes (boxed areas, B/D). Dorsal views, anterior to the left. Scale bar: 20 µm.

Lastly, I analysed the size of the telencephalon in embryos stained for *shh* and *krox20*. *Shh* is expressed in the floor plate, the ventral diencephalon in the anterior forebrain and close to the forebrain-midbrain boundary (arrow heads, Fig 25). The expression domain close to the forebrain-midbrain boundary is also referred to as *zona limitans intrathalamica: zli*. *Krox20* is expressed in rhombomeres 3 and 5 and its expression does not overlap with *dmrt5* (arrow, Fig. 25). A knock-down of *dmrt5* was not expected to influence the position of the *krox20* staining, which was used as an internal landmark. I measured the length of the most anterior *shh*-expression domain to the forebrain-midbrain boundary and the length from there to rhombomere 3 in wild type (n=9) and *dmrt5* morphant embryos (n=20). By analysing the size ratios of anterior versus posterior head regions, I was able to exclude that the general brain structure was changed. The ratios between anterior to posterior head region were not significantly different between wild type and *dmrt5* morphant embryos ($p_{dmrt5Mo- wt} = 0.27$, Fig. 25 a/b'). This finding implicates that the general brain structure was unaltered. Additionally to the general brain structure, I evaluated if the forebrain itself was changed in *dmrt5* morphants. To evaluate this, I was using the unchanged *shh*-expression domain close to the forebrain-midbrain boundary (arrow, Fig. 25 a''/b'') as well as the recess between the telencephalon and diencephalon (dotted line, Fig. 25 a''/b'') as internal landmarks. The measured average distance between both landmarks was 22.9 µm in wild type embryos and around 57.7 µm in

dmrt5 morphants (Fig. 26 a). The telen-/ diencephalon boundary was shifted anteriorly due to a decreased size of the dorsal telencephalon, while the location of the *shh*-expression domain was unchanged. The increase in distance was considered to be extremely significant ($p_{dmrt5Mo-wt}= 5.5E^{-10}$). This shows that *dmrt5* morphant telencephala are significantly smaller than in wild type embryos probably because of the previously described effects on neuronal stem and progenitor cells. To confirm that adjacent midbrain structures were unaffected, dorsal *wnt1* expression was scrutinized. The *wnt1* expression domain in the dorsal midbrain was not significantly changed between control embryos and *dmrt5* morphants ($p_{dmrt5Mo- wt}= 0.38$, Fig. 25 c/d and Fig. 26 b). This and the unchanged ventral midbrain expression domain of *shh* (Fig. 25 a'/b') showed that effects caused by the knock-down of *dmrt5* were restricted to the forebrain and didn't affect other brain regions.
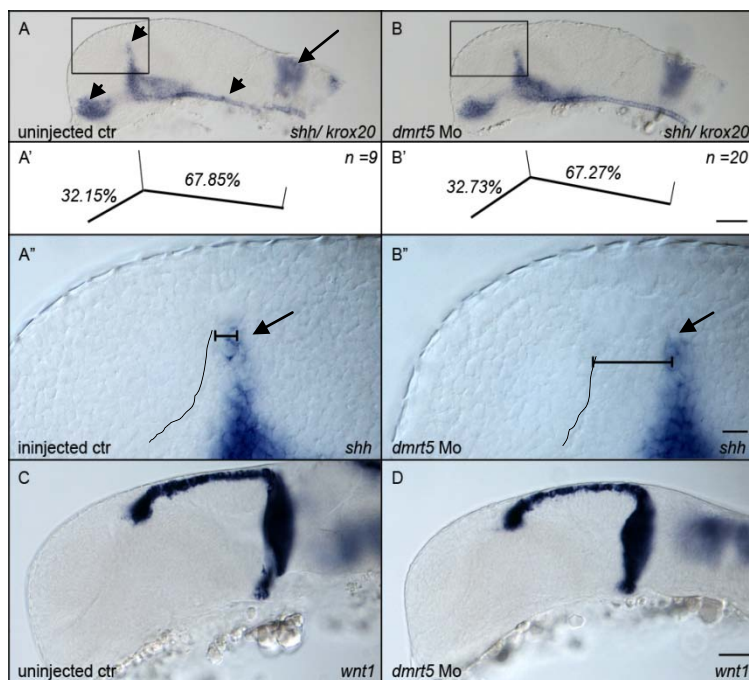
Fig. 25 dmrt5 morphants have smaller telencephala consistent with neuronal stem cell depletion: A-B'': A double *in-situ was carried out to* visualize *shh* (arrowhead) and *krox20* (arrow) expression. Boxed areas in A and B are the same areas as shown in A''/B''. A'/B': Schematic drawing of *shh/ krox20* expression domains observed in wild type and *dmrt5* morphants. Numbers shown are the average ratios between anterior (pituitary to forebrain-midbrain boundary) and posterior (forebrain-midbrain boundary to rhombomere 3) *shh*-expression domain. n $_{wt}$ = 9; n$_{dmrt5Mo}$ = 20. Close-up images A''/B'': observed distances between the telencephalon/diencephalon boundary and the ventral *shh*-expression domain adjacent to the *zona limitans intrathalamica* (ZLI). Can you increase the contrast here, so that boundary becomes more visible. C/D: Dorsal midbrain structures were stained for *wnt1* expression and to evaluate if *dmrt5* morphants show size differences in the midbrain. The length of the dorsal *wnt1* expression domain was measured and showed no differences between *dmrt5* morphants and controls. n= 9. Embryos are 24 hpf. Lateral views, anterior to the left. Scale bars: A-B': 100 µm, A''/ B'': 20 µm and C/D: 50 µm.
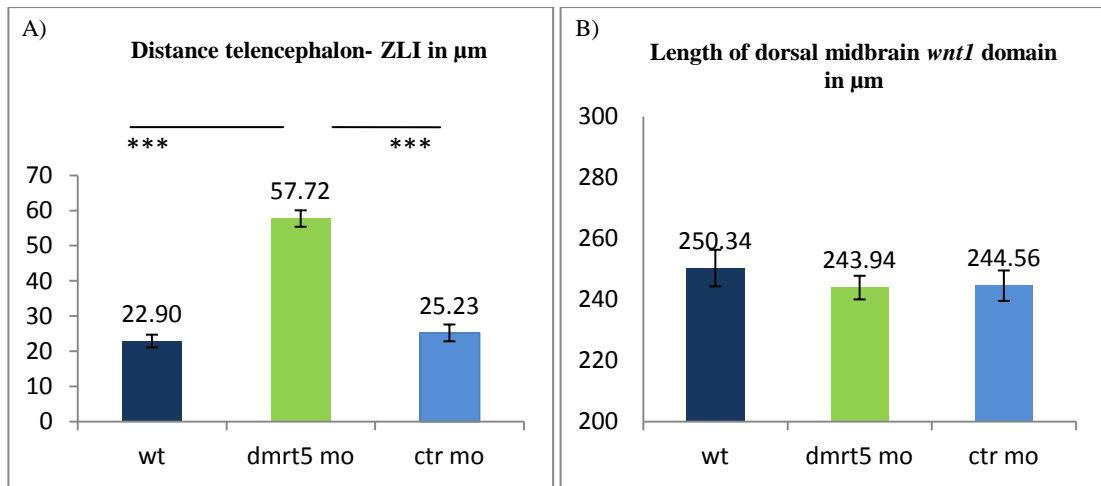
Fig. 26 Statistical analysis of measured distances in dmrt5 morphant and control embryo brains: A) Comparison of the measured distances between telen-/ diencephalon boundary to *shh*-stained ZLI expression domain as shown in figure 36 A"/B". *Dmrt5* morphants showed a significant increase in the distance. P-values: ***< 0.001, $p_{dmrt5Mo- wt}$= 5.5E^{-10}; $p_{dmrt5Mo-ctr\,mo}$= 7.3E^{-10}. n_{wt}= 9; $n_{dmrt5mo}$= 20, $n_{ctr\,mo}$= 11. B) Measured length of the dorsal midbrain as indicated by *wnt1* expression. No significant changes were observed between morphant and control embryos. n= 9.

In summary, *Dmrt5* seems to be an important regulator of dorsal telencephalic neurogenesis as it appears to control the timing and process of neural stem cell differentiation from early stem cells to more differentiated and neurogenic radial glia pools. The lack of neurogenic radial glia also explains the reduced numbers of differentiating and differentiated neurons.

3.5 Dmrt5 is required for stem cell survival and neuronal differentiation in the olfactory system:

Dmrt5 expression starts at the bud-stage in the forming pre-placodal olfactory fields (see page 57, Fig 11 c/c') and is maintained in olfactory epithelia as observed at 24 hpf and 52 hpf (see page 57, Fig. 11 e'), however with reduced expression levels after 52 hpf. Since I observed neuronal differentiation defects in the dorsal telencephalon where *dmrt5* expression overlaps with *neurogenin* expression, I also scrutinized proneural gene expression in olfactory epithelia. For that *neurogenin*, *neuroD* and *zash1a* expression was analysed by RNA *in-situ* hybridization in wild type and *dmrt5* morphant embryos at 25 hpf. At this stage *neurogenin* is only expressed in a few cells of the olfactory epithelium (arrow head, Fig. 27 a), while *neuroD* is expressed throughout the epithel (Fig. 27 e). *Zash1a* is expressed at the lateral edges of the olfactory epithel in a crescent like shape (Fig. 27 c). Similar to the situation in the

telencephalon, *neurogenin* (20/20) and *zash1a* (34/35) expression were down-regulated in morphants (Fig. 27 b/d). However, olfactory *neuroD* transcription was only slightly down-regulated (31/31 and 29/29 in *dmrt5* morphants injected with a morpholino concentration of 1.6 mg/ml, Fig. 27 f) and none of the *dmrt5* morphants showed a complete absence of *neuroD* transcripts. In addition, it is not clear if the observed reduction of *neuroD* expression was a direct consequence of the *dmrt5* knock-down or an indirect consequence of the reduced size of olfactory epithelia. Embryos at this stage showed slightly smaller olfactory epithelia which could explain the observed effects for olfactory *neuroD* expression.
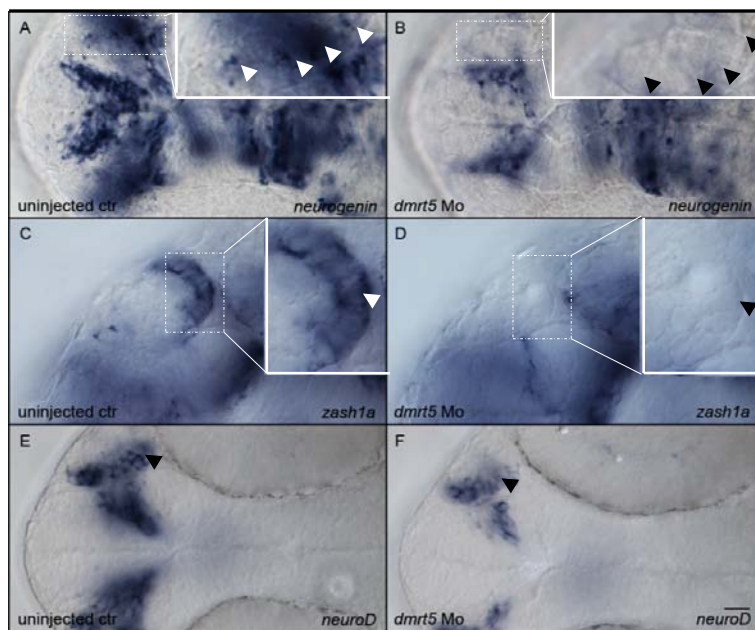
Fig. 27 Proneural gene expression is reduced in the olfactory placode of dmrt5 morphants: Expression of proneural genes *neurogenin* (A/B) and *zash1a* (C/D) were down-regulated in *dmrt5* morphants (B/D). Insets are close-up images of affected cells. *NeuroD* expression was slightly reduced but still present in morphants and may represent the reduced size of the olfactory epitehlium (E/F). A/C and E: wild type embryos; B/D and F: morphant embryos. Wild type domains that are affected in *dmrt5* morphants are marked with arrowheads. Embryos were at 25 hpf. Dorsal views, anterior to the left. Scale bars: 20 µm

Neurogenin and *zash1a* were down-regulated in the telencephalon and the olfactory epithelium. Contrary, *neuroD* expression was strongly down-regulated in the telencephalon but only mildly affected in the olfactory epithelium. This suggests that the underlying mechanisms controlling proneural gene expression may be different between both regions. Therefore, expression analysis of all previously tested telencephalic genes were expanded to the olfactory epithelium to test for potential changes in transcriptional networks that control neurogenesis. There were no apparent transcriptional changes detected in *sox2, notch3, her6 and pax6a*, genes that are considered to be responsible for the phenotypical changes observed in the *dmrt5* morphant telencephalon (data not shown). This finding confirms that

neurogenesis regulatory networks or the function of *dmrt5* in these networks are different between distinct brain regions.

However, since *dmrt5* morphants showed reduced proneural gene expression in the olfactory epithelium, I analysed if the lack of proneural gene expression may affect cell survival of undifferentiated stem- or progenitor cells in the developing nose. For that, apoptosis was examined by TUNEL-staining in wild type, control morpholino, control morpholino plus *p53* morpholino, *dmrt5* morpholino and *dmrt5* plus *p53* morpholino injected embryos at 24 hpf (Fig. 28). The concentration of *dmrt5* splice site morpholinos and control morpholinos was 3.125 mg/ml and the concentration of the p53 morpholino was 5 mg/ml. Wild type embryos were weakly stained and barely showed any apoptosis across the forebrain (4/5, Fig. 28 a). TUNEL staining of control morpholino injected embryos showed markedly increased unspecific apoptosis throughout the mid- and hindbrain (boxed area, Fig. 28 b/b') but importantly not in the olfactory epithelium (4/5). Apoptosis in the mid- and hindbrain was completely rescued by co-injection with *p53* morpholino indicating that the increase in apoptosis was caused by unspecific morpholino effects. On the other hand, *dmrt5* morphants showed extensive apoptosis in olfactory epithelium (4/5). The increase in olfactory apoptosis could not be rescued by *p53* morpholino co-injection, demonstrating that olfactory epithelium apoptosis was due to the *dmrt5* knock-down (4/5, Fig. 28 c/c').
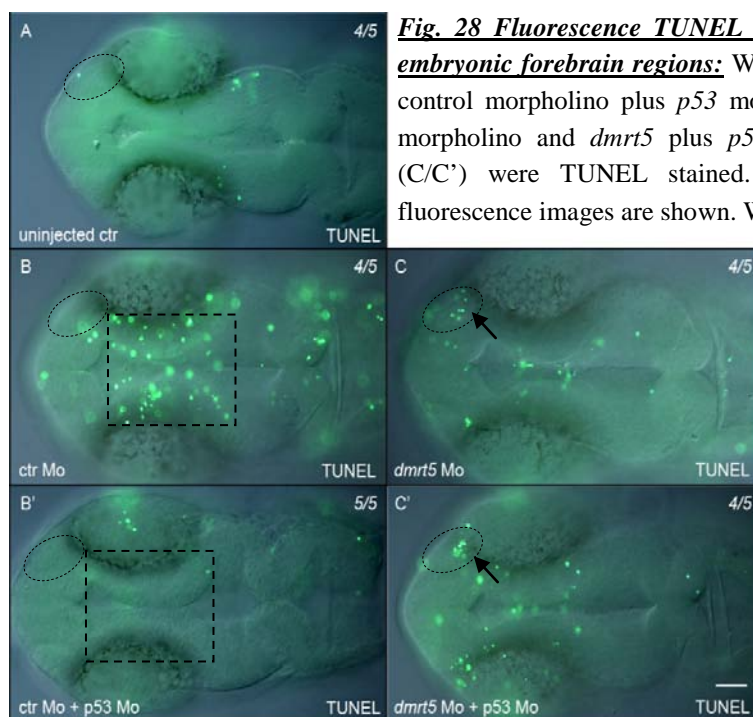
Fig. 28 Fluorescence TUNEL assays to visualize apoptosis in embryonic forebrain regions: Wild type (A), control morpholino, control morpholino plus *p53* morpholino injected (B/B'), *dmrt5* morpholino and *dmrt5* plus *p53* morpholino injected embryos (C/C') were TUNEL stained. Overlay of bright field and fluorescence images are shown. Wild type embryos showed barely any apoptosis in the forebrain. B) Control morpholino injected embryos showed unspecific apoptosis in mid- and hindbrain regions (boxed) that could be rescued by p53 morpholino co-injection (B'). C) Contrary, *dmrt5* morphants showed only little apoptosis in the midbrain but increased apoptosis in the olfactory epithelium (circled area, arrow). C') Olfactory epithelium apoptosis couldn't be rescued by *p53* morpholino co-injection. Scale bar: 50µm.

In addition to 24 hpf, apoptotic events were also examined at 31 and 48 hpf. At 31 hpf, apoptosis in olfactory epithelia was still significantly increased in *dmrt5* and *dmrt5/ p53* co-injected morphants compared to controls (Fig. 29 a). At 48 hpf, apoptosis in developing olfactory regions was still slightly elevated in *dmrt5* morphants when compared to controls although this increase was not significant (Fig. 29 b).
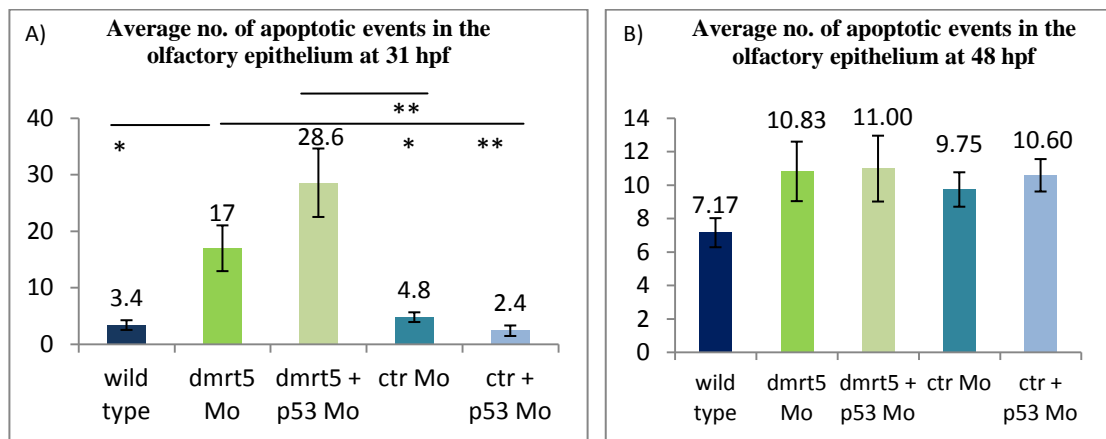
Fig. 29 Average number of apoptotic events in the olfactory epithelium: Average number of apoptotic events measured in the developing olfactory epithelium at 31 hpf and 48 hpf. A) Apoptosis was significantly increased at 31 hpf in *dmrt5* morphants in comparison to the used controls. n= 5 B) At 48 hpf, apoptotic levels in *dmrt5* morphants were comparable to those observed in wild type embryos. *Dmrt5* knock-down induced apoptosis was not rescuable by *p53* morpholino co-injection. n= 4-6. An unpaired t-test was used to calculate p-values. P-values: * < 0.05; ** p< 0.01.

As proneural gene expression was reduced and neuronal differentiation pathways may potentially be impaired in *dmrt5* morphants, I next tested if apoptotic cells had the identity of undifferentiated neuronal stem- and/or progenitor cells. This was done by labelling control and *dmrt5* morpholino injected embryos with BrdU that labels proliferative cells in S-phase or anti-pH3 antibodies, which marks dividing stem- and progenitor cells in M-phase. Based on the BrdU or pH3 labelling, the numbers of dividing cells in wild type and control morpholino as well as *dmrt5* morpholino injected embryos were determined. All tested control embryos (wild type and control morpholino injected embryos) displayed a crescent-shaped BrdU domain along the edges of the olfactory epithelium (Fig. 30 a/a'). This illustrated that embryos were rich in proliferative olfactory stem- and/or progenitor cells at 24 hpf. In contrast, *dmrt5* morphants lacked BrdU staining (Fig. 30 b/b') indicating that the number of

proliferating cells was reduced and suggesting that the identity of apoptotic cells were that of non-differentiating olfactory stem-/progenitor cells.
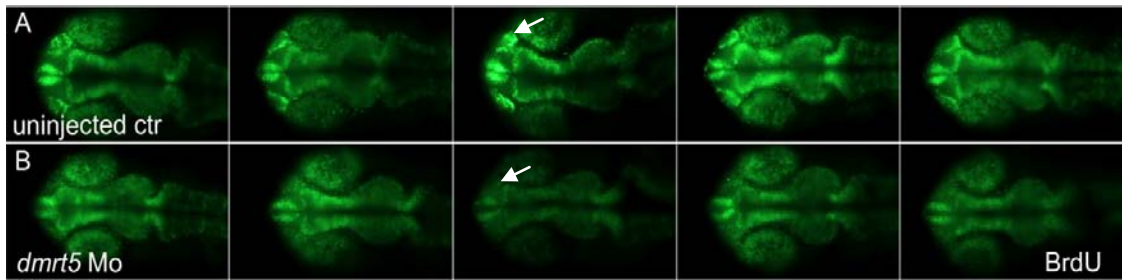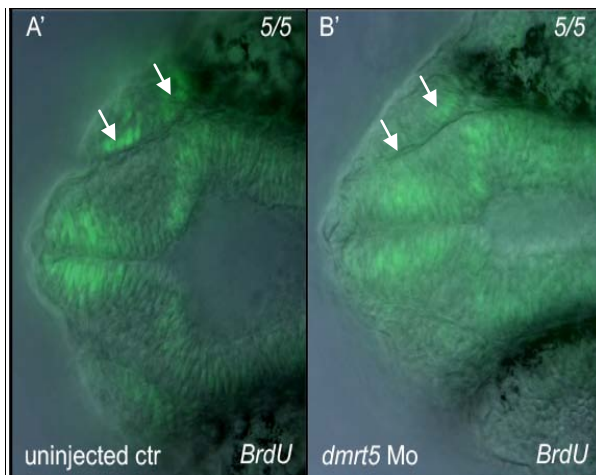
Fig. 30 BrdU labelled uninjected wild type and dmrt5 morphants: Examples of wild type (A) and *dmrt5* morpholino injected embryos (B), stained with BrdU and fixed at 24 hpf. *Dmrt5* morphants had reduced numbers of BrdU labelled olfactory stem and/or progenitor cells (arrow). Dorsal view, anterior to the left. A'/ B': Comparison of wild type and *dmrt5* morphants at higher magnification. Compared to wild type embryos, fewer BrdU labelled cells were detected along the edges of olfactory epithelia (arrowhead). Overlay of bright field and fluorescence images. Dorsal views, anterior to the top.

Furthermore, control and *dmrt5* morphant embryos were analysed for phospho-Histone3, which labels proliferative stem-/ progenitor cells (Fig. 31). When compared to control embryos, *dmrt5* deficient embryos showed a significant reduction in $pH3^+$ cells in the olfactory region. Numbers of cells counted positive for pH3 were reduced from 26.3_{wt}/ 27.6_{ctrMo} to 19.3 in *dmrt5* morphants ($p_{dmrt5Mo-wt} = 0.0149$; $p_{dmrt5Mo-ctr\ Mo} = 0.0002$, Fig. 31). Based on the observation that both markers for dividing stem and/or progenitor cells were reduced while apoptotic rates were increased in olfactory epithelia of *dmrt5* morphants, I suggest that undifferentiated olfactory stem and/or progenitor cells initiated programmed cell death upon *dmrt5* knock-down.

Average number of pH3$^+$ cells in olfactory vesicles

wild type: 26.3 *
dmrt5 morphant: 19.3
ctr morphant: 27.6 ***
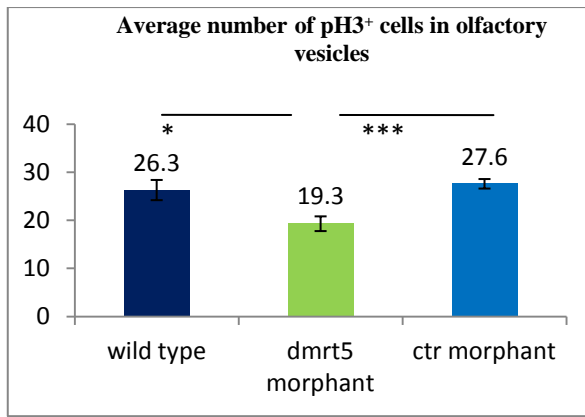
Fig. 31 Numbers of pH3$^+$ cells in olfactory regions of 24 hpf embryos: Numbers of pH3$^+$ cells in control- (wild type or control morpholino injected) and *dmrt5* morpholino injected embryos. Cell counting was performed as a blind study where five embryos from each sample set were randomly selected. A significant down-regulation of pH3$^+$ cells in the morphants could be detected. P-values were calculated using unpaired t-test. *= p< 0.05; ***= p< 0.001. n=5

Interestingly, at later stages I also detected defects in telencephalic areas that were adjacent to the developing olfactory epithelium, which will give rise to the olfactory bulbs. At 24 hpf, wild type, control morpholino and *dmrt5* morpholino injected embryos showed no obvious apoptotic differences in telencephalic regions adjacent to developing olfactory epithelia (see page 78, Fig. 28). However, examination of these telencephalic regions at 31 hpf revealed first signs of increased apoptosis (Fig. 32 a), which became more evident at 48 hpf (Fig. 32 b). The elevated apoptosis observed in control morpholino injected embryos were unspecific since *p53* morpholino co-injection rescued the apoptosis phenotype. Additionally, regions of apoptotic events in control morpholino injected embryos were found throughout the entire telen- and diencephalon (data not shown).On the other hand, *dmrt5* morpholino injected embryos showed a distinct apoptosis pattern positioned within the prospective olfactory bulbs, which was not rescuable by p53 co-injection (Fig. 32).

A) **Average no. of apoptotic events telen- / diencephalon at 31 hpf**

wild type: 9.6 *
dmrt5 mo: 18.4
dmrt5 + p53 mo: 15.8
ctr mo: 67
ctr + p53 mo: 9.8 *
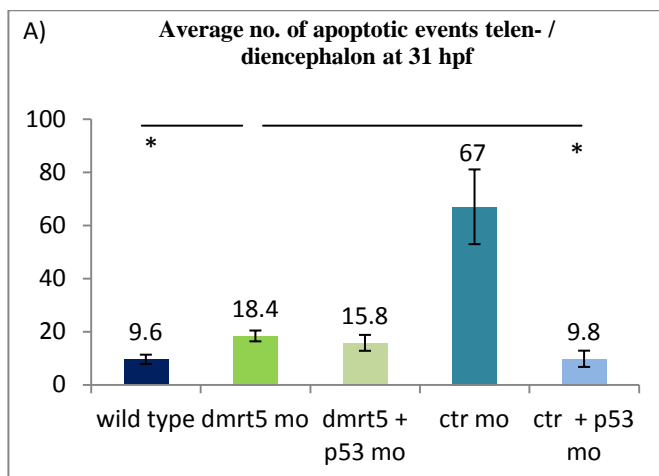
Fig. 32 Increased apoptosis in the developing olfactory bulbs: Number of telencephalic apoptosis events at A) 31 hpf and B) 48 hpf. Apoptosis at 48 hpf was further separated into events detected in telen- /diencephalon (blue columns) and lateral telencephalon/ olfactory bulb regions (green columns). A) At 31 hpf, a significant increase in apoptotic events was observed in *dmrt5* morphants when compared to wild type embryos. Embryos analysed: n= 5.

B)

Average no. of apoptotic events in the telencephalon at 48 hpf

Legend:
- ■ number of apoptotic events in the whole telen- /diencephalon
- ■ number of apoptotic events in higher telencephalic, olfactory brain centers

Bar values:
- wild type: 30.83 (blue), 10 (green)
- dmrt5 Mo: 41.67 (blue), 28.6 (green)
- dmrt5 + p53 Mo: 38.50 (blue), 22 (green)
- ctr Mo: 50.25 (*) (blue), 13.75 (green)
- ctr + p53 Mo: 41.80 * (blue), 11 (green)

Significance markers: *, ** over wild type/dmrt5 region

Continue Fig. 32: B) The overall telen- / diencephalon apoptosis values were not significantly different (blue columns), but apoptosis in the lateral telencephalon was significantly increased in *dmrt5* morphants when compared to controls. n= 4-6. An unpaired t-test was used to calculate p-values. P-values: (*) = 0.052; * < 0.05; ** p< 0.01.

A progressive increase in apoptosis over time and reduced numbers of stem- and/or progenitor cells resulted in morphological changes that became phenotypically visible in the olfactory system (olfactory epithelium and associated developing olfactory bulbs) in *dmrt5* morphants at 52 hpf (Fig. 33 b/d/f). The olfactory epithelium of *dmrt5* morpholino injected embryos appeared smaller and less structured when compared to that of wild type or control morpholino injected embryos. Five weeks old morphants also showed characteristically smaller olfactory bulbs (Fig. 33 h).
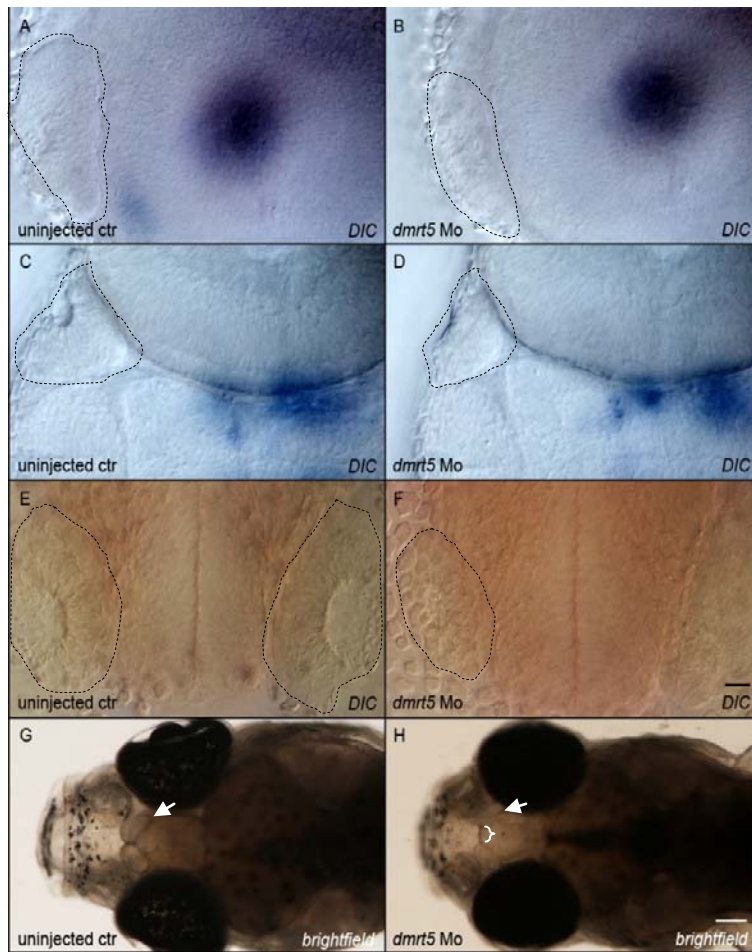
Fig. 33 Increased apoptosis and reduced cell division lead to smaller olfactory epithelia and olfactory bulbs: The knock-down of *dmrt5* resulted in embryos with smaller olfactory epithelia (circled area, B/D/F, second olfactory epithelia not clearly visible) when compared to wild type embryos (A/C/E). At later stages (5 weeks), differences in the size of the olfactory bulb became visible between wild type and Dmrt5 depleted fish (white arrow, G/H). Gaps, normally not visible in wild type, were detectable between both olfactory bulbs (bracket, H). Lateral (A/B), dorsal (C/D) and frontal (E/F) views of 52 hpf embryos; Dorsal views of 5 weeks old adolescent fish in G/H; Anterior is to the left (except frontal views). Images A-F DIC images, G/H bright field. Scale bars: A-F: 20 μm, G/H: 200 μm.

It was earlier shown that the development of higher olfactory structures within the telencephalon is dependent on the interaction with developing olfactory placodes and vice versa (Whitlock, 2004). This interaction is mediated through axonal projections from olfactory neurons to the telencephalon. Since undifferentiated olfactory stem/progenitor cells were dying in *dmrt5* morphants, followed by the increased apoptosis in lateral telencephalic fields, it could be possible that such interactions between olfactory placodes and telencephalic fields were disturbed. Therefore, I stained axonal projections with a fluorescent antibody against acetylated tubulin and visualized axons by confocal microscopy to evaluate if axon development is impaired in *dmrt5* morphants. As shown in figure 34 the size as well as the structure of olfactory epithelia was affected in *dmrt5* morphants when compared to wild type embryos. Besides this, reduced numbers of large nerves were found around the olfactory epithelium of *dmrt5* morphants (arrows, Fig. 34). The origin of these larger nerves is

unknown. However, the location adjacent to the olfactory epithelium suggests that these nerves may be involved in signal transmission from or to the nose. This would support the idea that an impaired crosstalk between olfactory epithelium and telencephalon could be partially responsible for the developmental defects observed in both structures. In addition to smaller noses and less nerves, less olfactory cilia (asterisk, Fig. 34) were detected in *dmrt5* morphants. This either indicates that the numbers of olfactory sensory neurons were reduced or that the development of cilia was impaired. The reduction in olfactory neurons could be explained by the increased cell death of olfactory stem or progenitor cells, while the lack of proneural gene expression may have influenced differentiation programs important for olfactory cilia development.
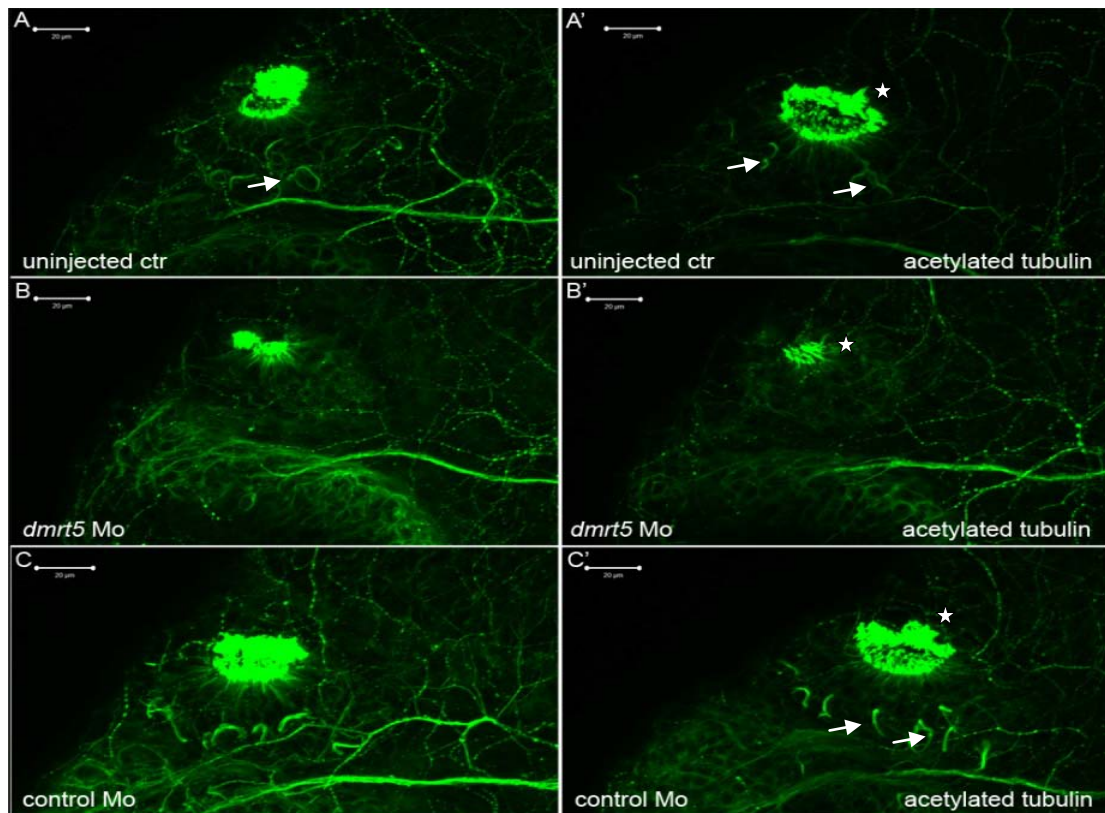
Fig. 34 Dmrt5 morphants exhibit reduced numbers of olfactory sensory neurons and olfactory nerves: Controls and *dmrt5* morphants were immunostained with an antibody against acetylated tubulin. While wild type (A/A') and *dmrt5* control morphants (C/C') showed well developed olfactory pits with numerous olfactory sensory neurons (OSN, marked by asterisk), *dmrt5* morphants illustrated considerably smaller olfactory pits and less OSN. Note that cilia of OSN are rich in acetylated tubulin giving an oversaturated signal from the olfactory pits. Depending on slightly different imaging angles, strong signals from clusters of cilia might prevent an optimal resolution of the olfactory pit (as seen in A or C). Additionally, *dmrt5* morphants were missing large nerves that were surrounding the olfactory epithelia (arrows). Slight differences in the signal intensities from these large nerves are seen between wild type and uninjected control embryos.

In summary, *dmrt5* morphant embryos are characterized by the down-regulation of proneural genes, *neurogenin* and *zash1a*, indicating that neuronal differentiation or specification processes are impaired in progenitor cells of the developing olfactory epithelium. Additionally, the number of olfactory stem- and/or progenitor cells is down-regulated. Higher apoptotic rates and reduced proliferative capacity were found in corresponding regions. This suggests a loss of undifferentiated stem cells pools. As a cumulative effect of persistently increased apoptosis, the morphants have smaller olfactory cups which show a less developed olfactory epithelium. Furthermore, telencephalic domains in close proximity to the developing nose are also marked by increased apoptosis. Although the apoptosis in olfactory associated telencephalic domains mainly occur at later stages, this eventually manifests as phenotypically visible smaller olfactory bulbs.

3.6 Dmrt5 regulates corticotrope differentiation in the pituitary

The early development of the pituitary is very dynamic and occurs during the first 30 hpf when cells are migrating from antero-lateral to more postero-medial positions. The pituitary is formed from pre-placodal fields which also express *dmrt5*. *Dmrt5* transcripts could be detected in these pre-placodal fields from bud-stage onwards (asterisk, Fig. 35 a). Based on their position and behaviour, *dmrt5* expressing cells stained in ventral head regions at 24 hpf were most probably migrating pituitary cells (arrowhead, Fig. 35 b). Definitive expression in pituitary cells was confirmed from 48 hpf onwards (Fig. 35 c/c'). Due to the expression of *dmrt5* in presumptive and terminally differentiated pituitary cells during the time window of pituitary formation, I analysed possible neuro-differentiation defects in these cells.

Fig. 35 dmrt5 expression in pituitary cells: Expression of *dmrt5* in pituitary pre-placodal fields started at bud-stage (asterisk, A) and could be detected throughout pituitary cell migration (arrowhead, B) and pituitary formation (C/C'). A: dorsal and lateral view; B/C: lateral views, anterior to the left; C': cross section through anterior of pituitary. Scale bars: A: 100 μm, B-C': 20 μm.

Proneural gene expression in potential migrating pituitary cells was analysed during the first 30 hpf and seemed to be normal in *dmrt5* morphants (data not shown). Therefore, wild type, control morpholino and *dmrt5* morpholino injected embryos were examined at 48 – 74 hpf, after the pituitary has been formed. Marker genes specific for pituitary endocrine cell populations, with overlapping expression domain to *dmrt5* in the anterior pituitary, were investigated. Expression of the following genes was analysed in controls and *dmrt5* morphants (cell type in brackets): *prolactin* (*prl*: lactotropes), *proopiomelanocortin* (*pomc*: corticotropes and melanotropes) and pituitary *glycoprotein alpha* (*gsu-a*: thyrotropes and gonadotropes). *Dmrt5* morphants showed a down-regulation of *pomc* expression restricted to corticotropes of the anterior pituitary (40/42, arrow head, Fig. 36) while melanotropes in the posterior pituitary maintained *pomc* expression (asterisk, Fig. 36). The down-regulation could not be rescued by p53 morpholino co-injection (18/22, data not shown). The other marker genes seemed to be unaffected upon *dmrt5* knock-down.

Previous reports have shown a transdifferentiation from *pomc* to *prl* expressing cell fates when Delta-Notch signalling is affected (Dutta *et al.*, 2008). To test whether lack of *dmrt5* expression promotes transdifferentiation of corticotropes to lactotropes, the *prl* expression domain was analysed in wild type and morphant embryos. If transdifferentiation would have occurred in *dmrt5* morphants, an elevated number of prl^+ cells and a concentrated *prl* domain with reduced *pomc* expression were expected. However, no obvious change in the number of prl^+ cells was detected (50/50, Fig. 36). Moreover, gaps in between single lactotropes remained *prl* negative which suggests that transdifferentiation from $pomc^+$ to prl^+ cells did not take place (Fig. 36 c/d). Indeed, the gaps between single stained cells seemed to be increased (Fig. 36 d inserts) with a slight but significant expansion of the *prl* domain to the posterior ($p_{dmrt5Mo-wt} = 0.000811$, $p_{dmrt5Mo-ctr\ Mo} = 0.001084$; Fig. 36 g). The identity of those cells that were unstained and intermingled with *prl* positive cells remains unknown, but the neuronal differentiation defects observed in the other brain regions suggest that pituitary (*pomc*) progenitor cells might have failed to differentiate and remained unstained for corticotrope

specific marker expression. In order to evaluate if the lack of *pomc* expressing cells was due to increased apoptosis of undifferentiated corticotrope progenitors, TUNEL stainings were performed at 24, 31 and 48 hpf (data not shown). The time window between 28 to 31 hpf is important for pituitary development, since it has repeatedly been shown that the lack of factors involved in pituitary formation could lead to increased apoptosis in pituitary cells in this period (Herzog *et al.*, 2004; Pogoda *et al.*, 2006). In contrast to the situation in previous reports, no apoptosis was observed in regions of interest during this critical time window. Since apoptosis of corticotropes or corticotrope progenitor cells could be excluded, I tested if defects during pituitary patterning could explain the lack of *pomc* positive corticitropes. For that expression of *pituitary homeobox 3* (*pitx3)* was analysed in morphants and controls. *Pitx3* is expressed before pituitary formation and demarcates pituitary pre-placodal fields (Dutta *et al.*, 2005). Its function is crucial for pituitary development and it labels all cells irrespective of their cell type.
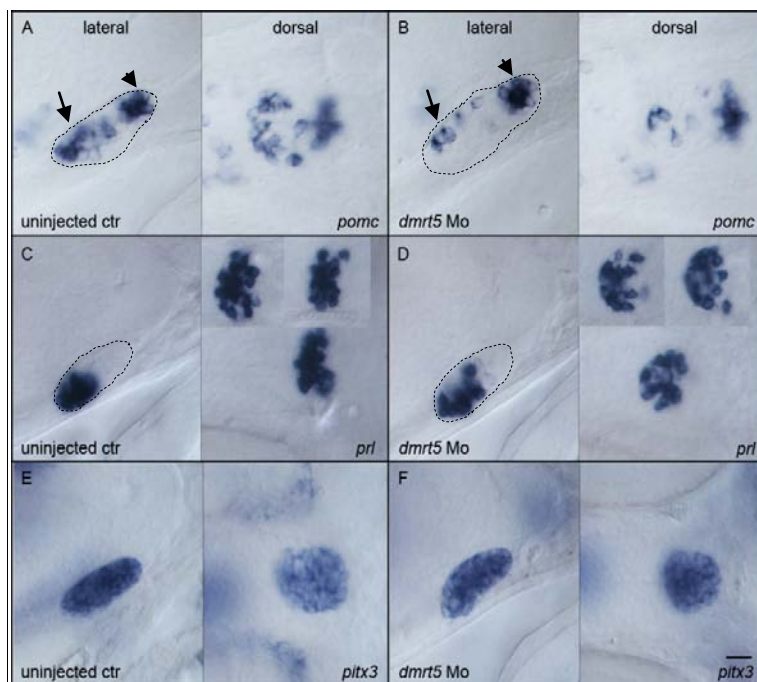
Fig. 36 Expression analysis of pomc, prl and pitx3 in dmrt5 morphants: Expression of *pomc* (A/B), *prl* (C/D) and *pitx3* (E/F) was analysed to reveal the function of *dmrt5* during pituitary development. *Dmrt5* morphants were characterized by a down-regulation of *pomc* in corticotropes (arrow, B), while *pomc* expression in melanotropes (arrow head b) was unaffected. *Prl* and *pitx3* expression showed also no obvious differences (D/F). A/C /E: wild type pituitaries; B/D/F: *dmrt5* morphant pituitaries. Dorsal views in C and D show several representative examples to demonstrate the more loose structure of *prl* domains in *dmrt5* morphants. Images are split in lateral close up (left) and dorsal close up (right). Outlines of pituitaries in lateral views are labelled with dotted lines. Scale bar: 20 μm
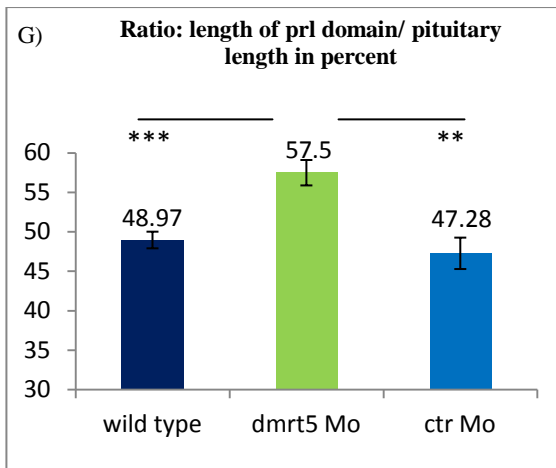
G) Ratio of length of the stained *prl* domain/ total length of pituitary. In *dmrt5* morphants, the *prl* domain was expanded posteriorly in comparison to controls. An unpaired t-test was used to calculate p-values: **= $p < 0.01$, ***= $p < 0.001$. N= 7- 10. **H)** Overview of the total size of measured pituitaries in morphant and control embryos. Pituitary size was unchanged in length and broadness, but the thickness was slightly but significantly increased in *dmrt5* morphants. Calculated p-value thickness: $p_{dmrt5Mo-wt} = 0.002961$. Number of tested embryos: n= 8-10.
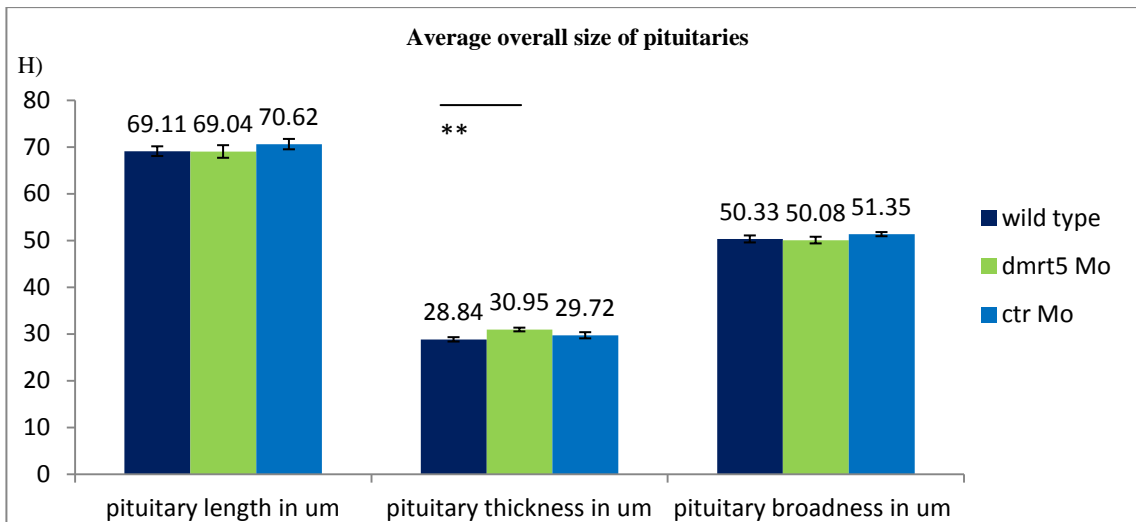
No changes in pituitary *pitx3* expression were visible between *dmrt5* morphants (35/35) and control embryos, suggesting that the basic pituitary patterning was not affected (Fig. 36 e/f). The length and width of the pituitary were also unchanged between controls and *dmrt5* morphants. The thickness of *dmrt5* pituitaries were slightly but significantly increased (Fig. 36 h). The measured pituitary dimensions in *dmrt5* morphants confirmed indirectly that *pomc* negative cells were still present at this stage and were not lost through increased apoptosis. To test if upstream regulators of POMC synthesis were possibly affected in *dmrt5* morphants, hypothalamic *crh* (*corticotrophin-releasing hormone)* expression was analysed. CRH is known to regulate POMC synthesis and is important during stress responses (Chandrasekar *et al.*, 2007; Alsop *et al.*, 2009; Alsop *et al.*, 2009), but no *crh* expression differences could be detected between *dmrt5* morphants and controls (20/22, data not shown).

Reduced levels of Dmrt5 result in the reduced expression of *pomc* in anterior pituitary cells without increasing *prl* expression in adjacent lactotropes. Increased apoptosis of *pomc* cells could be excluded since pituitary apoptotic rates and overall pituitary dimensions were normal. I therefore suggest that the observed data are consistent with neuronal differentiation or specification defects of corticotrope precursors, which fail to differentiate completely.

3.7 Dmrt5 regulates neuronal differentiation in the neurosecretory preoptic area and ventral midbrain

This chapter describes two other brain structures that were affected in Dmrt5 deficient embryos: the neurosecretory preoptic area (npa) and the ventral midbrain (vmb). Both tissues were identified and scored as affected based on down-regulated *neurogenin* expression (circles area, Fig. 37). Besides *neurogenin*, transcription of *zash1a* was also decreased in the ventral midbrain regions (Fig. 37 d). These observations are in line with the described data from the dorsal telencephalon and the olfactory epithelium and indicate that the loss of proneural genes may also affect neuronal differentiation in the npa and vmb. In the present study, I analysed the identity and function of affected neuronal stem cell and/or progenitor populations in the ventral midbrain and the preoptic area.
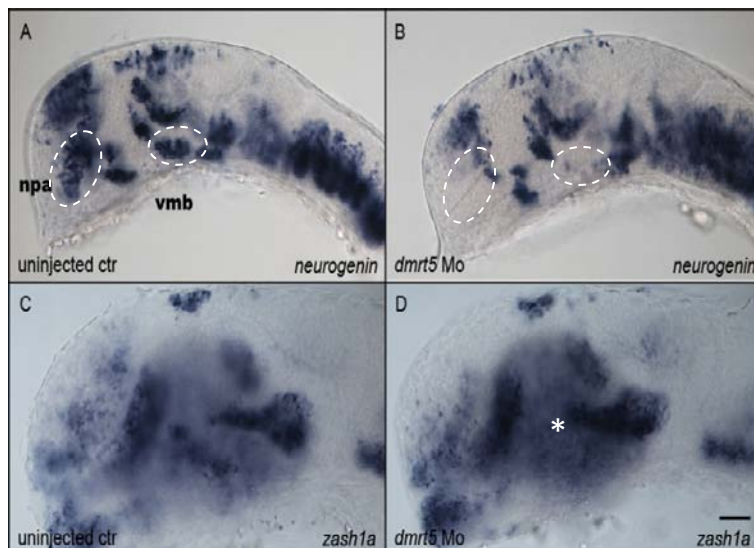
Fig. 37 Neuronal differentiation defects in the neurosecretory preoptic area and ventral midbrain: Proneural gene expressions of *neurogenin* (A/B) and *zash1a* (C/D) at 24 hpf. Additionally to previously identified regions, *neurogenin* expression was reduced in the neurosecretory preoptic area (**npa,** circled) and the ventral midbrain (**vmb,** circled) while adjacent expression domains remained unchanged (B).Ventral midbrain expression of *zash1a* was also decreased (asterisk, D). Lateral views, anterior is to the left. Scale bar: 50 μm.

Previous studies have shown that the preoptic area is the birth place of neuro-endocrine cells (Szarek *et al.*; Del Giacco *et al.*, 2008). Since proneural genes were down-regulated and

neural differentiation and specification defects were expected in *dmrt5* morphants, I looked at the expression of neuro-endocrine cell fate determinants of neuro-endocrine cell populations. Genes were chosen, whose expression overlapped with that of *dmrt5* and *neurogenin* in the preoptic area: *orthopedia homolog a (otpa), orthopedia homolog b (otpb)* and *simple-minded homolog 1a (sim1a)* (Del Giacco *et al.*, 2006; Eaton *et al.*, 2006; Eaton *et al.*, 2007; Eaton *et al.*, 2008). As demonstrated in figure 38, expression of all three hypothalamic neuro-endocrine fate determinants was strongly reduced in *dmrt5* morphants (arrow, *otpa:* 64/67, *otpb:* 63/63, *sim1a:* 59/60). The down-regulation of all three genes was not rescuable by p53 morpholino co-injection (data not shown). This indicates that Dmrt5 controls cell fate decisions in the neurosecretory preoptic area via regulation of *otpa/ otpb* and *sim1a* transcription. Noteworthy, the reduction of gene expression was restricted to those areas that overlapped with *dmrt5* in the preoptic area while most ventral expression domains of these three genes were unaffected in *dmrt5* morpholino injected embryos (asterisk, Fig. 38).
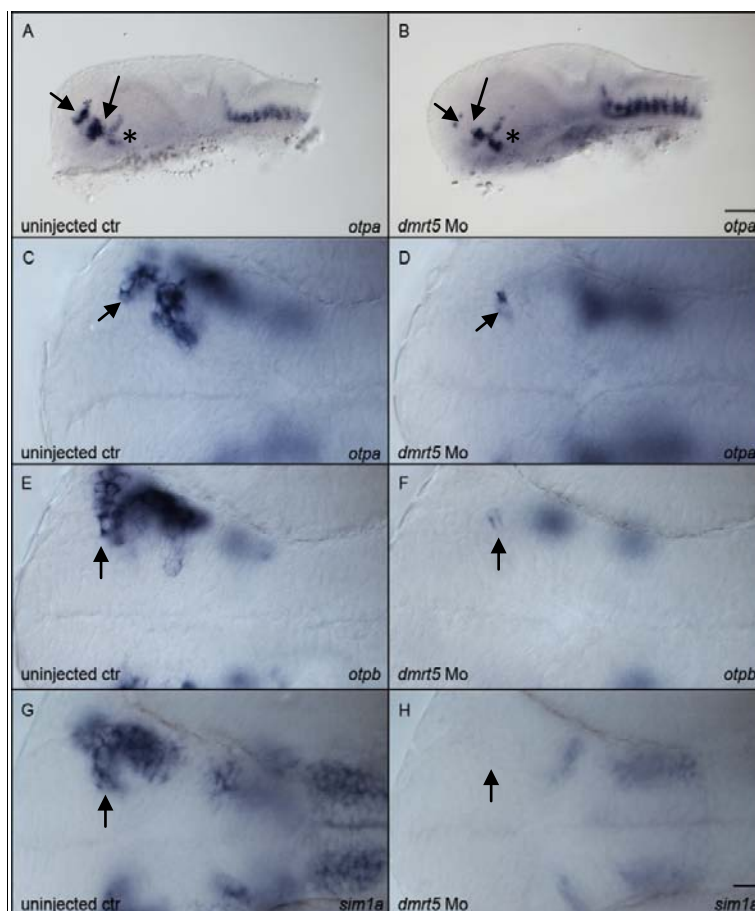
Fig. 38 Down-regulation of hypothalamic fate determinants in dmrt5 morphants: Dmrt5 deficient embryos show reduced expression of hypothalamic fate determinants: *otpa* (A- D), *otpb* (E/F) and *sim1a* (G/H) in preoptic areas. Images A/C/E and G: wild type embryos, Images B/D/F and H: *dmrt5* morphants. Ventral, diencephalic expression domains were unaffected in morphants (asterisk, B). A and B are lateral overview images. C-H: magnified dorsal views from the preoptic area. Arrows indicate affected cell populations and asterisk mark unaffected ventral diencephalic cell populations. Embryos A to F were at 24 hpf, embryos shown in G/H were fixed at 31 hpf. Anterior is to the left. Scale bars: A/B: 100 µm, C-H: 20 µm.

A knock-down of *dmrt5* resulted in the down-regulation of *otpa, otpb* and *sim1a*. It was shown previously that a down-regulation or a loss of these hypothalamic fate determinants affects the development of preoptic and hypothalamic neuro-endocrine cell populations (Lohr *et al.*, 2009). As regulators of neuro-endocrine cell development were reduced in *dmrt5* morphants, I next examined if these neuro-endocrine cell populations were developed normally in *dmrt5* morphants. For that, expression of marker genes for preoptic and hypothalamic neuro-endocrine cell populations was analysed. A*rginine vasopressin-like* (*avpl*) and *oxytocin-like* (*oxtl*) label pre-optic cell populations while *somatostatin1.1* (*sst1.1*), *thyrotropin releasing hormone* (*trh*), *tyrosine hydroxylase* (*th*) and *corticotrophin releasing hormone* (*crh*) mark hypothalamic neuro-endocrine cells.
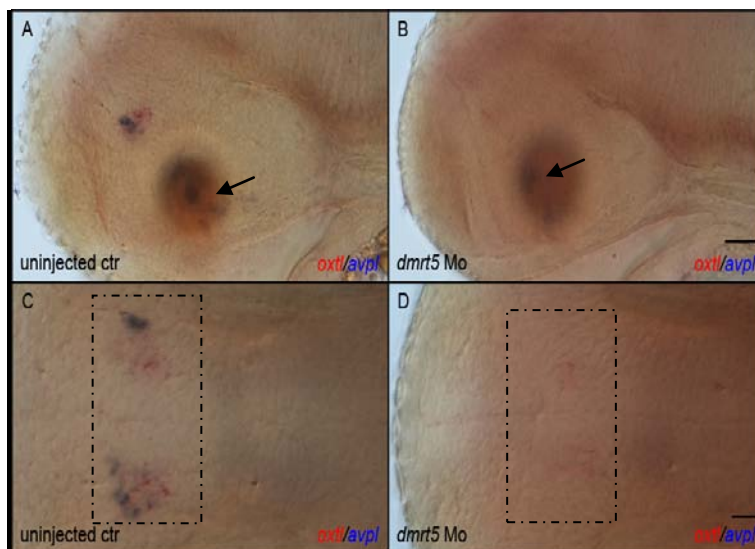
Fig. 39 Dmrt5 morphants show absence of neurosecretory cells in the preoptic area : Double in-situ staining of wild type (A/C) and *dmrt5* morphants (B/D). Expression of *oxtl* in red, *avpl* in blue. Neither *oxtl* nor *avpl* transcripts were detected in *dmrt5* morphants (B/D). A/B: lateral views, C/D dorsal views, expression domains of *oxtl* and *avpl* are boxed. Unchanged hypothalamic *avpl* expression domains were labelled with an arrow. Embryos were at 52 hpf, anterior to the left. Scale bars: A/B: 50 µm, C/D: 20 µm.

As shown in figure 39, expression of *oxtl* and *avpl* were both strongly down-regulated in the preoptic area. This was expected since transcription of endocrine fate determinants was reduced in the corresponding progenitor populations (see page 90, Fig. 38). However, hypothalamic transcripts of *avpl* were still detectable in *dmrt5* morphants (arrow, Fig. 39 c/d). This indicates that the effects on neuro-endocrine cell populations were restricted to the *otpa, otpb* and *sim1a* progenitor domains that overlap with *dmrt5*, while *dmrt5* non-overlapping domains were unaffected. In accordance with that, the expression of hypothalamic ventral

brain markers (*sst1.1, th, crh* and *avpl*) were comparable to that of wild type embryos (data not shown).

The defects observed in the ventral midbrain were similar to those found in the preoptic area. Transcriptional levels of *neurogenin, zash1a* and *sim1a* were decreased (see page 88, Fig. 37 and Fig 40 b). Considering a similar role of Sim1a in endocrine fate determination in preoptic area and ventral midbrain, the endocrine marker g*onadotropin releasing hormone 2* (*gnrh2*) was analysed in the ventral midbrain. Its expression was found to be down-regulated in *dmrt5* morphants (Fig. 40 d/f) and cell counts of *gnrh2* positive (*gnrh2*+) cells in ventral midbrain regions at 48 hpf and 74 hpf showed significant differences in cell numbers between *dmrt5* morphants and control embryos (Fig. 40 g/h).
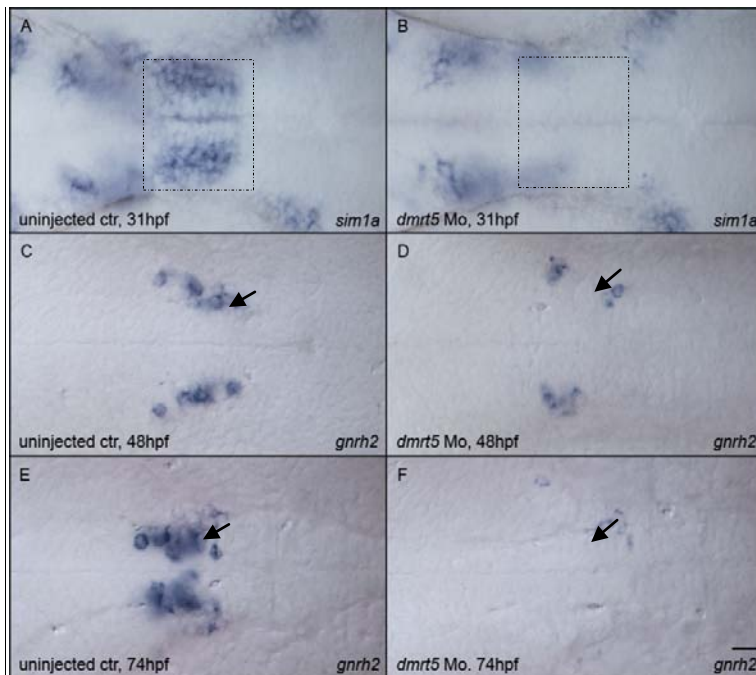
Fig. 40 Dmrt5 morphants show neuro-endocrine differentiation defects in ventral midbrain regions: Ventral midbrain expression pattern of *sim1a* (A/B) and *gnrh2* (C-F) were diminished in morphants (B/D/F) but not in controls (A/C/E). A/B: *sim1a* expression, down-regulated midbrain domains are labelled with arrows. C-F: *gnrh2* expression. Dorsal views, anterior to the left. Scale bar: 20 µm.
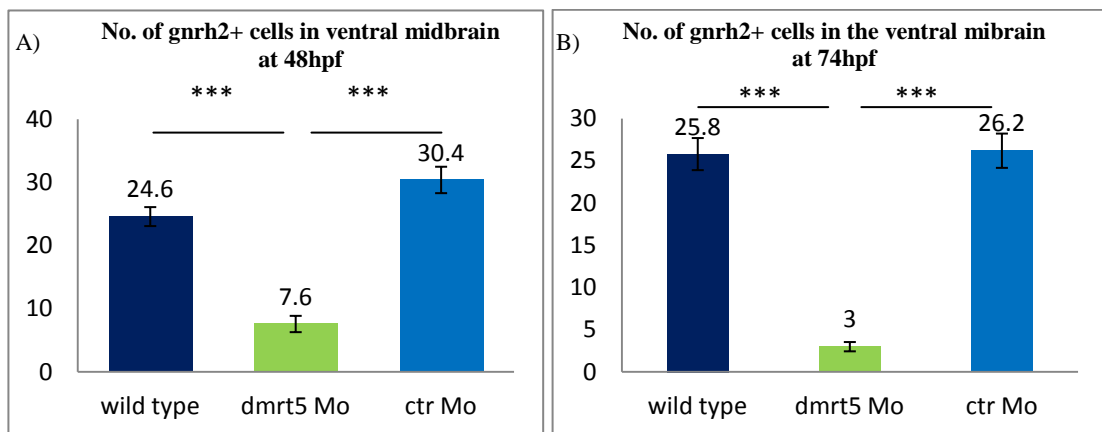
Fig. 41 Statistical analysis of gnrh2 positive (gnrh2⁺) cell populations: Control and morphant embryos at A) 48 hpf and B) 74 hpf. Only in Dmrt5 deficient embryos but not in the control morpholino injected embryos, the number of *gnrh2*⁺ were significantly reduced. An unpaired t-test was used to calculate p-values: 48 hpf: ***= $p < 0.001$. Number of analysed embryos: n= 5.

Taken together, the preoptic area and ventral midbrain of *dmrt5* morphants showed reduced proneural and cell fate determinant gene expression. As a consequence, neuronal differentiation and specification processes are defective resulting in a loss of specific neuro-endocrine cell populations. Hence, Dmrt5 is required for the development of the neuro-endocrine system and it is important to note that the observed effects on *gnrh2* positive cell populations could ultimately led to gonadal development defects. This would be the first time to show that a member of the *dmrt* gene family may influence gonadal development in a non-gonadal, non-autonomous manner and would provide an interesting link between brain and sex development.

3.8 Generation of *dmrt3* targeting zinc finger nucleases and *dmrt3* mutant zebrafish

In order to knock-out *dmrt3*, it was first necessary to determine optimal ZFN binding sites. As mentioned in the introduction, Dmrt proteins contain conserved DM-domains that are essential for DNA binding. A ZFN mediated genomic frameshift mutation upstream of these positions, would either lead a) to alterations of the amino acid sequence of the DM-domain or b) result in premature stop-codons and truncated Dmrt3 proteins without a DM-domain. In both cases, the DNA binding would be severely impaired rendering Dmrt3 proteins non-functional.

To identify the conserved DNA-binding DM-domain, the amino acid sequence of Dmrt3 was aligned with other Dmrt-proteins. Based on previous reports (Narendra *et al.*, 2002), key amino acids were identified that are essential for DNA binding (Fig. 42, asterisk). While the amino acid sequences were identical between Dmrt3 and other Dmrt-proteins at these conserved positions, the coding sequences differed. Therefore, generated ZFN will target only the *dmrt3* loci. The determined *dmrt3* target site was located within a RQR motif of the DNA recognition helix (green arrow, Fig.42), known to be essential for DNA binding. Consequentially, mutations within this motif are very likely to result in *dmrt3* null mutants.
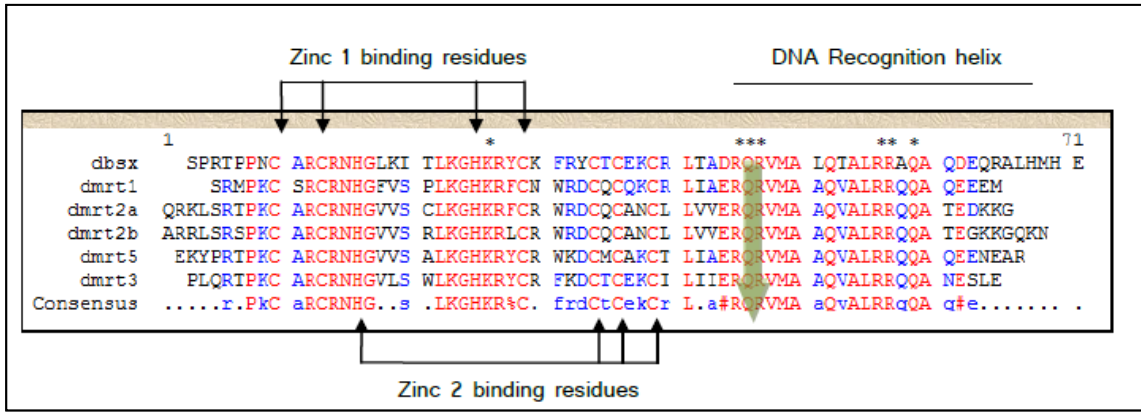
Fig. 42 Alignment of zebrafish and Drosophila DM-domains and selected dmrt3 ZFN binding site:
Alignment shows the amino acid sequence similarities between *D. melanogaster doublesex* (dbsx: ensemble: FBgn0000504) and zebrafish *dmrt1* (ENSDARG00000007349), *dmrt2a* (ENSDARG00000015072), *dmrt2b* (ENSDARG00000070013), *dmrt3a* (ENSDARG00000035290) and *dmrt5* (ENSDARG00000039412). The DM domain of these proteins contains two zinc binding and one DNA binding motif. The two zinc-binding domains are marked with black arrows; the DNA-binding domain is labelled as "DNA-recognition helix". Note the high degree of amino acid sequence conservation within the DM-domains. Amino acid residues essential for *dbsx* DNA binding are labelled with asterisks. Point mutations at any of these amino acid residues results in an impaired DNA binding (Narendra *et al.*, 2002). The green arrow indicates the location of the expected ZFN cleavage site within the *dmrt3* sequence.

To determine potential ZFN binding sites, bioinformatic tools ZiFit (http://bindr.gdcb.iastate.edu/ZiFiT/) and ZFPsearch (http://pgfe.umassmed.edu/ZFPsearch.html) were used. The chosen ZFN binding site (Fig. 43) contained an internal MspA1l restriction site in the spacer region for convenient identification of *dmrt3* ZFN knock-out embryos by RFLP analysis.

94
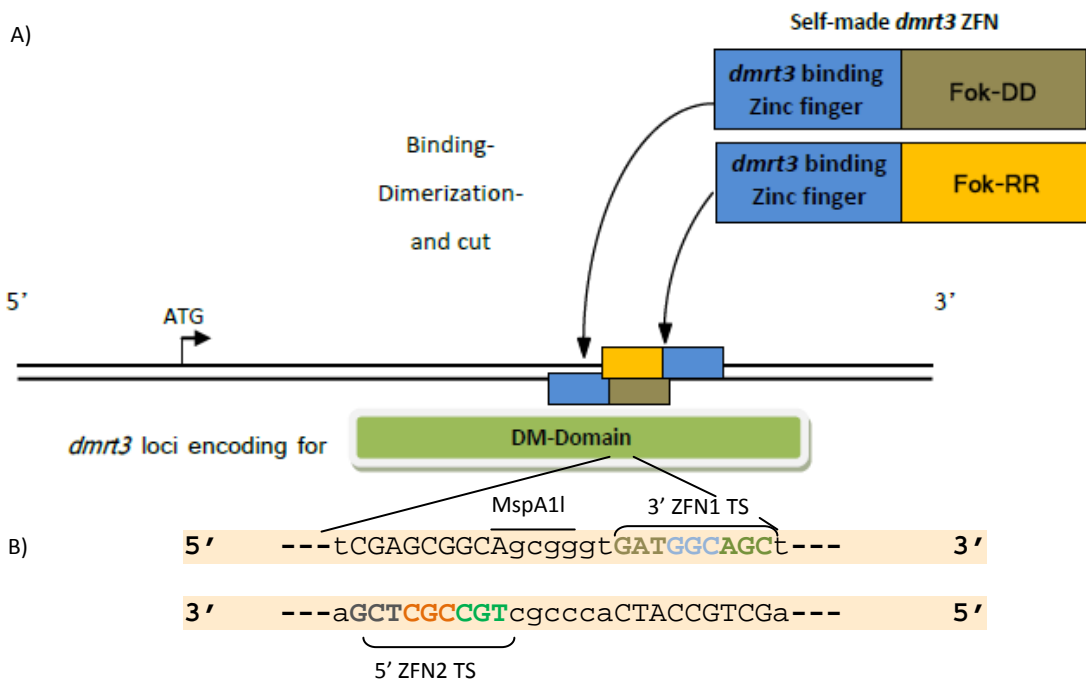
Fig. 43 Schematic drawing of designed ZFN and their binding sites with respect to the dmrt3 DM domain: A) The binding of the two ZFN to their target sites in the encoding sequence for the Dmrt3 DM domain is mediated via its two zinc finger proteins (blue boxes). Each of the zinc finger proteins contains three distinct zinc finger domains (ZFD; not indicated) that binds to specific target site nucleotide triplets. The cut of the target sequence is mediated via the FokI heterodimer (yellow/brown boxes). B) Target sequences of the ZFN's: Bold, capital letters indicate the two binding sites of the two ZFN. Differentially coloured nucleotide triplets mark specific binding sites of distinct ZFDs. The spacer region between left and right ZFN binding site is shown in small letters. A MspA1l restriction site spans the boundary between the left ZFN binding site and the spacer. 3' indicates that the target site (**TS**) is located downstream of the spacer region, while 5' labels the target site upstream of the spacer sequence.

Additionally, ZFPsearch provides the user with sequences for degenerated primers that were used to customize a template zinc finger in a way that it binds to the determined *dmrt3* target site. A list of used primers can be found in the Appendix A2 and the minimum diversity of resulting plasmid pools can be found in table 17.

Table 17 Overview of generated zinc finger libraries:

5p ZF (zinc finger 2) Module preparation	Library Diversity (Selection on target site vector)	3p ZF (zinc finger 1) Module prep.	Library Diversity (Selection on target site)
Module 1	18432 (ZF2TS1)	Module 1	221184 (ZF1TS1)
Module 2	110592 (ZF2TS1TS2) 110592 (ZF2TS2_2)	Module 2	6912 (ZF1TS1TS2)
Module 3	13824 (ZF2Dmrt3) 13824 (ZF2TS3_2)	Module 3	12288 (ZF1Dmrt3)

Table legend: Depending on the level of primer degeneration for zinc finger module (ZFM) synthesis, pools of different ZFM encoding amplicons had to be generated and cloned into ZF expression vectors. The numbers indicate the minimum size of different ZFM- encoding plasmid libraries and correspond to the level of primer degeneration that were used to generate the libraries. The abbreviations noted in brackets name the corresponding target sites. ZF= zinc finger; TS= target site; several sequential target sites are labelled TS1TS2, while particular single target sites are labelled TS"position of the triplet"_2.

After identification of the potential ZFN target site, the standard zinc finger zif268 (Addgene) had to be changed from its preferred binding site towards the identified *dmrt3* target site. This was done via PCR-based mutagenesis. Degenerated primers were used in a first round of PCR to amplify new, variable ZFMs (Fig. 44; lanes 2) at one out of three possible ZFM positions. PCR amplified fragments encoding for the other two ZFMs remained unchanged. Modified fragments and the unchanged two neighbouring ZFM were annealed with each other resulting

in amplicons that encode for a new zinc finger protein (Fig. 44; lane 3). The annealing of different modules was done with a modified PCR protocol (see 2.5.3; Table 12/13). Depending on the mode of selection (see 2.5.3; Fig. 8), different annealing strategies were used, but only one out of three zinc finger modules was changed at a time while the remaining two domains remained unchanged. The two unchanged neighbouring modules were used as anchors that position the new assembly over its target site.
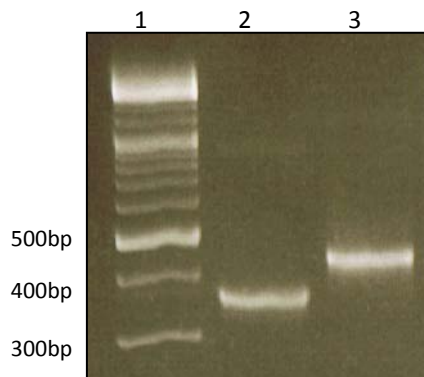
Fig. 44 Amplification and annealing of zinc finger module 1 using degenerated primers: Lane 1: DNA ladder. Lane 2: PCR amplified and customized fragment encoding for zinc finger module 1 (354bp). Lane 3: After annealing of ZFM1 with oligonucleotide 1 (Oligo1: 76bp) only one band with the corresponding size of the annealed fragment (412bp) were detectable on the TAE gel. The illustrated annealing of ZFM1 with oligo1 is exemplarily for all performed annealing steps of different module encoding fragments.

Annealed fragments were cloned into the plasmid pB1H2Ω2, from which zinc finger proteins are expressed as fusion proteins with an N-terminally fused RNA-polymerase. Expression plasmids were transformed into *his* deficient bacteria harbouring the corresponding *dmrt3* target site plasmid pH3U3. Only if the expressed zinc finger fusion protein binds to its target region in pH3U3, the RNA-polymerase is positioned in close proximity to the promoter of the Histidine-synthetase and the used bacterial strain is capable to survive the selection on the Histidine deficient selection media (for more details see chapter 2.5.2). In addition, the selection plates contained an increasing concentration gradient of 3-AT, allowing to distinguish between low affine and high affine *dmrt3* zinc finger proteins. By selecting only those colonies that are able to survive on high 3-AT concentrations, it was ensured to isolate plasmids encoding for zinc finger modules with high affinity to the *dmrt3-* target site. After transformation of plasmids encoding for modified zinc finger proteins, selection plates were incubated for two to five days at 37°C and removed when first bacterial colonies became visible (Fig. 45).
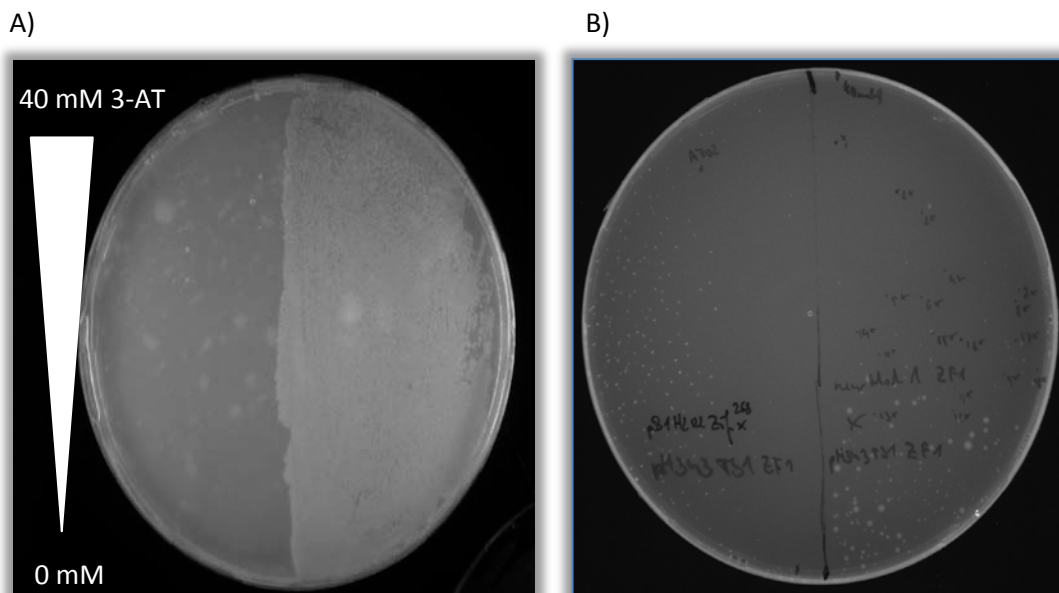
Fig.45 Selection of binding zinc fingers on NM-media plates: NM-media selection plates lack Histidine but contain a 3-AT gradient ranging from 0 mM to 40 mM. A) Positive control: original Zif268 selected against its preferred target site. The right half of the plate was covered with a bacterial lawn that showed a high to low density gradient from low to high concentrations of 3-AT. The left half of the plate remained empty for this experiment. B) Left half shows a negative control, where the template zinc finger was selected against the customized *dmrt3* target side. Experimental results on the right side of the plate showed a bacterial lawn density gradient from a high number of colonies at the lowest stringency to single colonies at high concentrations of 3-AT.

Colonies growing at relative high concentrations of 3-AT indicating high affinity binding of the selected ZFM to the *dmrt3* target site were pooled and ZFP encoding plasmids were isolated from these as plasmid libraries. After isolation of plasmids from 3-AT resistant colonies, single plasmids as well as the whole library were sequenced to identify changes in the sequence of the DNA binding domains. As shown in figure 46, sequencing results of single plasmids confirmed altered zinc finger domains within PCR mutagenized modules. The changes within these domains were variable in nature as expected due to the high degree of primer degeneration. The high variability in the zinc finger domain encoding sequence is also reflected by the 'N' residues at all altered positions in the sequencing results for the pooled library.

Fig. 46 Confirming modifications of particular zinc finger domains by sequencing: Sequence alignment of randomly picked ZF-expression plasmids after the first selection round. The sequence at the top shows the coding sequence for template zif268. All six zinc finger domains were highly diverse within sequences encoding the DNA-binding domain of the first ZFM. The lane "lib" illustrates the sequenced pool of all selected plasmids and shows that the whole library is varied as evident by 'N' residues.

Depending on the selection strategy, the modifications of different zinc finger domains were done in parallel for all three modules or sequentially one module after each other. While parallel selection was faster, it selected only modules that bound best to *dmrt3* nucleotide triplets flanked by two original zif268 target sites not taking the module context into account. Hence, the resulting whole *dmrt3* ZF protein may not contain modules that interact well with each other. Since the binding of one zinc finger module can influence the binding of the neighbouring module, the used sequential selection method addressed this problem better than the parallel selection method and increased the chances of a successful selection process. The disadvantage of this method was that one selection step had to be completely finished before the next module was tested.

After the last selection round, 13 different zinc finger proteins were identified for the 3' target sequence, while only one zinc finger protein was identified for the 5' target sequence. The selected ZFP were generated via the sequential selection method as modular assembly yielded no *dmrt3* binding ZFP. To address the question, which of the isolated 3' zinc finger proteins bound best to the desired *dmrt3* target site, a comparative affinity assay was performed (Fig. 47). Equal amounts of zinc finger expression plasmids encoding for one particular *dmrt3*-zinc finger protein were transformed into the same amount and batch of *his⁻* deficient bacteria. *His⁻* bacteria harbouring the complete *dmrt3* target site plasmid were plated out next to each other on 3-AT selection plates. Bacteria synthesizing high-affine ZFP were able to survive and

grow at higher concentrations of 3-AT. By comparing the maximum growth front of the different bacterial lawns, it was possible to distinguish high affine *dmrt3* ZFPs from lower-affinity ZFPs (Fig. 47).
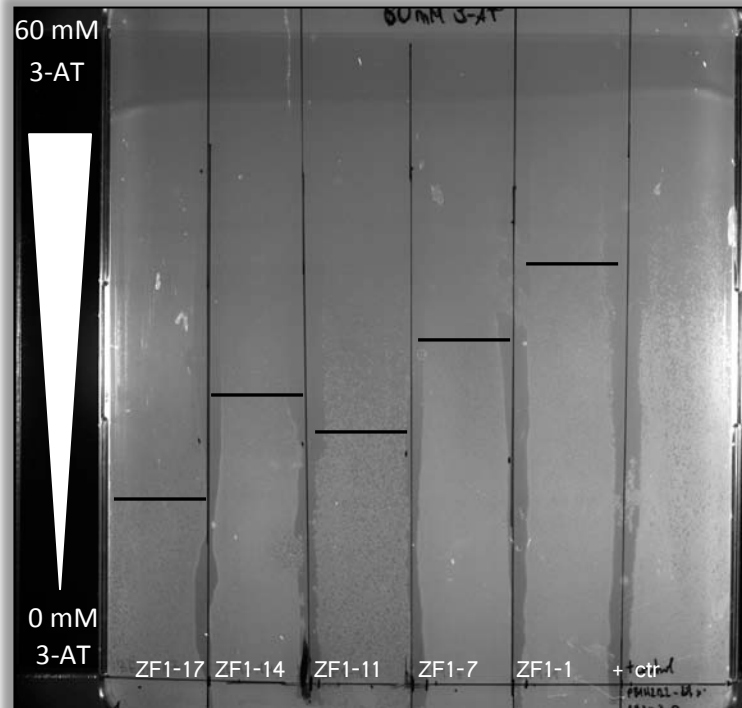
Fig. 47 Comparative ZF-binding assay: To find out which of the ZFP showed highest binding efficiencies, equal amounts of ZF encoding plasmids were transformed into *US0⁻* cells and plated out next to each other on 3-AT gradient plates. The 3-AT concentration ranged from 0 mM (bottom) to 60 mM (top). Positive control on the right: original zif268 selected against its original target site. Black bars represent the maximum growth front of the bacterial lawns. As shown in this picture, ZF1-1 transformed bacteria were able to survive the most stringent conditions whereas ZF1-17 transformed bacteria survived only less stringent conditions.

After identification of the three best binding 3' ZFPs and one 5' ZFP, a unique BamHI restriction site was introduced 3' of the completed ZF assembly by means of PCR mutagenesis and plasmids were digested with KpnI/BamHI. ZFP coding fragments were isolated and cloned into Fok-RR/Fok-DD endonuclease expression vectors resulting in plasmids encoding for four customized *dmrt3* zinc finger nucleases (Fig. 48 a), three for the 3' target site and one for the 5' target site. Since the Fok-endonuclease is active as dimer, two ZFNs have to interact with each other to introduce frameshift mutations. Based on the yield of distinct ZFN plasmids, three different ZFN combinations were possible from which all were tested. Plasmids encoding ZFNs for the right as well as the left *dmrt3* target site were linearized with NotI. Plasmids were purified and mRNAs encoding the desired ZFN were prepared according to the protocol. mRNA concentrations from 20 to 100 ng/µl were injected

into one-cell stage zebrafish embryos and surviving injected fish were analysed for genomic *dmrt3* frameshift mutations.
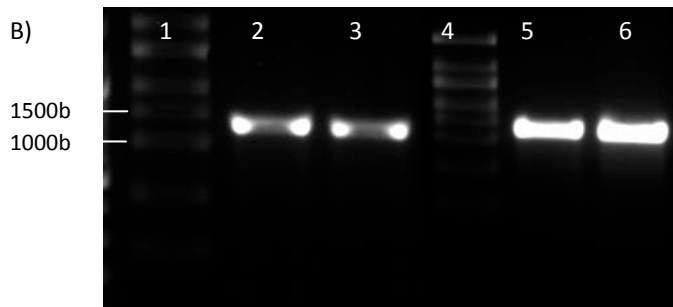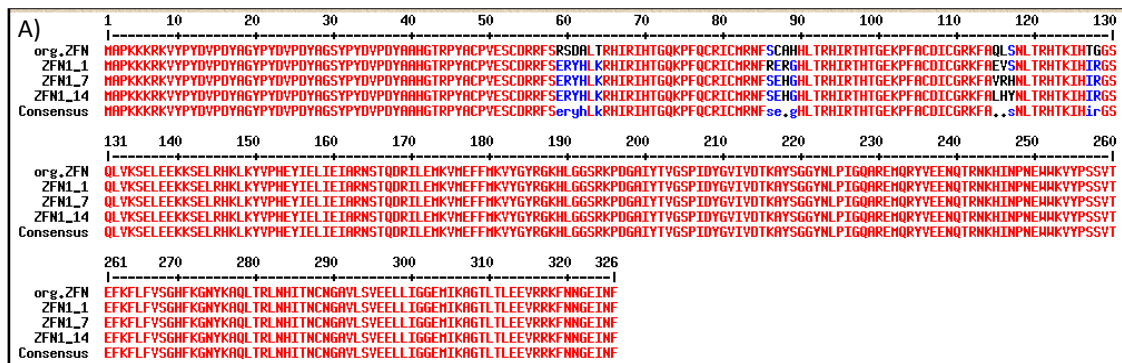
Fig. 48 Amino acid sequences of selected ZFNs and prepared mRNA: A) Amino acid sequence alignment of generated 3' ZFNs. The N-terminal end contained the three ZFDs (motifs different from the original zinc finger). The FokI-RR endonuclease domain extended from amino acid position 130 to the C-terminus. B) Qualitative and quantitative analysis of synthesized, polyadenylated, capped mRNA encoding for *dmrt3* binding ZFN's Lane 1 and 4: RNA ladder; Lane 2: ZFN1_1; Lane 2: ZFN1_14; Lane 5: ZFN1_7; Lane 6: ZFN2_24. Note that the picture shows two different gels from two separate mRNA synthesis experiments.

The evaluation of ZFN activity and identification of potential founder fish was done by analysing isolated genomic DNAs from ZFN injected zebrafish using the T7 endonuclease assay. The assays were used to identify mutations in the *dmrt3* locus. T7 endonuclease recognizes and cuts hair pin loops in DNA-hybrids, formed between normal and frameshift *dmrt3* gDNA (see 2.5.6, Fig. 10). The size of the undigested *dmrt3* homodimer was 382bp. If heterodimers between wild type and mutant *dmrt3* amplicons were formed, a T7 mediated cut around the spacer region was expected. Hence, T7 digested heterodimers were expected to be around 200bp in size. I analysed 72 ZFN mRNA injected embryos with T7 endonuclease but only 13 of the embryonic gDNA showed a partial digestion into smaller fragments whose sizes corresponded to the expected fragments. A representative result is shown in Fig. 49 a. Correct T7 activity under the used experimental conditions was confirmed as positive control fragments were digested almost completely (labelled '+', Fig. 49 a). Reactions yielding additional bands with sizes corresponding to the T7 digested *dmrt3* fragments were sequenced

(reaction products sequenced labelled with asterisk, Fig. 49). Unfortunately, no frameshift mutation within the *dmrt3* loci was detectable (Fig. 49 b). In addition to the "T7 pre-screening" of embryos, I also sequenced pools of ZFN mRNA injected embryos directly without T7 pre-screening. In total, 200 embryos were sequenced (20 pools with 10 embryos each) that were previously injected with the two ZFN combinations: ZFN1-7 x ZFN2-24 and ZFN1-14 x ZFN2-24. Unfortunately, all tested sequences were negative for a *dmrt3* mutation (data not shown). A possible explanation for positive T7 results could be that *dmrt3* amplicons formed internal loop-structures during the re-annealing, which then got digested by T7 giving "false-positive" results. Finally, expression of *dbx1a* was analysed as it was shown to be strongly down-regulated in *dmrt3* morphants (Rajaei, PhD Thesis, 2012). I analysed 10 embryos injected with the two ZFN combinations (ZFN1-1 x ZFN2_24 and ZFN1-14 x ZFN2_24) and compared the cell numbers of *dbx1a* positive (*dbx1a*$^+$) cells in a defined region of the spinal cord to wild type embryos. The ratio of *dbx1a*$^+$ cells per somite were unaffected in ZFN mRNA injected embryos (5.12 and 5.99 *dbx1a*$^+$ cells/somite compared to 5.79 *dbx1a*$^+$ cells/somite in wild type). Taken together, these data suggest that the self-designed customized ZFNs, although showing efficient binding in the *in-vitro* selection assay, were not affine enough to bind and cut the zebrafish *dmrt3* loci *in-vivo* in embryos.
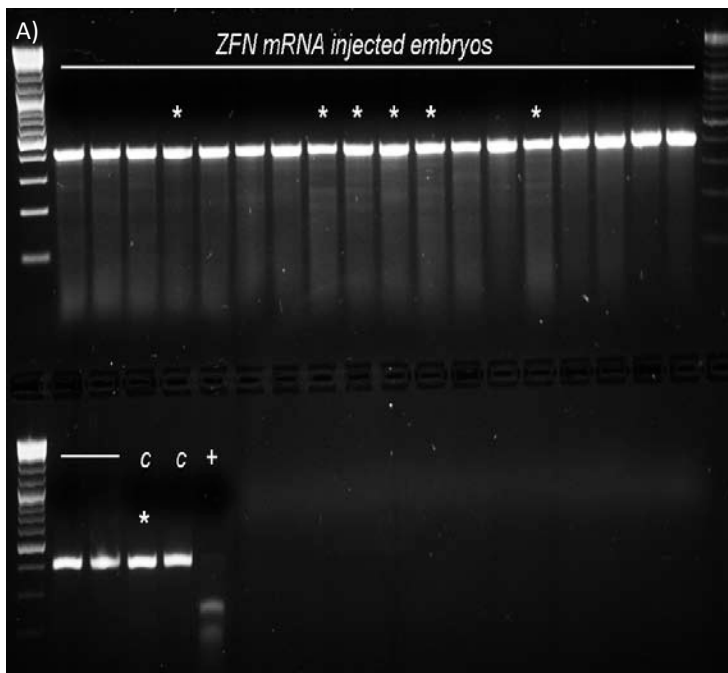
Fig. 49 T7 endonuclease screen of ZFN injected single embryos: A) T7 endonuclease treated *dmrt3* amplicons generated from gDNA of ZFN injected embryos were analysed on a 1.5% TAE gel. Lanes 1, 20 and 21: DNA ladder. Lanes 2-19 and 22-25: T7 digested *dmrt3* amplicons. Lanes 2-19 and 22/23 were *dmrt3* amplicons of ZFN mRNA injected embryos. Lanes 24/25: amplicons of uninjected control embryos (labelled 'c'). Last lane: various annealed ZFP encoding fragments used as positive control ('+'). gDNA from samples labelled with asterisks were sequenced.

B)

```
                                                                    ZFN2 TS              ZFN1 TS
                                                          ------------GCGGGT-----------
              131    140      150      160      170      180      190      200      210      220
              |-------+--------+--------+--------+--------+--------+--------+--------+--------+--------+--
native_dmrt3: AGCGCTACTGCCGATTTAAGGACTGCACTTGCGAGAAATGTATTCTGATAATCGAGCGGCAGCGGGTGATGGCAGCTCAGGTGGCGCTGAGG
ZFN_dmrt3_8:             CGATTTAAGGACTGCACTTGCGAGAAATGTATTCTGATAATCGAGCGGCAGCGGGTGATGGCAGCTCAGGTGGCGCTGAGG
ZFN_dmrt3_ctr:          CGATTTAAGGACTGCACTTGCGAGAAATGTATTCTGATAATCGAGCGGCAGCGGGTGATGGCAGCTCAGGTGGCGCTGAGG
ZFN_dmrt3_14:           CGATTTAAGGACTGCACTTGCGAGAAATGTATTCTGATAATCGAGCGGCAGCGGGTGATGGCAGCTCAGGTGGCGCTGAGG
ZFN_dmrt3_11:           CGATTTAAGGACTGCACTTGCGAGAAATGTATTCTGATAATCGAGCGGCAGCGGGTGATGGCAGCTCAGGTGGCGCTGAGG
ZFN_dmrt3_10:           CGATTTAAGGACTGCACTTGCGAGAAATGTATTCTGATAATCGAGCGGCAGCGGGTGATGGCAGCTCAGGTGGCGCTGAGG
ZFN_dmrt3_9:            CGATTTAAGGACTGCACTTGCGAGAAATGTATTCTGATAATCGAGCGGCAGCGGGTGATGGCAGCTCAGGTGGCGCTGAGG
ZFN_dmrt3_4:            CGATTTAAGGACTGCACTTGCGAGAAATGNATTCTGATAATCGAGCGGCAGCGGGNGANGGCAGCTCAGGNGGCGCTGAGG
Consensus     ..........CGATTTAAGGACTGCACTTGCGAGAAATGtATTCTGATAATCGAGCGGCAGCGGGtGAtGGCAGCTCAGGtGGCGCTGAGG
```

Fig. 49 continued: B) Alignment of sequenced *dmrt3* amplicons from ZFN injected embryos that showed additional bands after T7 endonuclease digest. The binding sequences (TS) of both ZFNs as well as the sequence of the spacer region that was expected to be cleaved by FokI are indicated above the alignment. None of the sequences showed mutations around the expected cleavage site of the ZFN.

Based on these results, our laboratory purchased a pair of tailor-made *dmrt3* ZFN from ToolGen (South Korea). These ZFNs were generated according to a protocol provided by ToolGen. Both ZFN pairs consist of a 3-module and a 4-module ZFP separated by a spacer of five to six base pairs. Therefore, binding affinity and specificity were expected to be higher than our own self-made ZFNs. Predicted binding locations were directly 3' of the *dmrt3* start codon and introduced frameshift mutations were expected to result in pre-mature translational stops and non-functional Dmrt3 proteins (Fig. 50). Plasmid information can be found in the Appendix A2.

A)
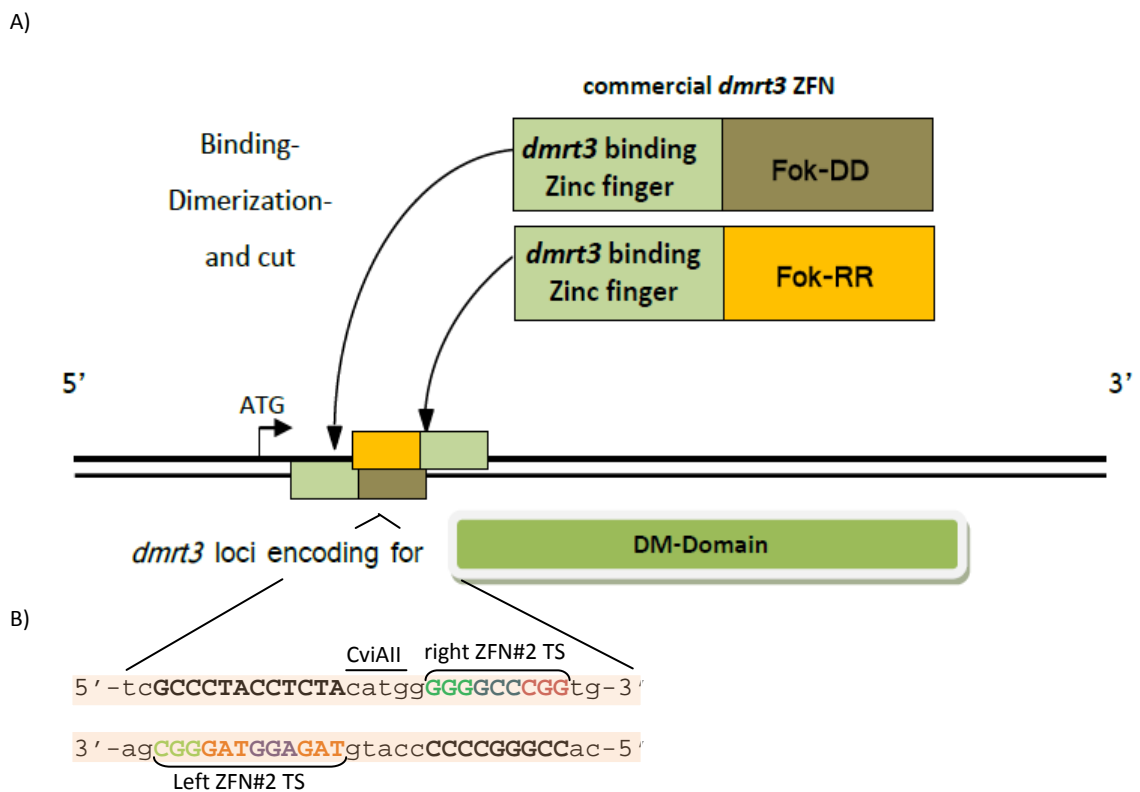
**Fig. 50 Schematic overview about the predicted target sequences of the commercial ZFNs and their**
**location with respect to the DM domain:** A) The binding of the two ZFN to their target site in the
encoding sequence for the _dmrt3_ DM domain is mediated via its two zinc finger proteins (green boxes).
The cut of the target sequence is mediated via the two FokI heterodimer (yellow/brown boxes). B)
Target sequence of ZFN's: Bold, capital letters indicate the two binding sites, while differentially
coloured nucleotide triplets mark the binding sites of distinct zinc finger modules. The spacer region
between left and right ZFN binding site is shown in small letters. A CviAII restriction site spans the
boundary between the left ZFN binding site and the spacer and can be used for diagnostic purposes.
The predicted cleavage site is around 25-30bp downstream of the start codon.

Only ZFN pair #2 were processed since it had a higher _in-vitro_ activity than ZFN pair #1
(personal communication, ToolGene). Plasmids encoding ZFN pair #2 were linearized with
XhoI and purified according to the protocol. Capped mRNA was transcribed using T7
polymerase according to the protocol. Synthesized mRNAs needed to be polyadenylated (Fig.
51) since XhoI cuts before the plasmid-internal poly-A signal.
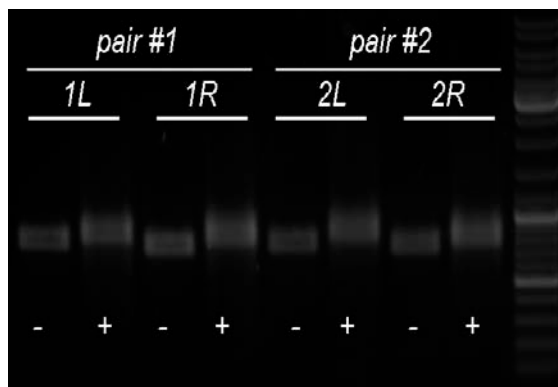
**Fig. 51 Polyadenylation reaction of transcribed**
**ZFN mRNA:** mRNAs encoding two different
ZFN pairs were transcribed from ZFN encoding
template plasmids and polyadenylated. Lanes
labelled with '-': unprocessed mRNA's. Lanes
labelled with '+': polyadenylated ZFN mRNA's.
A size shift from unprocessed to processed
mRNA indicates a successful poly-A reaction. L
and R are abbreviations for the left and the right
target site binding ZFN.

Capped mRNAs at a concentration between 20 to 100 ng/µl were injected into 1-cell stage
zebrafish embryos. Genomic DNAs from pools as well as single embryos were isolated and
analysed for frameshift mutations introduced by _dmrt3_ ZFN using RFLP analysis. Using a
restriction enzyme cutting site for CviAII located in the spacer region between the left and the
right ZFN binding site, gDNA based amplicons from different ZFN-injected embryos were
screened for frameshift mutations. At first, 100 pooled embryos (10x 10 ZFN mRNA injected
embryos) were screened to evaluate the activity of the used ZFN in a large scale approach.
For this, I isolated pooled gDNA, amplified fragments of the _dmrt3_ loci that flanked the new
ZFN target site and digested the amplicon with CviAII. Native _dmrt3_ amplicons containing
the CviAII restriction site were digested in the middle of the sequence resulting in fragments
of around 350bp in size (arrow, Fig. 52). _dmrt3_ fragments cleaved by ZFN were devoid of the

CviAII restriction site. Thus, the presence of undigested amplicons with a size at around 700bp (asterisk, Fig. 52) was indicative for mutated *dmrt3* loci and active ZFNs. As shown in figure 21, 8 out of 10 pools were partially insensitive to CviAII-digestion since fragments with a size of around 700bp were detected on TAE gels. Amplicons from uninjected control embryos were completely digested. This shows that enzyme conditions were optimal and suggests that the undigested fragments were mutated *dmrt3* amplicons. After evaluating that the commercial ZFNs were active in zebrafish embryos, I repeated the injections and analysed single embryos using the same CviAII assay as for pooled embryos. Results recapitulated the obtained data from the pooled embryos assay and showed that ZFNs were very efficient in introducing frameshift mutations into the genomic *dmrt3* locus. 15 out of 19 tested embryos showed amplicons insensitive to CviAII digestion while 8 out of 8 uninjected control embryos were completely digested (data not shown). To verify that the commercial ZFNs mutated the genomic *dmrt3* locus, undigested fragments were gel extracted, cloned and sequenced. Sequencing data confirmed frameshift mutations in the *dmrt3* loci and showed that one fish can have several mutation variants (Fig. 53).
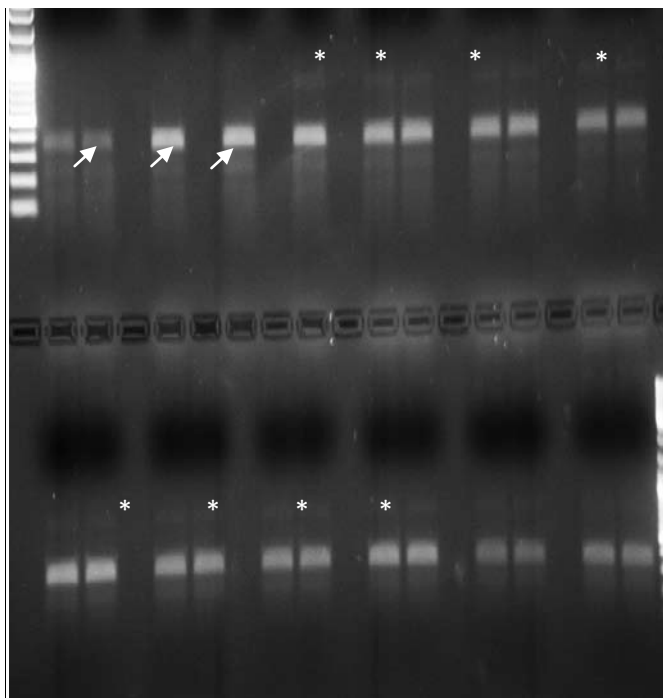
Fig. 52 CviAII restriction fragment length polymorphism assay to evaluate ZFNs activity: Dmrt3 amplicons were generated from pooled gDNA and digested by CviAII. Lanes 1 and 37: DNA ladder. Lanes 2, 5 and 7: DNA fragments obtained from uninjected wild type fish. Fragments were completely digested (arrows). Lanes 9-36: DNA fragments from ZFN mRNA injected embryos. In 8 out of 10 samples, some of the *dmrt3* amplicons remained undigested leaving a higher molecular weight band (asterisk). This suggests that ZFNs mutated the CviAII restriction site in the spacer region. Double lanes are belonging to one sample.

```
                        ZFN#2L                 ZFN#2R
                   -----------catg     g---------
Native_dmrt3:  TCGCCCTACCTCTACATG----GGGGGCCCGGTGTCCCAGCC
   dmrt3_12:   TCGCCCTACCTCTACATG----GGGGGCCCGGTGTCCCAGCC
    dmrt3_3:   TCGCCCTACCTCTACATGCATGGGGGGCCCGGTGTCCCAGCC   (+4)
    dmrt3_1:   TCGCCCTACCTCTAAA-------GTCGCCCGGTGTCCCAGCC   (+1,△4)
    dmrt3_2:   TCGCCCTACCTCT-----------CGCCCGGTGTCCCAGCC   (△8)
   dmrt3_11:   TCGCCCTACCTCTA-------------------GTGTCCCAGCC   (△13)
    dmrt3_9:   TCGCCCTACCTC----------GCCC----TCCCAGCC   (△14)
```

Fig. 53 Sequence confirmation of dmrt3 frameshift mutations: To confirm the identity of CviAII undigested fragments, CviAII resistant *dmrt3* amplicons of one promising candidate were cloned into TOPO blunt vector and sequenced. Several distinct frameshift mutations in the *dmrt3* locus could be identified after sequencing multiple TOPO clones of one CviAII digestion resistant *dmrt3* amplicon. The first lane shows the native *dmrt3* sequence. Except lane 2 (clone 12), all clones showed mutations of different nature. Various insertions and deletions were introduced into the *dmrt3* locus. The changes in the sequence are indicated on the right site: insertions and the length of inserted sequence as '**+x**', deletions and the length of deletion as '**Δx**'. The two ZFN binding sites are indicated above the sequences and the spacer region is shown in lowercase letters. The CviAII restriction site is highlighted in yellow.

ZFN mRNA injected embryos were raised, gDNA was isolated from fin clips and potential founders were identified using the above mentioned RFLP assay. From 22 tested founders, 9 fish were carrying *dmrt3* mutations (data not shown). At the moment, positively tested fish are individually kept until they are sexually matured. In the future, these *dmrt3* mosaic mutants will be crossed with each other and wild type fish to identify founder fish. F1 generation embryos will be analysed using RFLP assays, sequencing the gDNA loci and WISH techniques to analyse for changes in marker gene expression such as *dbx1a* that was previously found down-regulated in *dmrt3* morphants

In summary, I generated *dmrt3* knock-out zebrafish using tailor-made zinc finger nucleases. We will use *dmrt3* mutants to support previously generated *dmrt3* knock-down data for the spinal cord (Rajaei, PhD Thesis 2012) and expand the functional analysis of *dmrt3* into forebrain regions. Furthermore, since the morpholino mediated *dmrt3* knock-down was not 100% efficient, additional functions of Dmrt3 could become visible in *dmrt3* null mutants that were not detectable in *dmrt3* morphants.

4. Discussion

In *Xenopus*, *dmrt4* is expressed in the anterior neural ridge and becomes restricted to the telencephalon and the olfactory placodes at later stages (Huang *et al.*, 2005). Xdmrt4 is located upstream of the two proneural bHLH transcription factors *neurogenin* and *xebf2* and regulates their expression. Both factors are important for neuronal determination and differentiation within the olfactory epithelium. When *xdmrt4* was knocked-down, the expression of *neurogenin* and *xebf2* was down-regulated and neuronal differentiation was impaired. Consistent with this finding, the expression of the pan-neuronal marker NCAM was down-regulated indicating that terminal differentiation was affected (Huang *et al.*, 2005). The study by Huang *et al.* (2005) gave a first indication about the function of a DM-transcription factor as an essential regulator of neuronal differentiation in the olfactory epithelium. However, they failed to show whether the initial neuronal determination and differentiation defects in the olfactory epithelium also resulted in a reduced production, differentiation or survival of terminally differentiated olfactory neurons at later stages. In addition, the functions of *xdmrt4* for telencephalic neuronal determination and differentiation remained completely unaddressed.

The zebrafish genome does not contain a *dmrt4* ortholog (Volff *et al.*, 2003; Hong *et al.*, 2007). Instead, two other members of the *dmrt* family in zebrafish are expressed in the developing olfactory placodes and forebrain from earliest stages onwards: *dmrt3*, which starts to be expressed in the early forebrain at 14 hpf, and *dmrt5*, which commences at bud-stage (10 hpf). Their spatio-temporal expression patterns in zebrafish are comparable with that of *dmrt4* in *Xenopus*, and coincide with early neuron formation. This suggests possible roles for both zebrafish *dmrt* genes during forebrain neurogenesis.

The question if *dmrt5* has a role during neuronal development in zebrafish was recently addressed by Yoshizawa *et al.* (2011). In this study, the authors analysed the function of *dmrt5* in the dorsal telencephalon by analysing *dmrt5* mutant zebrafish. It was shown in *dmrt5* mutants that *her6* expression was ectopically up-regulated in the dorsal telencephalon. As

Her6 blocks proneural gene expression (Pasini *et al.*, 2001; Scholpp *et al.*, 2009), *neurogenin* expression was down-regulated leading to neuronal differentiation defects in this brain region (Yoshizawa *et al.*, 2011). The study of Yoshizawa *et al*. indicated that Dmrt5 may have a comparable role in the zebrafish telencephalon to that of Xdmrt4 during the development of the olfactory epithelium in *Xenopus*. However, the study of Yoshizawa *et al*. lacks a) a detailed analysis investigating the underlying molecular mechanisms of how Dmrt5 controls telencephalic brain development and b) an analysis of early neural stem cell populations. Furthermore, they did not address the functional consequences of the differentiation defect in the dorsal telencephalon as well as other additional roles of Dmrt5 in the olfactory epithelium, pituitary, preoptic area and the ventral midbrain.

Lastly, it is known from more recent work in mouse (Gennet *et al.*, 2010) that the mammalian ortholog of *dmrt5* (*Dmrta2*) is also expressed in the olfactory epithelium, the telencephalon and additionally in the ventral midbrain. Dmrta2 is required for the determination and differentiation of ventral midbrain cell fates from neural progenitor populations and a reduced expression of *Dmrta2* led to compromised midbrain differentiation (Gennet *et al.*, 2010). In addition, they revealed that the overexpression of *Dmrta2* in neuralized stem cells led to increased numbers of dopaminergic neurons, which are normally formed from progenitor pools of the ventral midbrain. Interestingly and in contrast to mammals, zebrafish dopaminergic neurons do not originate from the midbrain (Rink *et al.*, 2001; Rink *et al.*, 2002; Ryu *et al.*, 2006; Schweitzer *et al.*, 2012). However, based on the study of Gennet *et al.* (2010) it could be that zebrafish Dmrt5 also controls neuronal differentiation and determination of midbrain progenitor pools, yet the identity of these pools may differ between mammals and zebrafish. So far, nothing is known about the function of *dmrt5* in the ventral midbrain of zebrafish.

The aim of this study was to reveal the roles of *dmrt3* and *dmrt5* during fore- and midbrain formation in zebrafish embryos. Although several studies examined the role of DM-transcription factors for the development of the central nervous system (Huang *et al.*, 2005;

Gennet *et al.*, 2010; Yoshizawa *et al.*, 2011), these studies only addressed either distinct aspects of development (only early neuronal determination as in Huang *et al.*, 2005; or only neuronal differentiation as in Yoshizawa *et al.*, 2011) and/or they analysed only particular brain regions (the olfactory placode as in Huang *et al.*, 2005; the dorsal telencephalon as in Yoshizawa *et al.*, 2011; or the ventral midbrain as in Gennet *et al.*, 2010). In addition, these studies were done in five different models: *Xenopus*, zebrafish, chick, mouse and neuralized stem cell cultures. This study tries to provide a more comprehensive analysis of the functions of *dmrt3* and/or *dmrt5* as well as the underlying molecular mechanisms. Moreover and in contrast to previous studies, analysis of *dmrt3/5* functions was not restricted to one particular brain region of interest. All brain compartments in which *dmrt3/5* are expressed during brain development of zebrafish were included in this study, namely the dorsal telencephalon, olfactory epithelium, ventral midbrain, preoptic area and the pituitary. This provides the possibility to analyse and compare the function of *dmrt* genes between different brain regions within one species. To analyse the detailed function of *dmrt3* and *dmrt5* I used knock-down and knock-out approaches using gene specific splice block morpholinos and zinc finger nucleases, respectively.

4.1. Evaluation of *dmrt3* and *dmrt5* splice site morpholinos for gene-specific knock-down

For knock-down of *dmrt3* function, I used splice site morpholinos that were previously characterized extensively in our lab (Rajaei, PhD Thesis 2012). I followed the recommendations and morpholino injections were done at a dose of 3.125 mg/ml (personal communication Flora Rajaei). The used morpholino dose injections of 3.125 mg/ml resulted in a knock-down of endogenous *dmrt3* by 67%, which proved to be sufficient to impair spinal cord interneuron formation in the absence of apoptosis.

The *dmrt5* splice site morpholinos used in my experiments were newly designed and uncharacterized. I therefore first evaluated their splice blocking efficiency and compatibility with overall embryogenesis. A combined concentration of 3.125 mg/ml per each *dmrt5* morpholino was sufficient to block splicing of 97% of the *dmrt5* pre-mRNA transcripts

without affecting overall embryo morphology. Concentrations higher than 3.125 mg/ml per morpholino were avoided due to non-specific side effects (data not shown). Based on these results (Fig. 14), I used concentrations of 3.125 mg/ml (*dmrt3/ dmrt5*) splice site morpholino during the course of the study. An exception was the *dmrt3/dmrt5* double knock-down approach, for which I reduced the concentration to 1.6 mg/ml per morpholino per gene because injection with concentrations of 3.125 mg/ml per morpholino per gene resulted in unwanted morphological alterations and increased apoptosis throughout the bodies of *dmrt3/ dmrt5* double morphants.

To determine the specificity of the *dmrt* knock-down and exclude non-specific morpholino defects, observed phenotypes were compared to phenotypes of embryos that were injected with control morpholinos that failed to bind and block *dmrt* splicing (control morpholino sequences: see table 1). Representative results of control morpholino injected zebrafish phenotypes are given in the main text (Fig. 15, 16, 19, 26, 28, 29, 31, 32, 34, 36, 41) as well as in the Appendix A1. In general, the injection of control morpholinos into zebrafish embryos did not change the phenotype of control morphants when compared to wild type embryos. These data indicate that the observed *dmrt3/dmrt5* knock-down phenotype was specific due to a gene specific down-regulation of *dmrt3/5* and not due to unspecific morpholino-induced defects.

The only difference between the phenotype of control morphants and uninjected embryos was the observed up-regulation of apoptosis in *dmrt5* control morpholino injected embryos (Fig. 28, 29 and 32). It was shown previously that some morpholinos induce unspecific apoptosis via the activation of the pro-apoptotic protein p53 (Robu *et al.*, 2007). The observed increase of apoptosis in control morphants, proved to be unspecific as it was completely rescuable by the co-injection of a p53 morpholino. Contrary to this, none of the observed *dmrt5* knock-down phenotypes were rescuable upon co-injection with p53 morpholinos, indicating that these defects were specific due to the knock-down of *dmrt5* (only shown for the TUNEL assay).

It is also noteworthy, that there are several instances where the observed defects only affected particular cell types, while directly adjacent cell types and brain structures were completely normal. As example, *pomc* positive corticotropes of the anterior pituitary were affected upon the knock-down of *dmrt5*, while *pomc* positive melanotropes were developing normally (Fig. 36). These observations indicate the knock-down did not cause a general developmental delay of morphants.

Lastly, I want to point out that a part of the dorsal telencephalon data (alterations of the following markers: *her6*, *neurogenin*, *neuroD*, HuC/HuD) are consistent with the findings made in the *dmrt5* mutant line used by Yoshizawa *et al.*, 2011 indicating gene specific knock-down activities of the used *dmrt5* splice-blocking morpholinos. Taken together, the examined phenotypes in *dmrt5* morphants are most likely specific due to a gene specific knock-down of *dmrt5*.

4.2. Dmrt3 and Dmrt5 as regulators of neurogenin expression in zebrafish

After the evaluation of morpholino activity and specificity, I addressed the function of Dmrt proteins during zebrafish fore- and midbrain neurogenesis. As previous studies indicated a role for Dmrt proteins during neurogenesis, I analyzed the fore- and midbrain expression profile of *neurogenin* in *dmrt* morphants to determine if neurogenesis was affected in these regions. While *dmrt3* morphants showed no change in *neurogenin* expression, *dmrt5* morphants showed a significant down-regulation of *neurogenin* in the dorsal telencephalon, preoptic area, olfactory placode and ventral midbrain. *Dmrt3/dmrt5* double morphants exhibited exactly the same defects in *neurogenin* expression pattern as the *dmrt5* morphants, demonstrating that double morphants had no synergistic effects with regards to *neurogenin* down-regulation. Thus, I conclude that only *dmrt5* but not *dmrt3* regulates *neurogenin* expression in the developing zebrafish forebrain. The observed down-regulation of *neurogenin* in the dorsal telencephalon upon the knock-down of *dmrt5* confirms previously published *dmrt5* mutant data (Yoshizawa et al., 2011) but is also consistent with data from *Xenopus*. It seems that zebrafish Dmrt5 is a functional homologue to *Xenopus* Dmrt4 with

regards to the Dmrt-regulated *neurogenin* expression during the development of the olfactory epithelium. Besides these two regions, I observed a down-regulation of *neurogenin* in the ventral midbrain of *dmrt5* morphants, which confirms and explains the neuronal specification and differentiation role of Dmrt5 during ventral midbrain development as it was indicated in mouse and chick (Gennet *et al.*, 2010). In addition, I also observed a down-regulation of *neurogenin* expression in the preoptic area of *dmrt5* morphants. A possible neuro-regulatory function of a member of Dmrt proteins during preoptic area formation hasn't been shown so far.

Due to the fact that previous studies analysed individual brain regions in different species, it was not possible to directly compare different regions within one species. One similarity between all affected brain regions was that the down-regulation of *neurogenin* expression was restricted to those domains that overlap with *dmrt5* expression. Importantly, non-overlapping domains that do not express *dmrt5* were unaffected in *dmrt5* morphants. These data strongly imply that *dmrt5* may play a crucial role during neurogenesis in distinct forebrain regions through direct or indirect regulation of *neurogenin* expression in a cell-autonomous manner. However, I also observed tissue specific differences between different brain regions which will be discussed in the following sections.

4.3. Dmrt5 regulates the switch from neuroectodermal stem cells to radial glia cells

In zebrafish embryos, *dmrt5* starts to be expressed at 10 hpf in multipotent neuroectodermal stem cells of the anterior neural ridge and the prospective telencephalon. These cells will give rise to the olfactory placode as well as cells of the dorsal telencephalon. As *neurogenin* expression was down-regulated in *dmrt5* morphants, neuronal determination and differentiation defects can be expected in these neuroectodermal stem cell populations. In wild type zebrafish embryos at 24 hpf, the dorsal telencephalon can be divided into a proliferative and a differentiating region. The proliferative region, or ventricular zone, is marked by the expression of *blbp* and *gfap* which serve as marker genes for neural stem cells, in particular radial glia cells (Kriegstein *et al.*, 2003; Raymond *et al.*, 2006; Pellegrini *et al.*,

2007; Marz *et al.*, 2010). In addition to the expression of *blbp* and *gfap*, dorsal telencephalic radial glia cells are characterized by expression of *notch3*. The overlapping expression of radial glia markers *blbp* and *gfap* with *notch3* indicates that Notch signalling may be involved in dorsal telencephalic radial glia maintenance as described previously (Wolfe *et al.*, 1999; Kageyama *et al.*, 2008; Yoon *et al.*, 2008; Chapouton *et al.*, 2010). The stem-cell maintaining function of Notch signalling is probably mediated via Notch effectors *her4* and *her15* (Takke *et al.*, 1999; Shankaran *et al.*, 2007; Yeo *et al.*, 2007), which are also co-expressed in *blbp/gfap/notch3*-positive radial glia cells. *Her* genes encode for transcriptional repressors of proneural gene expression. They are required to maintain stem cell populations by suppressing neuronal differentiation and specification processes governed by proneural genes (Fig. 54 a).

Radial glia cells can give rise to new radial glia cells and immature neurons or neuronal precursor cells with restricted proliferative capacities. These immature neurons migrate from the ventricular zone towards the lateral telencephalon and activate expression of proneural genes (*neurogenin, zash1a, zash1b, neuroD*) as well as the postmitotic neuronal marker HuC/HuD (Barami *et al.*, 1995; Kim *et al.*, 1996). These neuronal differentiation markers are restricted to areas that do not overlap with areas that show expression of radial glia markers (*notch3, her4, her15, blbp* and *notch3*; Fig. 54 a).

In *dmrt5* morphants, neurogenesis was severely impaired. Embryos injected with *dmrt5* morpholinos showed a down-regulation of radial glia markers *blbp* and *gfap* as well as a reduced expression of Notch-signalling markers (*notch3, her4 and her15*). These data suggest that the number of radial glia cells was reduced in *dmrt5* morphants. One possible consequence of impaired Notch signalling and radial glia maintenance is pre-mature differentiation of radial glia into neurons. However, this possibility was excluded since numbers of differentiating and differentiated neurons were strongly reduced in *dmrt5* morphants. This was evident by reduced expression of proneural genes (*neurogenin*, *zash1a*, *zash1b*, *neuroD*), postmitotic neuronal marker HuC/HuD as well as markers for distinct dorsal

telencephalic cell populations (*fezf2*, *pou50* and *dmrt3*). Increased apoptosis of undifferentiated neural stem cells could also be excluded as explanation for reduced radial glia cells since TUNEL staining did not reveal any elevated numbers of apoptotic cells in *dmrt5* morphants (Fig. 28). Consequently, these data suggest that the described differentiation defects in *dmrt5* morphants were likely due to early specification defects at the transition from neuroectodermal stem cells to neurogenic radial glia cells (Fig. 54 b). To support this hypothesis, I performed a set of RNA *in-situ* hybridisation experiments to analyse expression of *pax6a* and *sox2* which are markers for early neuroectodermal cell types (Krauss *et al.*, 1991; Amirthalingam *et al.*, 1995; Okuda *et al.*, 2006). It was shown that *sox2* belongs to one of the earliest neuronal markers in neuroectodermal cells (Mizuseki *et al.*, 1998). As shown in Fig. 24, *pax6a* as well as *sox2* were ectopically up-regulated in *dmrt5* morphants, which indicates that *dmrt5* morphants might be characterized by the presence of increased numbers of early neural stem cells. The ectopic up-regulation of *sox2* not only indicates expansion of early neural stem cells. Its ectopic expression may also explain the failure of *dmrt5* morphants to generate radial glia. It was shown in chick that Sox2 function is required to maintain early neural stem cells while its ectopic miss-expression inhibits neuronal differentiation (Graham *et al.*, 2003). In *dmrt5* morphants, *sox2* is ectopically expressed and therefore may prevent the maturation from early stem to neurogenic radial glia cells. In addition to the ectopic expression of neural specifier molecules in the dorsal telencephalon, *dmrt5* morphants were also ectopically expressing *her6* in this area. Earlier research in mouse and zebrafish showed that *her6* (the ortholog of *Hes1* in mouse) is expressed broadly in neuroectodermal stem cells but its expression is gradually down-regulated to restricted areas as neural differentiation proceeds (Ohtsuka *et al.*, 2001; Pasini *et al.*, 2001; Scholpp *et al.*, 2009). The prolonged maintenance of early neural stem cells could serve as an explanation, why *dmrt5* morphants were ectopically expressing *her6* in the dorsal telencephalon. Moreover, it has been reported in mice that the ectopic overexpression of *Hes1* (the ortholog of zebrafish *her6*) inhibits neuronal differentiation (Ishibashi *et al.*, 1994; Ohtsuka *et al.*, 2001). Thus, the observed ectopic expression of *her6* could explain why early neural stem cells failed to generate radial

glia cells in *dmrt5* morphants. Based on the observations made in my study, I propose the following model: Dmrt5 is required to initiate the switch from neuroectodermal cells to radial glia cells by down-regulating the expression of early-stem cell promoting transcription factors such as *sox2* or *her6*. The loss of Dmrt5 function therefore results in a prolonged expression of these factors which prevents the gradual change from early stem cells to cells with radial glia identity (Fig. 23 and 54 b). As a secondary consequence of failed radial glia formation in *dmrt5* morphants, the number of neurons positive for e.g. HuC/HuD and *neurogenin* was reduced. It seems that Dmrt5 plays a crucial role during telencephalic neuroectodermal specification and acts as a switch that promotes cellular identity changes from neuroectodermal stem cell to radial glia.
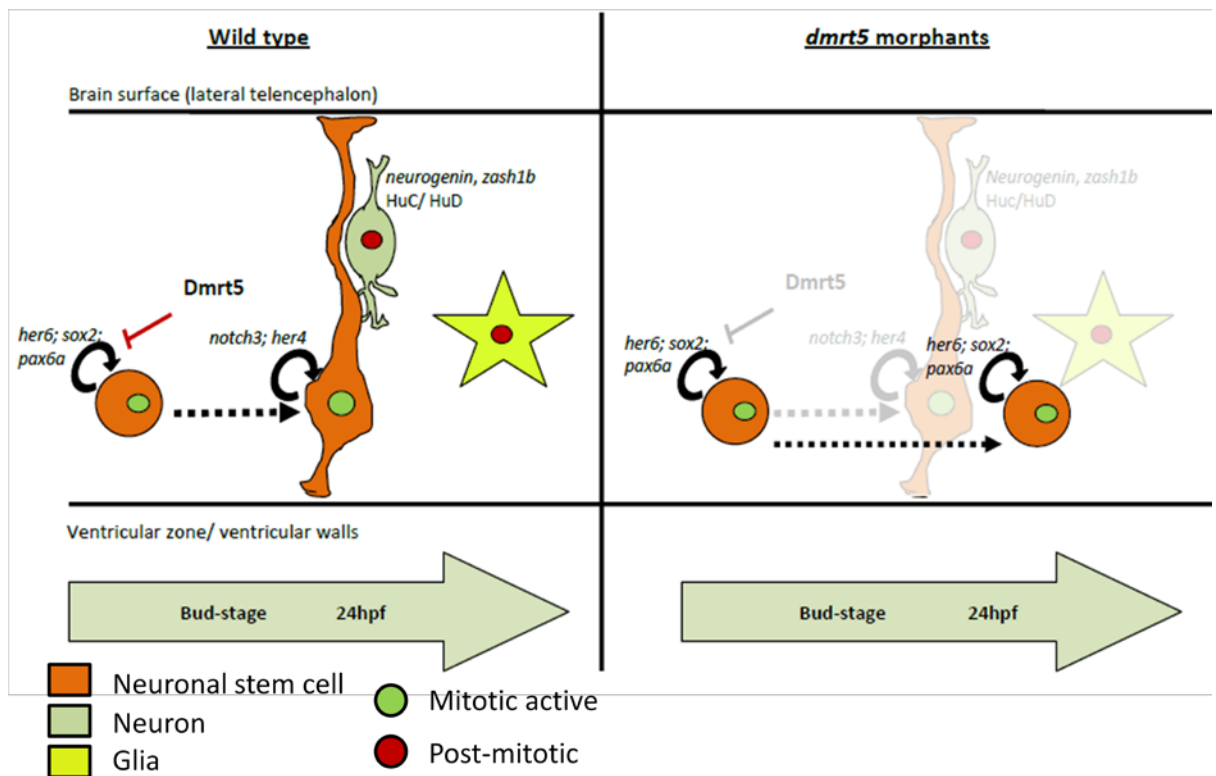
Fig. 54 Model for dmrt5 regulated dorsal telencephalon development: In wild type embryos (left side), early neuro-ectodermal stem cells express *her6*, *sox2* and *pax6a*, which maintain neural stem cell fates and repress differentiation. At bud stage, *dmrt5* expression emerges in a subset of cells of the presumptive telencephalon, leading to the down-regulation of these early stem cell markers. This initiates a developmental switch and early stem cells gradually differentiate into radial glia cells that can be found close to the ventricular surface at 24 hpf. This fate change is accompanied by characteristic changes of dorsal telencephalic cells. Radial glia cells express *notch3* and *her4*, which are important for the maintenance of this stem cell population. Ultimately, neurogenic radial glia cells give

rise to daughter cells with a neuronal cell fate. Newly differentiated neurons start expression of proneural genes as well as the postmitotic marker HuC/HuD and migrate into regions of the dorso-lateral telencephalon. In morphants with reduced Dmrt5 levels (right side), neuro-ectodermal stem cells maintain expression of *sox2*, *her6* and *pax6a*. Consequentially, early stem cells fail to form radial glia and radial glia markers are missing (*blbp, gfap, notch3, her4*). Due to a lack of neurogenic radial glia cells, less neurons were formed and the expression of respective marker genes were also reduced.

This model is supported by *her* gene expression data in zebrafish, which are in accordance with findings in mouse (Hatakeyama *et al.*, 2004; Kageyama *et al.*, 2008). It was reported that the development of radial glia from neuro-ectodermal stem cells is a gradual process that involves a change in *Hes* (*her*) gene expression. In mouse, early stem cells are characterized by expression of *Hes1 (her6)* and *Hes3* followed by the expression of *Hes1 (her6)* and *Hes5* (*her4*) in radial glia cells. It seems that the combinatorial changes of transcriptionally active *Hes* genes coincide with the maturation process from predominantly symmetrically dividing early stem cells to neurogenic, asymmetrically dividing radial glia cells. In zebrafish, *her6* expression starts early in neuroectodermal cells but is subsequently down-regulated as a pre-requisite for neuronal differentiation (Pasini *et al.*, 2001; Scholpp *et al.*, 2009). As shown with my data, radial glia cells are positive for *her4* and *her15* expression, indicating that dorsal telencephalic neural stem cells are undergoing a similar "*her* gene maturation" from *her6* in early stem cells to *her4/her15* in radial glia in zebrafish as described in mouse (Hatakeyama *et al.*, 2004; Kageyama *et al.*, 2008). Based on the data from mouse and zebrafish, the following role of *her6* in early neuroectodermal cells could be possible. Assuming that a down-regulation of *her6* in neuroectodermal stem cells is a permitting pre-requisite for the expression and function of neuro-determining proneural genes, the *her6* down-regulation may contribute to the switch from early neuroectodermal stem cells to more differentiated radial glia cells with their respective marker gene expression (such as *her4* and *her15*). In *dmrt5* morphants, *her6* expression was ectopically up-regulated while the induction of radial glia marker expression (*her4/her15)* was down-regulated. It could be therefore possible that the persistent *her6* expression is partially responsible for the absent switch of neuroectodermal stem to radial glia cells. In this model, Dmrt5 is required to switch-off *her6* expression, providing a transcriptional environment that allows the expression of early neuro-

determination factors and the gradual change from early stem cells to radial glia cells. In summary, it seems likely that *dmrt5* plays an important role during the development of the dorsal zebrafish telencephalon by initiating the switch from neuroectodermal cells to radial glia.

4.4. Dmrt5 regulates neurogenesis the olfactory system

The aim of this study was to understand how Dmrt proteins regulate forebrain development. The early onset of *dmrt5* expression in olfactory pre-placodal fields around bud-stage and sustained expression at later stages suggests that *dmrt5* is involved in regulation of neural differentiation in this area similar to the situation described in *Xenopus* olfactory placodes (Huang *et al.*, 2005). Therefore, I analysed the expression of proneural genes *neurogenin*, *neuroD* and *zash1a* in *dmrt5* morphants and wild type embryos at 25 hpf. In wild type embryos, all three proneural genes are expressed in distinct cell populations of the olfactory epithelium (Fig. 27) which partially overlap with BrdU positive proliferative progenitor/stem cells (Fig. 30). This suggests that a particular proneural gene may have specific roles in distinct progenitor domains.

In *dmrt5* morphants, expression of *neurogenin* and *zash1a* was strongly reduced or lost while *neuroD* expression was only slightly reduced. The down-regulation of *neurogenin* and *zash1a* indicates that neuronal differentiation and specification were affected in the developing olfactory placode of *dmrt5* morphants. However, previous studies suggested that a loss of Neurogenin function can be partially compensated by NeuroD (Madelaine *et al.*, 2011). Since *dmrt5* morphants exhibited residual expression of *neuroD*, the expected defects in neuronal differentiation might be prevented by functional compensation through NeuroD. Therefore, it was expected that neuronal differentiation defects could be limited to those aspects of olfactory placode development that are exclusively governed by Neurogenin and Zash1a but not by NeuroD. However, *dmrt5* morphants still showed drastic defects in the developing olfactory epithelium as apoptosis was significantly increased at 24 and 31 hpf when compared to controls. Dying cells were probably olfactory progenitor/or stem cells as indicated by

reduced signals from proliferative markers BrdU and pH3. Stem or progenitor cells may require direct cell-cell interactions with surrounding cells. If these supporting cells develop normal while stem or progenitor cells fail to differentiate in time, they miss essential signals from their environment and thus undergo apoptosis. Thus, a possible explanation for the increased cell death in the pool of olfactory progenitors in *dmrt5* morphants could be the loss of environmental cues due to failure of differentiation. Consequently, the development of the olfactory epithelium was severely impaired in *dmrt5* morphants affecting the size of the olfactory epithelium, the structure (smaller olfactory pits), the number of olfactory sensory neurons as well as their olfactory cilia (see Fig. 33/34). Due to the observed reduction in the number of olfactory sensory neurons (**OSN**), a loss or a reduction of the olfactory sensory nerve is expected. Additionally, it was previously shown that Neurogenin1 is required in the developing olfactory system to control aspects of olfactory nerve fasciculation and axon path finding (Madelaine *et al.*, 2011). As *dmrt5* morphants showed a reduced expression of proneural genes in the olfactory epithelium, fasciculation problems of the olfactory nerve were anticipated. However, the lack of olfactory sensory nerves as well as possible fasciculation problems have to be confirmed by the use of a retrograde lipophilic dye like DiI applied to the olfactory pit or employment of suitable transgenic lines that drive reporter gene expression under control of an olfactory sensory neuron specific promoter, such as the olfactory promoter for *omp*. Additionally to the defects observed in the olfactory epithelium, I observed a reduced number of larger nerves around the developing olfactory epithelium (white arrow, Fig. 34). These nerves are most probably branches of the lateral line nerve and their absence in this region of *dmrt5* morphants could be explained by path finding defects that also affects other nerve populations other than the olfactory nerve.

Moreover, knock-down of *dmrt5* not only influenced stem and/or progenitor cells in the nose, but also had a negative impact on olfactory bulb development. The number of apoptotic cells in lateral telencephalic regions in *dmrt5* morphants was comparable to control embryos at 24 hpf. However, at 31hpf apoptosis was significantly increased in the morphant situation. At 48

hpf, apoptosis in *dmrt5* morphants had increased further and concentrated in lateral telencephalic domains. Affected telencephalic cells are presumably progenitor cell populations that are involved in olfactory bulb development. The described phenotype could also explain why olfactory bulbs in adolescent *dmrt5* morphants were smaller compared to wild type embryos. It was shown in previous studies that the interaction between the developing olfactory placode and the olfactory bulbs (lateral telencephalon) is from bilateral importance for their development (Whitlock *et al.*, 2000; Wang *et al.*, 2001). Olfactory sensory neurons send out axonal terminals into the olfactory bulbs and support their development via stimulating signals (Wang *et al.*, 2001). In *dmrt5* morphants, the loss of olfactory progenitor cells resulted in reduced numbers of olfactory sensory neurons. Consequently, fewer olfactory sensory neuron axons reach the developing olfactory bulbs. As a result of the reduced interaction or lack of inductive signals from the olfactory neurons, telencephalic cells underwent apoptosis. Therefore, it seems possible that the observed telencephalic effect is secondary and occurs as a consequence of olfactory epithelium cell apoptosis and/or failure of migration or axon guidance into telencephalic olfactory regions. This could explain why I observed increased apoptosis in the olfactory epithelium first, before it was increased in the developing olfactory bulbs.

In summary, I conclude that *dmrt5* is an important regulator for the development of the olfactory system. It controls proneural gene expression in olfactory progenitor cells which is essential for their differentiation into olfactory sensory neurons.

4.5 Comparison between telencephalic and olfactory defects in *dmrt5* morphants

Upon *dmrt5* knock-down, both the dorsal telencephalon as well as the olfactory system were characterized by a down-regulation of *neurogenin* expression. However, *dmrt5* morpholino induced expression changes of other proneural genes showed remarkable differences between the two structures. *NeuroD*, which is expressed in both regions, was strongly down-regulated in the dorsal telencephalon upon *dmrt5* morpholino injection while its expression was only slightly affected in the adjacent olfactory epithelium. In addition to that, expression of

regulators of neural development such as *pax6a, her6* and *sox2* was altered in the dorsal telencephalon of *dmrt5* morphants, while it was unchanged in the olfactory epithelium. The differences seen in the expression analysis in the nose and the dorsal telencephalon of *dmrt5* morphants have indicated that the genetic networks must be controlled differently in these two regions. Therefore, it seems that *dmrt5* may play distinct roles in different tissues. It is tempting to speculate that these diverse specific functions of Dmrt5 are mediated via so far unknown tissue specific transcriptional co-regulators. This idea could explain why knock-down of *dmrt5* manifests in different phenotypes e.g. the described differences in *neuroD* expression.

4.6. Role of Dmrt5 for Corticotrope differentiation

Besides the dorsal telencephalon and olfactory epithelium, I also observed *dmrt5* expression in pituitary pre-placodal fields at bud-stage and migrating pituitary cells at 24 hpf (Fig. 35). The spatio-temporal pattern of *dmrt5* expression suggests a role for *dmrt5* during pituitary formation. Remarkably, the expression of *dmrt5* was restricted to the anterior pituitary indicating that Dmrt5 influences only the anterior subset of pituitary cells. A potential differentiation defect in anterior pituitary cells was assessed via analysing marker gene expression specific for anterior pituitary cell populations. In *dmrt5* morphants, the expression of the corticotrope and melanotrope marker *pomc* (Hansen *et al.*, 2003) was reduced in corticotropes while melanotrope expression domains remained unaffected. To assess the possibility of apoptosis among *pomc* progenitor cells, TUNEL stainings were performed at 31 and 48 hpf but showed no obvious differences between *dmrt5* morphants and controls. The size as well as the pituitary patterning was also normal in *dmrt5* morphants as indicated by the unaffected expression of the pituitary patterning marker *pitx3* (Dutta *et al.*, 2005). Subsequently, I tested the possibility of a potential transdifferentiation from corticotropes to lactotropes, through the expression analysis of the lactotrope marker gene *prl* (Herzog *et al.*, 2003). Transdifferentiation from corticotropes to lactotropes was excluded since the *prl* positive domain was not expanded. However, the *prl* expression domain was slightly loosened

and shifted posteriorly. At last, expression of the hypothalamic upstream regulator of POMC synthesis, *crh* (Chandrasekar *et al.*, 2007), was analysed but no difference in the expression pattern was evident between the controls and *dmrt5* morphants.

Taken together, at least two possible scenarios could explain the observed phenotype (Fig. 55). I) The knock-down of *dmrt*5 function could have negatively influenced the differentiation program and *pomc* progenitor cells transdifferentiate into cell populations of the medial pituitary (gonadotropes, somatotropes, and thyrotropes). Or II) Corticotrope progenitor cells might remain undifferentiated due the *dmrt5* knock-down. Less differentiated cells are usually characterized by a bigger cell size. This would explain why the morphant *prl* expression domains were not as concentrated as they were in control embryos. Furthermore, the larger cell size of undifferentiated corticotrope progenitors and an altered cell-cell interaction would explain why the *prl* expression domain was shifted posteriorly. Considering the role of Dmrt5 as differentiation regulator and its effects on neural stem and/or progenitor cells, the second scenario seems the more favourable option.
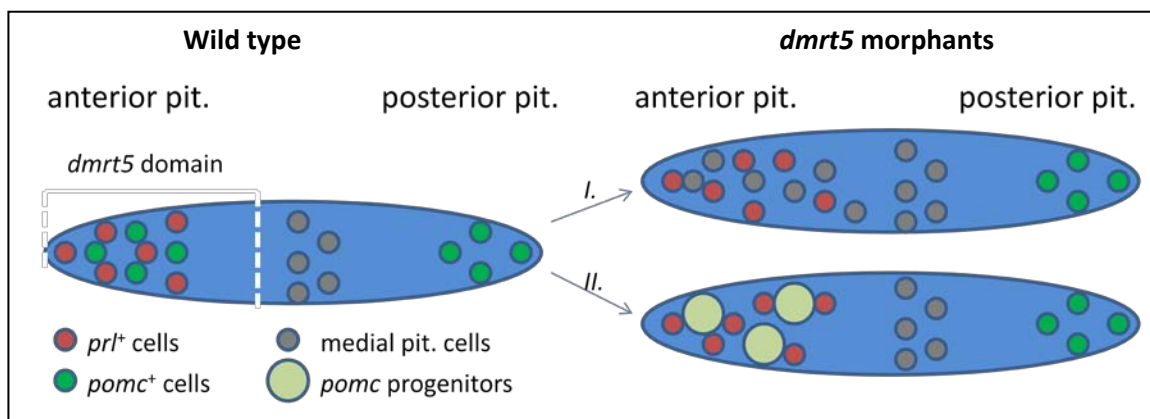
Fig. 55 Proposed model for dmrt5 function during pituitary development: Dmrt5 expression is restricted to anterior pituitary cell populations where it controls corticotrope differentiation. Two hypotheses are possible to explain the underlying molecular mechanism of the observed phenotype. I) Dmrt5 inhibits medial pituitary fates and acts permissively for corticotrope cell fates or II) Dmrt5 is required for proper differentiation of corticotrope progenitor cells, which remains undifferentiated in *dmrt5* morphants.

There were some limitations in the study of the pituitary. Due to their vastly mobile nature of the cells during the first 30 hpf, it was difficult to specifically locate gene expression patterns of the tested proneural genes to the migrating pituitary cells. Therefore, the pituitary was the

only tested structure where a conclusive effect on proneural gene expression could not be shown by RNA *in-situ* hybridisation experiments. The suggested model is based on the loss of a terminally differentiated cell populations and the seemingly conserved role of Dmrt5 as a regulator of proneural gene expression in the other four brain regions.

4.7 Dmrt5 controls neuro-endocrine cell differentiation in the preoptic area and ventral midbrain

The preoptic area and ventral midbrain are known to be the birth places of neuro-endocrine cell populations (Lohr *et al.*, 2011). Effects detected in these areas are both described in this section since underlying mechanisms and affected genes appeared to be similar. In accordance to the observed effects in telencephalon and olfactory epithelia, a knock-down of Dmrt5 function also decreased proneural gene expression (*neurogenin* and *zash1a*) in the preoptic area and ventral midbrain. As a consequence of the diminished proneural gene expression in these domains, an effect on the neuro-endocrine forebrain system was expected. Hence, expression patterns of genes involved in cell fate regulation and cell type specific marker genes were analysed. The three investigated genes *otpa, otpb* and *sim1a* are crucial for development of the neuro-secretory preoptic area and hypothalamus (Del Giacco *et al.*, 2006; Eaton and Glasgow, 2006; Blechman *et al.*, 2007; Eaton and Glasgow, 2007; Eaton *et al.*, 2008). As shown in this study, down-regulation of all three genes was evident in regions of the preoptic area while ventral diencephalic expression domains were only slightly reduced or unaffected. In addition, *sim1a* expression was extenuated in specific ventral midbrain regions. Due to their described roles as neuro-endocrine fate determinants, follow up examinations of neuro-endocrine marker genes (*avpl* and *oxytocin*) were performed to determine the identity of the affected cell populations. In agreement with previous reports by Eaton *et al.*, expression of *avpl* and *oxytocin* was strongly reduced in the preoptic area of *dmrt5* morphants (Eaton *et al.*, 2008). Both genes encode for small peptides with hormonal activity, which are released into the bloodstream from the neuro-endocrine region of the pituitary (Lohr and Hammerschmidt, 2011). It is known that these peptides, among others, are involved during

ion maintenance and osmoregulation (Busby *et al.*, 2010; Gutnick *et al.*, 2011). The lack of expression of both genes could explain the lethality of *dmrt5* morphants between 8 and 11 dpf as a result of impaired osmoregulation, which is of significant importance for survival of aquatic animals. The morphants developed normally during the first few days except that the majority of morphants did not inflate their swim bladder. Around 8 dpf, most of the Dmrt5 depleted zebrafish larvae died and some of them showed indications of impaired osmoregulation, such as massive eye edema or heart edema. In parallel to endocrine cell populations of the preoptic area, I also evaluated the impact of *otpa*, *otpb* and *sim1a* deficiency in hypothalamic neurons. Surprisingly and in contrast to other studies (Del Giacco *et al.*, 2006; Eaton and Glasgow, 2006; Blechman *et al.*, 2007; Eaton and Glasgow, 2007; Eaton *et al.*, 2008), the hypothalamic expression domains of hormone-encoding genes were unaffected in *dmrt5* morphants. Hypothalamic expression patterns of *sst1.1, th, crh, trh* and even *avpl* were unaffected. Although expression levels of hypothalamic fate determinants were reduced the described effects were restricted to the preoptic area and not found in the ventral diencephalon or hypothalamus. The impact on differentiated neuronal populations was limited to altered expression domains of *otpa*, *otpb* and *sim1a,* which suggest that the remaining unchanged expression domains of hypothalamic fate determinants were sufficient to promote normal neuronal development. The obtained discrepancies between our study and other studies stem from different experimental approaches. Our study was based on knock-down of *dmrt5,* which indirectly influenced the neuro-secretory preoptic area by decreasing the expression levels of preoptic fate determinants. In contrast, the previous studies were aimed directly at *otpa*, *otpb* and *sim1a.* As a consequence, ventral diencephalic expression domains of these genes remained unaffected in our approach, while other studies showed the opposite.

Besides the impact on cell populations of the preoptic area, *sim1a* expression diminution was also observed in the ventral midbrain. Sim1a in the ventral midbrain could act as fate determinant in a similar fashion as in the preoptic area or hypothalamus. I saw an effect on the

expression pattern of the neuro-endocrine marker *gnrh2* expression in *dmrt5* morphants. *Gnrh2* positive cell populations in the ventral midbrain were significantly reduced in *dmrt5* morphants when compared to controls. At the moment it is unknown whether the down-regulation of *gnrh2* expression is a direct consequence of the failed neuronal specification due to reduced *sim1a* expression. Underlying molecular mechanisms leading to the reduced *gnrh2* expression are still under investigation. In addition, we are also trying to reveal functional consequences of the GnRH2 reduction. GnRHs regulate sex determination and/or differentiation processes via regulating the levels of sex hormones, follicle stimulating hormone (FSH) and luteinizing hormone (Kwok *et al.*, 2005; So *et al.*, 2005). Therefore, it is of great interest to assess if *dmrt5* morphants have an altered sexual development. Studies have shown that *dmrt* genes are expressed in gonads and control certain aspects of sex determination and/or differentiation in a gonad cell-autonomous manner (Raymond *et al.*, 2000; Kim *et al.*, 2007). In contrast, *dmrt5* is expressed in the fore- and midbrain and controls the development of *gnrh2*$^+$ cells. Based on the described involvement of *dmrt* genes during sex development and a defect on *gnrh2* positive cell populations, it is tempting to speculate that the loss of *gnrh2* expression may affect sex development. However, the sex hormone regulating gonadotropins in zebrafish is GnRH3 and not GnRH2 (Abraham *et al.*, 2010). Expression of *gnrh3* was tested but found to be unaltered in *dmrt5* morphants (data not shown). As a result, it is rather unlikely that the expression levels of FSH and LH are changed. Nevertheless, it cannot be excluded that partial facets of sexual development and/or behaviour will be affected in *dmrt5* morphants. Oka *et al.* showed that *gnrh2*- positive neurons regulate neuronal activity as neuro-modulators in multiple brain regions (Oka, 2010). In addition, it was shown in goldfish and musk shrews that GnRH2 administration changed sexual behaviour (Kauffman *et al.*, 2004; Kauffman *et al.*, 2004; Matsuda *et al.*, 2008). Hence, it could be possible that *dmrt5* morphants exhibit altered sexual behaviours due to reduced levels of *gnrh2* expression. With regards to the family of *dmrt* genes, this would be the first time to show that a member of the *dmrt* family regulates sex development and/or behaviour through a gonad independent mechanism. As *gnrh2*$^+$ cells act most probably neuro-

modulatory on other neuronal cell populations, a lack of *gnrh2* expression would lead to alternate activities in those GnRH2- modulated neuron populations. That means, instead of acting cell-autonomously on specific gonadal cell populations, Dmrt5 could act indirectly on sexual behaviour via controlling *gnrh2*$^+$ cell development and the activity of Gnrh2 regulated neuron populations.

4.8 Future experiments

There are a few more aspects regarding the function of *dmrt5* that are worth examining in future studies. It would be very helpful to identify direct and indirect Dmrt5 target genes via a comparative ChIP and microarray analysis. Dmrt5-ChIP experiments will reveal information about target promoter regions bound by Dmrt5, while loss-of-function (*dmrt5* morphants) and gain-of-function (*dmrt5* BAC transgenic lines) microarray data will help to identify and distinguish directly bound and regulated from indirectly regulated genes. Those genes that are directly regulated by Dmrt5 should appear in overlapping data-sets of ChIP and microarray experiments, while indirectly regulated genes should be only present in the microarray data. One of the addressed questions would be whether Dmrt5 directly binds to the promoters of *sox2* and *her6*. Both genes are neuroectodermal markers as well as factors involved in stem cell maintenance but yet it is unclear if both, only one or none of the genes are direct targets of Dmrt5 (ChIP-microarray data set). If both genes may appear in the ChIP-microarray data set, it seems that Dmrt5 regulates multiple genes that are acting synergistically to each other to maintain early neural stem cell character. If only one of those genes is directly regulated, but the other one indirectly (only microarray data set), it may help to understand the cascade and order of genes that are involved during neural stem cell maintenance as well as at which level of this regulatory hierarchy may Dmrt5 act.

The cortex is a structure in the mammalian brain that is homologous to the zebrafish telencephalon and is important for behavioural patterns. As zebrafish *dmrt5* morphants developed smaller telencephala due to a lack of radial glia and neurons, it could be possible that Dmrt5 morphants show altered behaviour patterns. However, it is very difficult to track a

potential change of behaviour to a particular telencephalic cell population due to the lack of reference data. Therefore, I didn't follow this question during my study. Nevertheless, as the cortex is the mammalian homologue to the zebrafish telencephalon and there are several instances of functional homology between zebrafish *dmrt5* and *dmrt* gens of more recent vertebrate groups, I would also expect smaller cortices in *Dmrt5* knock-out (KO) mice. Due to the fact that the cortex is important for behavioural patterns and the accessibility of brain maps in mice that links particular behaviours to distinct cell populations within the mouse cortex, it should be very interesting to analyse Dmrt5 KO mice for behavioural changes. In this model, one might be able to asses whether the entire cortex or only particular cortical layers are affected by a Dmrt5 knock-out. In addition, it would also be of interest to see if affected cortex structures were linked to distinct sensory, motor or associative fields. If so, *dmrt5* KO mice could be tested specifically for a particular behaviour that is thought to be exclusively linked to the affected brain region. These studies could link the function of Dmrt5 during cortex development and the development and differentiation of neuronal progenitors to behavioural aspects. If links could be established between a behavioural disorder in model organism and the lack of Dmrt5, this information could provide useful hints for understanding so far idiopathic human behavioural disorders.

Another behavioural assay could be conducted in zebrafish for the analysis of Dmrt5 function during olfactory system development. In wild type embryos, small molecules are detected via olfactory sensory neurons, which send out sensory information into the olfactory bulbs where these information gets further processed (Li *et al.*, 2005). The observed phenotypical changes in the olfactory system of *dmrt5* morphants imply that morphants may have problems during olfaction. Firstly, since olfactory sensory neurons detect small molecules and initiate olfaction, the reduced numbers of neurons might reduce the overall capability of chemoreception in *dmrt5* morphants. Secondly, the observed changes in higher olfactory brain centers suggest that *dmrt5* morphants may also have problems in processing olfactory neuronal input. I therefore conducted preliminary behavioural tests to analyse embryonic

olfaction according to a publication from Lindsay and Vogt (Lindsay *et al.*, 2004). In this publication, zebrafish medium was incubated with fish food and filter sterilized to prepare fish food-conditioned medium. The conditioned medium evoked an increased reactivity in young zebrafish larvae after it was added to the larvae, while normal unconditioned medium didn't increase zebrafish activity. To date, experimental outcome is pending since the experimental setting requires further fine-tuning before valid data can be acquired. Once the experimental setting is optimized, *dmrt5* depleted embryos will be checked for behavioural changes during olfaction such as an increased activity of zebrafish larvae after administration of fish food conditioned medium (Lindsay and Vogt, 2004).

Next, based on the experimental data obtained from the analysis of the pituitary in *dmrt5* morphants, it seems that corticotropes progenitors either I) transdifferentiated into medial pituitary cell types or II) remained completely undifferentiated. The first possibility could be tested by double WISH, through the analysis of *prl* and medial pituitary markers. *Prl* positive cells in anterior pituitary parts should not intermingle with medial pituitary cell populations. However, if lactotropes would be found intermingled with gonadotropes, thyrotropes or somatotropes, transdifferentiation processes might have taken place. This would explain the loss of *pomc* positive cells and the loosened *prl* positive cell cluster. Since the *prl* positive adjacent cells are from unusual origin, cell-cell interaction may be influenced and the whole *prl* positive domain is loosened and shifted posteriorly. In this scenario, Dmrt5 acts as the permitting factor of corticotrope differentiation by blocking medial pituitary cell fates. To address possibility II) The active and terminally differentiated neuro-endocrine cells can be distinguished from undifferentiated cells based on their sub-cellular compartments. If corticotrope cells remained undifferentiated, I would expect to see less active and smaller organelles involved in hormone synthesis (e.g. Golgi-apparatus). The use of electron-microscopy could help to identify undifferentiated pomc progenitor cells in the pituitaries of *dmrt5* morphants.

Lastly, findings made in the ventral midbrain of *dmrt5* morphants suggest an indirect role of Dmrt5 during sex development via a possible alteration of gonadotropin expression levels. The expression changes could result in alterations of sexual behaviour or gonad development. Hypothetically, these *dmrt5* morpholino mediated alterations of sexual behaviour or gonad development need to be tested by behavioural studies and gonad analysis in *dmrt5* morphant adults. The use of *dmrt5* morphants that are devoid of Dmrt5 function during the first few days of development provides a great tool to separate early Dmrt5 functions on gonadal development and sex differentiation via *gnrh2* from those functions that are mediated through its gonadal expression at much later stages (Guo *et al.*, 2004).

4.9 Conclusion

As a final conclusion, the presented data strongly suggest a possible role for Dmrt3 during terminal differentiation of dorsal telencephalic and olfactory placode neurons and an essential role for Dmrt5 in transcriptional regulation of genetic networks involved in neuronal differentiation. Dmrt5 controls neuronal differentiation and specification throughout the developing embryonic brain in a context sensitive manner. The best example to illustrate this functional diversity are the described impacts on the olfactory epithelium and telencephalon. While telencephalic expression of *neuroD* was reduced in *dmrt5* morphants, olfactory epithelium expression of *neuroD* remained unaffected. In contrast, olfactory stem and/or progenitor cells became apoptotic in morphants while telencephalic stem cells were maintained at an early stage. A possible explanation for these tissue specific effects in morphants could be that Dmrt5 interacts with various tissue specific co-regulators. However, all of the characterized brain regions showed impaired neuronal differentiation that manifest as severe morphological and/or physiological defects of the forebrain.

Future experiments using *dmrt5* knock-down and *dmrt3* knock-out approaches will help to elucidate yet unanswered questions and complete the hypothesized models for Dmrt3 and Dmrt5 function during fore- and midbrain development.

5. References

Abraham, E., Palevitch, O., Gothilf, Y. and Zohar, Y. (2010). "*Targeted gonadotropin-releasing hormone-3 neuron ablation in zebrafish: effects on neurogenesis, neuronal migration, and reproduction*." **Endocrinology** 151(1): 332-40.

Akazawa, C., Sasai, Y., Nakanishi, S. and Kageyama, R. (1992). "*Molecular characterization of a rat negative regulator with a basic helix-loop-helix structure predominantly expressed in the developing nervous system*." **J Biol Chem** 267(30): 21879-85.

Alberts, B., Johnson, A. and Lewis, J. e. a. (2002). "*Molecular Biology of the Cell. 4th edition.*".

Alexandre, P., Reugels, A. M., Barker, D., Blanc, E. and Clarke, J. D. (2010). "*Neurons derive from the more apical daughter in asymmetric divisions in the zebrafish neural tube*." **Nat Neurosci** 13(6): 673-9.

Alsop, D. and Vijayan, M. (2009). "*The zebrafish stress axis: molecular fallout from the teleost-specific genome duplication event*." **Gen Comp Endocrinol** 161(1): 62-6.

Alsop, D. and Vijayan, M. M. (2009). "*Molecular programming of the corticosteroid stress axis during zebrafish development*." **Comp Biochem Physiol A Mol Integr Physiol** 153(1): 49-54.

Amirthalingam, K., Lorens, J. B., Saetre, B. O., Salaneck, E. and Fjose, A. (1995). "*Embryonic expression and DNA-binding properties of zebrafish pax-6*." **Biochem Biophys Res Commun** 215(1): 122-8.

Bae, Y. K., Shimizu, T. and Hibi, M. (2005). "*Patterning of proneuronal and inter-proneuronal domains by hairy- and enhancer of split-related genes in zebrafish neuroectoderm*." **Development** 132(6): 1375-85.

Baek, J. H., Hatakeyama, J., Sakamoto, S., Ohtsuka, T. and Kageyama, R. (2006). "*Persistent and high levels of Hes1 expression regulate boundary formation in the developing central nervous system*." **Development** 133(13): 2467-76.

Bally-Cuif, L. and Hammerschmidt, M. (2003). "*Induction and patterning of neuronal development, and its connection to cell cycle control*." **Curr Opin Neurobiol** 13(1): 16-25.

Barami, K., Iversen, K., Furneaux, H. and Goldman, S. A. (1995). "*Hu protein as an early marker of neuronal phenotypic differentiation by subependymal zone cells of the adult songbird forebrain*." **J Neurobiol** 28(1): 82-101.

Bertrand, N., Castro, D. S. and Guillemot, F. (2002). "*Proneural genes and the specification of neural cell types*." **Nat Rev Neurosci** 3(7): 517-30.

Bibikova, M., Carroll, D., Segal, D. J., Trautman, J. K., Smith, J., Kim, Y. G. and Chandrasegaran, S. (2001). "*Stimulation of homologous recombination through targeted cleavage by chimeric nucleases*." **Mol Cell Biol** 21(1): 289-97.

Bibikova, M., Golic, M., Golic, K. G. and Carroll, D. (2002). "*Targeted chromosomal cleavage and mutagenesis in Drosophila using zinc-finger nucleases*." **Genetics** 161(3): 1169-75.

Blader, P., Fischer, N., Gradwohl, G., Guillemot, F. and Strahle, U. (1997). "*The activity of neurogenin1 is controlled by local cues in the zebrafish embryo*." **Development** 124(22): 4557-69.

Blechman, J., Borodovsky, N., Eisenberg, M., Nabel-Rosen, H., Grimm, J. and Levkowitz, G. (2007). "*Specification of hypothalamic neurons by dual regulation of the homeodomain protein Orthopedia*." **Development** 134(24): 4417-26.

Bownes, M. (1994). "*The regulation of the yolk protein genes, a family of sex differentiation genes in Drosophila melanogaster*." **Bioessays** 16(10): 745-52.

Brayer, K. J. and Segal, D. J. (2008). "*Keep your fingers off my DNA: protein-protein interactions mediated by C2H2 zinc finger domains*." **Cell Biochem Biophys** 50(3): 111-31.

Busby, E. R., Roch, G. J. and Sherwood, N. M. (2010). "*Endocrinology of zebrafish: a small fish with a large gene pool*." **Zebrafish,eds Perry S. F., Ekker M., Farrell A.P., Brauner C. J.**: 173–247.

Cathomen, T. and Joung, J. K. (2008). "*Zinc-finger nucleases: the next generation emerges*." **Mol Ther** 16(7): 1200-7.

Cau, E. and Blader, P. (2009). "*Notch activity in the nervous system: to switch or not switch?*" **Neural Dev** 4: 36.

Chandrasekar, G., Lauter, G. and Hauptmann, G. (2007). "*Distribution of corticotropin-releasing hormone in the developing zebrafish brain*." **J Comp Neurol** 505(4): 337-51.

Chapouton, P., Skupien, P., Hesl, B., Coolen, M., Moore, J. C., Madelaine, R., Kremmer, E., Faus-Kessler, T., Blader, P., Lawson, N. D. and Bally-Cuif, L. (2010). "*Notch activity levels control the balance between quiescence and recruitment of adult neural stem cells*." **J Neurosci** 30(23): 7961-74.

Collignon, J., Sockanathan, S., Hacker, A., Cohen-Tannoudji, M., Norris, D., Rastan, S., Stevanovic, M., Goodfellow, P. N. and Lovell-Badge, R. (1996). "*A comparison of the properties of Sox-3 with Sry and two related genes, Sox-1 and Sox-2*." **Development** 122(2): 509-20.

Del Giacco, L., Pistocchi, A., Cotelli, F., Fortunato, A. E. and Sordino, P. (2008). "*A peek inside the neurosecretory brain through Orthopedia lenses*." **Dev Dyn** 237(9): 2295-303.

Del Giacco, L., Sordino, P., Pistocchi, A., Andreakis, N., Tarallo, R., Di Benedetto, B. and Cotelli, F. (2006). "*Differential regulation of the zebrafish orthopedia 1 gene during fate determination of diencephalic neurons*." **BMC Dev Biol** 6: 50.

Dong, Z., Yang, N., Yeo, S. Y., Chitnis, A. and Guo, S. (2012). "*Intralineage directional Notch signaling regulates self-renewal and differentiation of asymmetrically dividing radial glia*." **Neuron** 74(1): 65-78.

Doyon, Y., McCammon, J. M., Miller, J. C., Faraji, F., Ngo, C., Katibah, G. E., Amora, R., Hocking, T. D., Zhang, L., Rebar, E. J., Gregory, P. D., Urnov, F. D. and Amacher, S. L. (2008).

"*Heritable targeted gene disruption in zebrafish using designed zinc-finger nucleases*." **Nat Biotechnol** 26(6): 702-8.

Dutta, S., Dietrich, J. E., Aspock, G., Burdine, R. D., Schier, A., Westerfield, M. and Varga, Z. M. (2005). "*pitx3 defines an equivalence domain for lens and anterior pituitary placode*." **Development** 132(7): 1579-90.

Dutta, S., Dietrich, J. E., Westerfield, M. and Varga, Z. M. (2008). "*Notch signaling regulates endocrine cell specification in the zebrafish anterior pituitary*." **Dev Biol** 319(2): 248-57.

Eaton, J. L. and Glasgow, E. (2006). "*The zebrafish bHLH PAS transcriptional regulator, single-minded 1 (sim1), is required for isotocin cell development*." **Dev Dyn** 235(8): 2071-82.

Eaton, J. L. and Glasgow, E. (2007). "*Zebrafish orthopedia (otp) is required for isotocin cell development*." **Dev Genes Evol** 217(2): 149-58.

Eaton, J. L., Holmqvist, B. and Glasgow, E. (2008). "*Ontogeny of vasotocin-expressing cells in zebrafish: selective requirement for the transcriptional regulators orthopedia and single-minded 1 in the preoptic area*." **Dev Dyn** 237(4): 995-1005.

Elrod-Erickson, M., Rould, M. A., Nekludova, L. and Pabo, C. O. (1996). "*Zif268 protein-DNA complex refined at 1.6 A: a model system for understanding zinc finger-DNA interactions*." **Structure** 4(10): 1171-80.

Feng, L., Hatten, M. E. and Heintz, N. (1994). "*Brain lipid-binding protein (BLBP): a novel signaling system in the developing mammalian CNS*." **Neuron** 12(4): 895-908.

Fishell, G. and Kriegstein, A. R. (2003). "*Neurons from radial glia: the consequences of asymmetric inheritance*." **Curr Opin Neurobiol** 13(1): 34-41.

Fortini, M. E. (2009). "*Notch signaling: the core pathway and its posttranslational regulation*." **Dev Cell** 16(5): 633-47.

Geling, A., Itoh, M., Tallafuss, A., Chapouton, P., Tannhauser, B., Kuwada, J. Y., Chitnis, A. B. and Bally-Cuif, L. (2003). "*bHLH transcription factor Her5 links patterning to regional inhibition of neurogenesis at the midbrain-hindbrain boundary*." **Development** 130(8): 1591-604.

Geling, A., Plessy, C., Rastegar, S., Strahle, U. and Bally-Cuif, L. (2004). "*Her5 acts as a prepattern factor that blocks neurogenin1 and coe2 expression upstream of Notch to inhibit neurogenesis at the midbrain-hindbrain boundary*." **Development** 131(9): 1993-2006.

Gennet, N., Gale, E., Nan, X., Farley, E., Takacs, K., Oberwallner, B., Chambers, D. and Li, M. (2010). "*Doublesex and mab-3-related transcription factor 5 promotes midbrain dopaminergic identity in pluripotent stem cells by enforcing a ventral-medial progenitor fate*." **Proc Natl Acad Sci U S A** 108(22): 9131-6.

Graham, V., Khudyakov, J., Ellis, P. and Pevny, L. (2003). "*SOX2 functions to maintain neural progenitor identity*." **Neuron** 39(5): 749-65.

Greenwald, I. and Rubin, G. M. (1992). "*Making a difference: the role of cell-cell interactions in establishing separate identities for equivalent cells*." **Cell** 68(2): 271-81.

Guillemot, F. (1999). "*Vertebrate bHLH genes and the determination of neuronal fates*." **Exp Cell Res** 253(2): 357-64.

Guo, Y., Cheng, H., Huang, X., Gao, S., Yu, H. and Zhou, R. (2005). "*Gene structure, multiple alternative splicing, and expression in gonads of zebrafish Dmrt1*." **Biochem Biophys Res Commun** 330(3): 950-7.

Guo, Y., Li, Q., Gao, S., Zhou, X., He, Y., Shang, X., Cheng, H. and Zhou, R. (2004). "*Molecular cloning, characterization, and expression in brain and gonad of Dmrt5 of zebrafish*." **Biochem Biophys Res Commun** 324(2): 569-75.

Gutnick, A., Blechman, J., Kaslin, J., Herwig, L., Belting, H. G., Affolter, M., Bonkowsky, J. L. and Levkowitz, G. (2011). "*The hypothalamic neuropeptide oxytocin is required for formation of the neurovascular interface of the pituitary*." **Dev Cell** 21(4): 642-54.

Hansen, I. A., To, T. T., Wortmann, S., Burmester, T., Winkler, C., Meyer, S. R., Neuner, C., Fassnacht, M. and Allolio, B. (2003). "*The pro-opiomelanocortin gene of the zebrafish (Danio rerio)*." **Biochem Biophys Res Commun** 303(4): 1121-8.

Hatakeyama, J., Bessho, Y., Katoh, K., Ookawara, S., Fujioka, M., Guillemot, F. and Kageyama, R. (2004). "*Hes genes regulate size, shape and histogenesis of the nervous system by control of the timing of neural stem cell differentiation*." **Development** 131(22): 5539-50.

Hemmati-Brivanlou, A. and Melton, D. (1997). "*Vertebrate embryonic cells will become nerve cells unless told otherwise*." **Cell** 88(1): 13-7.

Herzog, W., Sonntag, C., von der Hardt, S., Roehl, H. H., Varga, Z. M. and Hammerschmidt, M. (2004). "*Fgf3 signaling from the ventral diencephalon is required for early specification and subsequent survival of the zebrafish adenohypophysis*." **Development** 131(15): 3681-92.

Herzog, W., Zeng, X., Lele, Z., Sonntag, C., Ting, J. W., Chang, C. Y. and Hammerschmidt, M. (2003). "*Adenohypophysis formation in the zebrafish and its dependence on sonic hedgehog*." **Dev Biol** 254(1): 36-49.

Hirata, H., Tomita, K., Bessho, Y. and Kageyama, R. (2001). "*Hes1 and Hes3 regulate maintenance of the isthmic organizer and development of the mid/hindbrain*." **EMBO J** 20(16): 4454-66.

Hong, C. S., Park, B. Y. and Saint-Jeannet, J. P. (2007). "*The function of Dmrt genes in vertebrate development: it is not just about sex*." **Dev Biol** 310(1): 1-9.

Huang, X., Hong, C. S., O'Donnell, M. and Saint-Jeannet, J. P. (2005). "*The doublesex-related gene, XDmrt4, is required for neurogenesis in the olfactory system*." **Proc Natl Acad Sci U S A** 102(32): 11349-54.

Ishibashi, M., Ang, S. L., Shiota, K., Nakanishi, S., Kageyama, R. and Guillemot, F. (1995). "*Targeted disruption of mammalian hairy and Enhancer of split homolog-1 (HES-1) leads to*

up-regulation of neural helix-loop-helix factors, premature neurogenesis, and severe neural tube defects." **Genes Dev** 9(24): 3136-48.

Ishibashi, M., Moriyoshi, K., Sasai, Y., Shiota, K., Nakanishi, S. and Kageyama, R. (1994). "*Persistent expression of helix-loop-helix factor HES-1 prevents mammalian neural differentiation in the central nervous system*." **EMBO J** 13(8): 1799-805.

Itoh, M., Kim, C. H., Palardy, G., Oda, T., Jiang, Y. J., Maust, D., Yeo, S. Y., Lorick, K., Wright, G. J., Ariza-McNaughton, L., Weissman, A. M., Lewis, J., Chandrasekharappa, S. C. and Chitnis, A. B. (2003). "*Mind bomb is a ubiquitin ligase that is essential for efficient activation of Notch signaling by Delta*." **Dev Cell** 4(1): 67-82.

Kageyama, R., Ohtsuka, T. and Kobayashi, T. (2008). "*Roles of Hes genes in neural development*." **Dev Growth Differ** 50 Suppl 1: S97-103.

Kageyama, R., Ohtsuka, T., Shimojo, H. and Imayoshi, I. (2008). "*Dynamic Notch signaling in neural progenitor cells and a revised view of lateral inhibition*." **Nat Neurosci** 11(11): 1247-51.

Kauffman, A. S. and Rissman, E. F. (2004). "*A critical role for the evolutionarily conserved gonadotropin-releasing hormone II: mediation of energy status and female sexual behavior*." **Endocrinology** 145(8): 3639-46.

Kauffman, A. S. and Rissman, E. F. (2004). "*The evolutionarily conserved gonadotropin-releasing hormone II modifies food intake*." **Endocrinology** 145(2): 686-91.

Kersey, P., Bower, L., Morris, L., Horne, A., Petryszak, R., Kanz, C., Kanapin, A., Das, U., Michoud, K., Phan, I., Gattiker, A., Kulikova, T., Faruque, N., Duggan, K., McLaren, P., Reimholz, B., Duret, L., Penel, S., Reuter, I. and Apweiler, R. (2005). "*Integr8 and Genome Reviews: integrated views of complete genomes and proteomes*." **Nucleic Acids Res** 33(Database issue): D297-302.

Kim, C. H., Bae, Y. K., Yamanaka, Y., Yamashita, S., Shimizu, T., Fujii, R., Park, H. C., Yeo, S. Y., Huh, T. L., Hibi, M. and Hirano, T. (1997). "*Overexpression of neurogenin induces ectopic expression of HuC in zebrafish*." **Neurosci Lett** 239(2-3): 113-6.

Kim, C. H., Ueshima, E., Muraoka, O., Tanaka, H., Yeo, S. Y., Huh, T. L. and Miki, N. (1996). "*Zebrafish elav/HuC homologue as a very early neuronal marker*." **Neurosci Lett** 216(2): 109-12.

Kim, P., Helms, A. W., Johnson, J. E. and Zimmerman, K. (1997). "*XATH-1, a vertebrate homolog of Drosophila atonal, induces a neuronal differentiation within ectodermal progenitors*." **Dev Biol** 187(1): 1-12.

Kim, S., Bardwell, V. J. and Zarkower, D. (2007). "*Cell type-autonomous and non-autonomous requirements for Dmrt1 in postnatal testis differentiation*." **Dev Biol** 307(2): 314-27.

Kimmel, C. B., Ballard, W. W., Kimmel, S. R., Ullmann, B. and Schilling, T. F. (1995). "*Stages of embryonic development of the zebrafish*." **Dev Dyn** 203(3): 253-310.

Kimmel, C. B., Hatta, K. and Eisen, J. S. (1991). "*Genetic control of primary neuronal development in zebrafish*." **Development** Suppl 2: 47-57.

Korzh, V., Sleptsova, I., Liao, J., He, J. and Gong, Z. (1998). "*Expression of zebrafish bHLH genes ngn1 and nrd defines distinct stages of neural differentiation*." **Dev Dyn** 213(1): 92-104.

Krauss, S., Johansen, T., Korzh, V. and Fjose, A. (1991). "*Expression of the zebrafish paired box gene pax[zf-b] during early neurogenesis*." **Development** 113(4): 1193-206.

Kriegstein, A. R. and Gotz, M. (2003). "*Radial glia diversity: a matter of cell fate*." **Glia** 43(1): 37-43.

Krishna, S. S., Majumdar, I. and Grishin, N. V. (2003). "*Structural classification of zinc fingers: survey and summary*." **Nucleic Acids Res** 31(2): 532-50.

Kwok, H. F., So, W. K., Wang, Y. and Ge, W. (2005). "*Zebrafish gonadotropins and their receptors: I. Cloning and characterization of zebrafish follicle-stimulating hormone and luteinizing hormone receptors--evidence for their distinct functions in follicle development*." **Biol Reprod** 72(6): 1370-81.

Lee, J. E. (1997). "*Basic helix-loop-helix genes in neural development*." **Curr Opin Neurobiol** 7(1): 13-20.

Levitt, P. and Rakic, P. (1980). "*Immunoperoxidase localization of glial fibrillary acidic protein in radial glial cells and astrocytes of the developing rhesus monkey brain*." **J Comp Neurol** 193(3): 815-40.

Li, J., Mack, J. A., Souren, M., Yaksi, E., Higashijima, S., Mione, M., Fetcho, J. R. and Friedrich, R. W. (2005). "*Early development of functional spatial maps in the zebrafish olfactory bulb*." **J Neurosci** 25(24): 5784-95.

Li, Q., Zhou, X., Guo, Y., Shang, X., Chen, H., Lu, H., Cheng, H. and Zhou, R. (2008). "*Nuclear localization, DNA binding and restricted expression in neural and germ cells of zebrafish Dmrt3*." **Biol Cell** 100(8): 453-63.

Lindsay, S. M. and Vogt, R. G. (2004). "*Behavioral responses of newly hatched zebrafish (Danio rerio) to amino acid chemostimulants*." **Chem Senses** 29(2): 93-100.

Liour, S. S. and Yu, R. K. (2003). "*Differentiation of radial glia-like cells from embryonic stem cells*." **Glia** 42(2): 109-17.

Lohr, H. and Hammerschmidt, M. (2011). "*Zebrafish in endocrine systems: recent advances and implications for human disease*." **Annu Rev Physiol** 73: 183-211.

Lohr, H., Ryu, S. and Driever, W. (2009). "*Zebrafish diencephalic A11-related dopaminergic neurons share a conserved transcriptional network with neuroendocrine cell lineages*." **Development** 136(6): 1007-17.

Madelaine, R., Garric, L. and Blader, P. (2011). "*Partially redundant proneural function reveals the importance of timing during zebrafish olfactory neurogenesis*." **Development** 138(21): 4753-62.

Marz, M., Chapouton, P., Diotel, N., Vaillant, C., Hesl, B., Takamiya, M., Lam, C. S., Kah, O., Bally-Cuif, L. and Strahle, U. (2010). "*Heterogeneity in progenitor cell subtypes in the ventricular zone of the zebrafish adult telencephalon*." **Glia** 58(7): 870-88.

Matson, C. K. and Zarkower, D. (2012). "*Sex and the singular DM domain: insights into sexual regulation, evolution and plasticity*." **Nat Rev Genet** 13(3): 163-74.

Matsuda, K., Nakamura, K., Shimakura, S., Miura, T., Kageyama, H., Uchiyama, M., Shioda, S. and Ando, H. (2008). "*Inhibitory effect of chicken gonadotropin-releasing hormone II on food intake in the goldfish, Carassius auratus*." **Horm Behav** 54(1): 83-9.

Matsuda, M., Nagahama, Y., Shinomiya, A., Sato, T., Matsuda, C., Kobayashi, T., Morrey, C. E., Shibata, N., Asakawa, S., Shimizu, N., Hori, H., Hamaguchi, S. and Sakaizumi, M. (2002). "*DMY is a Y-specific DM-domain gene required for male development in the medaka fish*." **Nature** 417(6888): 559-63.

Matthews, J. M. and Sunde, M. (2002). "*Zinc fingers--folds for many occasions*." **IUBMB Life** 54(6): 351-5.

Meeker, N. D., Hutchinson, S. A., Ho, L. and Trede, N. S. (2007). "*Method for isolation of PCR-ready genomic DNA from zebrafish tissues*." **Biotechniques** 43(5): 610, 612, 614.

Meng, A., Moore, B., Tang, H., Yuan, B. and Lin, S. (1999). "*A Drosophila doublesex-related gene, terra, is involved in somitogenesis in vertebrates*." **Development** 126(6): 1259-68.

Meng, X., Noyes, M. B., Zhu, L. J., Lawson, N. D. and Wolfe, S. A. (2008). "*Targeted gene inactivation in zebrafish using engineered zinc-finger nucleases*." **Nat Biotechnol** 26(6): 695-701.

Meng, X. and Wolfe, S. A. (2006). "*Identifying DNA sequences recognized by a transcription factor using a bacterial one-hybrid system*." **Nat Protoc** 1(1): 30-45.

Misson, J. P., Edwards, M. A., Yamamoto, M. and Caviness, V. S., Jr. (1988). "*Identification of radial glial cells within the developing murine central nervous system: studies based upon a new immunohistochemical marker*." **Brain Res Dev Brain Res** 44(1): 95-108.

Mizuseki, K., Kishi, M., Matsui, M., Nakanishi, S. and Sasai, Y. (1998). "*Xenopus Zic-related-1 and Sox-2, two factors induced by chordin, have distinct activities in the initiation of neural induction*." **Development** 125(4): 579-87.

Mizutani, K., Yoon, K., Dang, L., Tokunaga, A. and Gaiano, N. (2007). "*Differential Notch signalling distinguishes neural stem cells from intermediate progenitors*." **Nature** 449(7160): 351-5.

Murphy, M. W., Zarkower, D. and Bardwell, V. J. (2007). "*Vertebrate DM domain proteins bind similar DNA sequences and can heterodimerize on DNA*." **BMC Mol Biol** 8: 58.

Narendra, U., Zhu, L., Li, B., Wilken, J. and Weiss, M. A. (2002). "*Sex-specific gene regulation. The Doublesex DM motif is a bipartite DNA-binding domain*." **J Biol Chem** 277(45): 43463-73.

Nieto, M., Schuurmans, C., Britz, O. and Guillemot, F. (2001). "*Neural bHLH genes control the neuronal versus glial fate decision in cortical progenitors*." **Neuron** 29(2): 401-13.

Ninkovic, J., Tallafuss, A., Leucht, C., Topczewski, J., Tannhauser, B., Solnica-Krezel, L. and Bally-Cuif, L. (2005). "*Inhibition of neurogenesis at the zebrafish midbrain-hindbrain boundary by the combined and dose-dependent activity of a new hairy/E(spl) gene pair*." **Development** 132(1): 75-88.

Noctor, S. C., Flint, A. C., Weissman, T. A., Dammerman, R. S. and Kriegstein, A. R. (2001). "*Neurons derived from radial glial cells establish radial units in neocortex*." **Nature** 409(6821): 714-20.

Noctor, S. C., Flint, A. C., Weissman, T. A., Wong, W. S., Clinton, B. K. and Kriegstein, A. R. (2002). "*Dividing precursor cells of the embryonic cortical ventricular zone have morphological and molecular characteristics of radial glia*." **J Neurosci** 22(8): 3161-73.

Noyes, M. B., Meng, X., Wakabayashi, A., Sinha, S., Brodsky, M. H. and Wolfe, S. A. (2008). "*A systematic characterization of factors that regulate Drosophila segmentation via a bacterial one-hybrid system*." **Nucleic Acids Res** 36(8): 2547-60.

Ohtsuka, T., Sakamoto, M., Guillemot, F. and Kageyama, R. (2001). "*Roles of the basic helix-loop-helix genes Hes1 and Hes5 in expansion of neural stem cells of the developing brain*." **J Biol Chem** 276(32): 30467-74.

Oka, Y. (2010). "*Electrophysiological characteristics of gonadotrophin-releasing hormone 1-3 neurones: insights from a study of fish brains*." **J Neuroendocrinol** 22(7): 659-63.

Okuda, Y., Yoda, H., Uchikawa, M., Furutani-Seiki, M., Takeda, H., Kondoh, H. and Kamachi, Y. (2006). "*Comparative genomic and expression analysis of group B1 sox genes in zebrafish indicates their diversification during vertebrate evolution*." **Dev Dyn** 235(3): 811-25.

Pasini, A., Henrique, D. and Wilkinson, D. G. (2001). "*The zebrafish Hairy/Enhancer-of-split-related gene her6 is segmentally expressed during the early development of hindbrain and somites*." **Mech Dev** 100(2): 317-21.

Pellegrini, E., Mouriec, K., Anglade, I., Menuet, A., Le Page, Y., Gueguen, M. M., Marmignon, M. H., Brion, F., Pakdel, F. and Kah, O. (2007). "*Identification of aromatase-positive radial glial cells as progenitor cells in the ventricular layer of the forebrain in zebrafish*." **J Comp Neurol** 501(1): 150-67.

Pevny, L. H., Sockanathan, S., Placzek, M. and Lovell-Badge, R. (1998). "*A role for SOX1 in neural determination*." **Development** 125(10): 1967-78.

Pogoda, H. M., von der Hardt, S., Herzog, W., Kramer, C., Schwarz, H. and Hammerschmidt, M. (2006). "*The proneural gene ascl1a is required for endocrine differentiation and cell survival in the zebrafish adenohypophysis*." **Development** 133(6): 1079-89.

Rajaei, F. (PhD Thesis 2012). "*Dmrt3 controls V0D interneuron formation and is regulated by Tcf3 and retinoic acid signalling in zebrafish* ".

Rakic, P. (1972). "*Mode of cell migration to the superficial layers of fetal monkey neocortex.*" **J Comp Neurol** 145(1): 61-83.

Rakic, P. (1995). "*A small step for the cell, a giant leap for mankind: a hypothesis of neocortical expansion during evolution.*" **Trends Neurosci** 18(9): 383-8.

Raymond, C. S., Murphy, M. W., O'Sullivan, M. G., Bardwell, V. J. and Zarkower, D. (2000). "*Dmrt1, a gene related to worm and fly sexual regulators, is required for mammalian testis differentiation.*" **Genes Dev** 14(20): 2587-95.

Raymond, C. S., Shamu, C. E., Shen, M. M., Seifert, K. J., Hirsch, B., Hodgkin, J. and Zarkower, D. (1998). "*Evidence for evolutionary conservation of sex-determining genes.*" **Nature** 391(6668): 691-5.

Raymond, P. A., Barthel, L. K., Bernardos, R. L. and Perkowski, J. J. (2006). "*Molecular characterization of retinal stem cells and their niches in adult zebrafish.*" **BMC Dev Biol** 6: 36.

Reversade, B. and De Robertis, E. M. (2005). "*Regulation of ADMP and BMP2/4/7 at opposite embryonic poles generates a self-regulating morphogenetic field.*" **Cell** 123(6): 1147-60.

Reversade, B., Kuroda, H., Lee, H., Mays, A. and De Robertis, E. M. (2005). "*Depletion of Bmp2, Bmp4, Bmp7 and Spemann organizer signals induces massive brain formation in Xenopus embryos.*" **Development** 132(15): 3381-92.

Rink, E. and Wullimann, M. F. (2001). "*The teleostean (zebrafish) dopaminergic system ascending to the subpallium (striatum) is located in the basal diencephalon (posterior tuberculum).*" **Brain Res** 889(1-2): 316-30.

Rink, E. and Wullimann, M. F. (2002). "*Development of the catecholaminergic system in the early zebrafish brain: an immunohistochemical study.*" **Brain Res Dev Brain Res** 137(1): 89-100.

Robu, M. E., Larson, J. D., Nasevicius, A., Beiraghi, S., Brenner, C., Farber, S. A. and Ekker, S. C. (2007). "*p53 activation by knockdown technologies.*" **PLoS Genet** 3(5): e78.

Ryu, S., Holzschuh, J., Mahler, J. and Driever, W. (2006). "*Genetic analysis of dopaminergic system development in zebrafish.*" **J Neural Transm Suppl**(70): 61-6.

Sasai, Y., Kageyama, R., Tagawa, Y., Shigemoto, R. and Nakanishi, S. (1992). "*Two mammalian helix-loop-helix factors structurally related to Drosophila hairy and Enhancer of split.*" **Genes Dev** 6(12B): 2620-34.

Sato, T., Rocancourt, D., Marques, L., Thorsteinsdottir, S. and Buckingham, M. (2010). "*A Pax3/Dmrt2/Myf5 regulatory cascade functions at the onset of myogenesis.*" **PLoS Genet** 6(4): e1000897.

Saude, L., Lourenco, R., Goncalves, A. and Palmeirim, I. (2005). "*terra is a left-right asymmetry gene required for left-right synchronization of the segmentation clock*." **Nat Cell Biol** 7(9): 918-20.

Scholpp, S., Delogu, A., Gilthorpe, J., Peukert, D., Schindler, S. and Lumsden, A. (2009). "*Her6 regulates the neurogenetic gradient and neuronal identity in the thalamus*." **Proc Natl Acad Sci U S A** 106(47): 19895-900.

Schweitzer, J., Lohr, H., Filippi, A. and Driever, W. (2012). "*Dopaminergic and noradrenergic circuit development in zebrafish*." **Dev Neurobiol** 72(3): 256-68.

Shankaran, S. S., Sieger, D., Schroter, C., Czepe, C., Pauly, M. C., Laplante, M. A., Becker, T. S., Oates, A. C. and Gajewski, M. (2007). "*Completing the set of h/E(spl) cyclic genes in zebrafish: her12 and her15 reveal novel modes of expression and contribute to the segmentation clock*." **Dev Biol** 304(2): 615-32.

Shen, M. M. and Hodgkin, J. (1988). "*mab-3, a gene required for sex-specific yolk protein expression and a male-specific lineage in C. elegans*." **Cell** 54(7): 1019-31.

Shimojo, H., Ohtsuka, T. and Kageyama, R. (2008). "*Oscillations in notch signaling regulate maintenance of neural progenitors*." **Neuron** 58(1): 52-64.

Skeath, J. B. and Carroll, S. B. (1992). "*Regulation of proneural gene expression and cell fate during neuroblast segregation in the Drosophila embryo*." **Development** 114(4): 939-46.

Smith, J., Bibikova, M., Whitby, F. G., Reddy, A. R., Chandrasegaran, S. and Carroll, D. (2000). "*Requirements for double-strand cleavage by chimeric restriction enzymes with zinc finger DNA-recognition domains*." **Nucleic Acids Res** 28(17): 3361-9.

So, W. K., Kwok, H. F. and Ge, W. (2005). "*Zebrafish gonadotropins and their receptors: II. Cloning and characterization of zebrafish follicle-stimulating hormone and luteinizing hormone subunits--their spatial-temporal expression patterns and receptor specificity*." **Biol Reprod** 72(6): 1382-96.

Stern, C. D. (2005). "*Neural induction: old problem, new findings, yet more questions*." **Development** 132(9): 2007-21.

Szarek, E., Cheah, P. S., Schwartz, J. and Thomas, P. "*Molecular genetics of the developing neuroendocrine hypothalamus*." **Mol Cell Endocrinol** 323(1): 115-23.

Takizawa, T., Nakashima, K., Namihira, M., Ochiai, W., Uemura, A., Yanagisawa, M., Fujita, N., Nakao, M. and Taga, T. (2001). "*DNA methylation is a critical cell-intrinsic determinant of astrocyte differentiation in the fetal brain*." **Dev Cell** 1(6): 749-58.

Takke, C., Dornseifer, P., v Weizsacker, E. and Campos-Ortega, J. A. (1999). "*her4, a zebrafish homologue of the Drosophila neurogenic gene E(spl), is a target of NOTCH signalling*." **Development** 126(9): 1811-21.

Volff, J. N., Zarkower, D., Bardwell, V. J. and Schartl, M. (2003). "*Evolutionary dynamics of the DM domain gene family in metazoans*." **J Mol Evol** 57 Suppl 1: S241-9.

Wang, X., Gao, C. and Norgren, R. B., Jr. (2001). "*Cellular interactions in the development of the olfactory system: an ablation and homotypic transplantation analysis.*" **J Neurobiol** 49(1): 29-39.

Whitlock, K. E. (2004). "*A new model for olfactory placode development.*" **Brain Behav Evol** 64(3): 126-40.

Whitlock, K. E. and Westerfield, M. (2000). "*The olfactory placodes of the zebrafish form by convergence of cellular fields at the edge of the neural plate.*" **Development** 127(17): 3645-53.

Winkler, C., Hornung, U., Kondo, M., Neuner, C., Duschl, J., Shima, A. and Schartl, M. (2004). "*Developmentally regulated and non-sex-specific expression of autosomal dmrt genes in embryos of the Medaka fish (Oryzias latipes).*" **Mech Dev** 121(7-8): 997-1005.

Wolfe, S. A., Greisman, H. A., Ramm, E. I. and Pabo, C. O. (1999). "*Analysis of zinc fingers optimized via phage display: evaluating the utility of a recognition code.*" **J Mol Biol** 285(5): 1917-34.

Yeo, S. Y., Kim, M., Kim, H. S., Huh, T. L. and Chitnis, A. B. (2007). "*Fluorescent protein expression driven by her4 regulatory elements reveals the spatiotemporal pattern of Notch signaling in the nervous system of zebrafish embryos.*" **Dev Biol** 301(2): 555-67.

Yoon, K. J., Koo, B. K., Im, S. K., Jeong, H. W., Ghim, J., Kwon, M. C., Moon, J. S., Miyata, T. and Kong, Y. Y. (2008). "*Mind bomb 1-expressing intermediate progenitors generate notch signaling to maintain radial glial cells.*" **Neuron** 58(4): 519-31.

Yoshizawa, A., Nakahara, Y., Izawa, T., Ishitani, T., Tsutsumi, M., Kuroiwa, A., Itoh, M. and Kikuchi, Y. (2011). "*Zebrafish Dmrta2 regulates neurogenesis in the telencephalon.*" **Genes Cells** 16(11): 1097-109.

Zarkower, D. (2001). "*Establishing sexual dimorphism: conservation amidst diversity?*" **Nat Rev Genet** 2(3): 175-85.

Appendix

A.1 *dmrt5* control morpholino injected embryos showed identical phenotypes as wild type embryos

The following images show whole mount *in-situ* hybridization results of control morpholino injected embryos. The stage and magnification are identical with wild type and *dmrt5* morphant images shown in the main text. To simplify the comparison between control and *dmrt5* morphant *in-situ* results, images are grouped similar like in the main results part and are labelled with corresponding figure numbers. The label on the left side of each panel, describes the region of interest as well as the image theme (for example: proneural genes, *her* genes etc.). In general, the *dmrt5* control morpholino images are showing identical *in-situ* staining like wild type embryos.

Control morpholino experiments are shown for the following figures:

Fig. 20 Knock-down of *dmrt5* leads to down-regulation of proneural genes *zash1b* and *neuroD*:

Fig. 21 *Dmrt5* morphants show neuronal differentiation defects in the telencephalon:

Fig. 22 The knock-down of *dmrt5* influences her gene expression in the telencephalon:

Fig. 23 *Dmrt5* knock-down results in reduced radial glia pools:

Fig. 24 Loss of *dmrt5* results in ectopic *pax6a* and *sox2* expression:

Fig. 25 Neuronal stem cell depleted *dmrt5* morphants have smaller telencephalon:

Fig. 27 Proneural gene expression is reduced in *dmrt5* morphants:

Fig. 30 BrdU labelled uninjected wild type and *dmrt5* morphants:

Fig. 33 Increased apoptosis and reduced cell division led to smaller olfactory epithelia and olfactory bulbs:

Fig. 36 Expression analysis of *pomc*, *prl* and *pitx3* in *dmrt5* morphants:

Fig. 37 Neuronal differentiation defects in the neurosecretory preoptic area and ventral midbrain:

Fig. 38 Down-regulation of hypothalamic fate determinants in *dmrt5* morphants:

Fig. 39 Alterations of neurosecretory preoptic area hormone production in *dmrt5* morphants:

Fig. 40 *Dmrt5* morphants show neuro-endocrine differentiation defects in ventral midbrain regions:

A.1 Chapter 3.5: Role of *dmrt5* for dorsal telencephalon, olfactory region and pituitary development

3.5.1 *Dmrt5* knock-down results in dorsal telencephalic differentiation defects

Control morpholino experiment to

Fig. 20
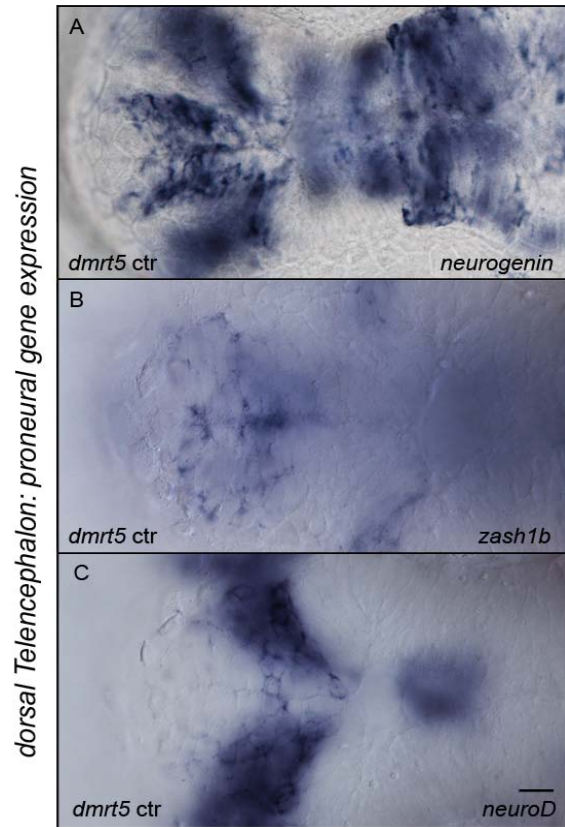
Fig. 21
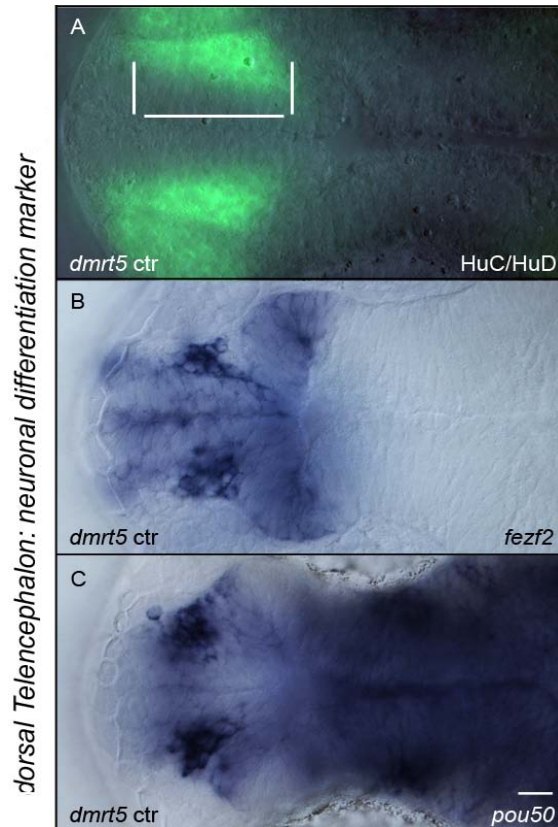
Fig. 22
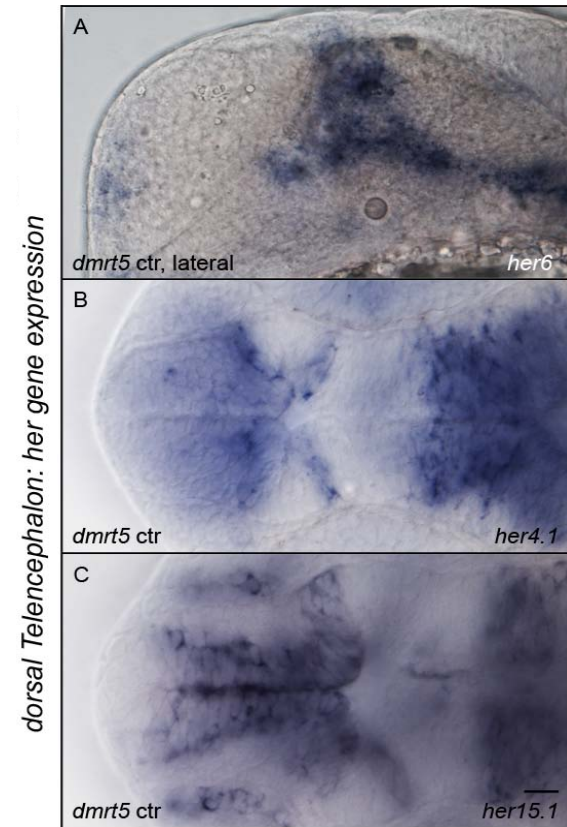
3.5.2 The loss of *dmrt5* leads to the maintenance of very early neuronal stem cell populations

Control morpholino experiment to

Fig. 23

dorsal Telencephalon: radial glia maintenance and radial glia marke

A — dmrt5 ctr — notch3
B — dmrt5 ctr — her4.1
C — dmrt5 ctr — gfap
D — dmrt5 ctr — blbp

Fig. 24

dorsal Telencephalon: early neuronal stem cell marker

A — dmrt5 ctr — pax6a
B — dmrt5 ctr — sox2

Fig.25

dorsal Telencephalon: morphology

A — dmrt5 ctr — shh/ krox20
A' — 32.32% — 67.68% — n =11
A" — dmrt5 ctr — shh
B — dmrt5 ctr — wnt1
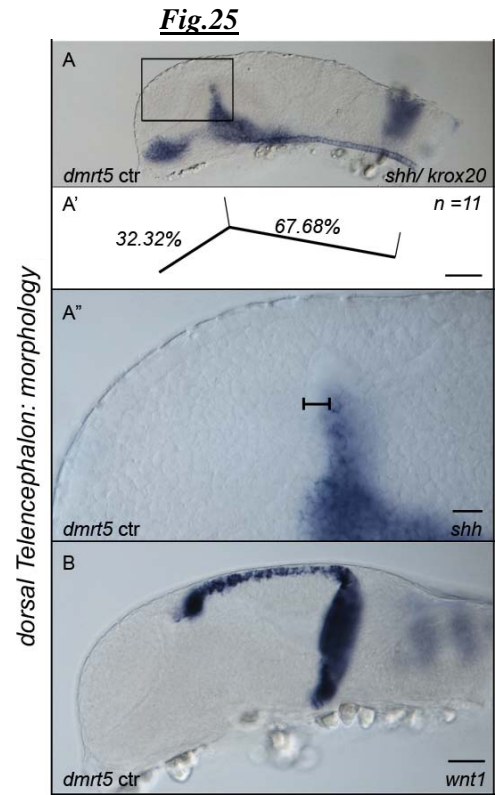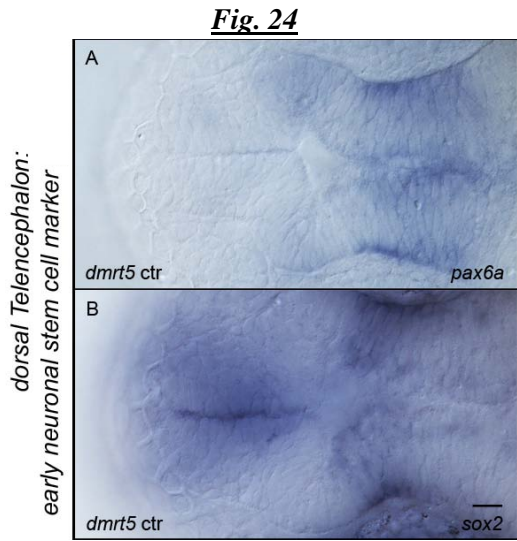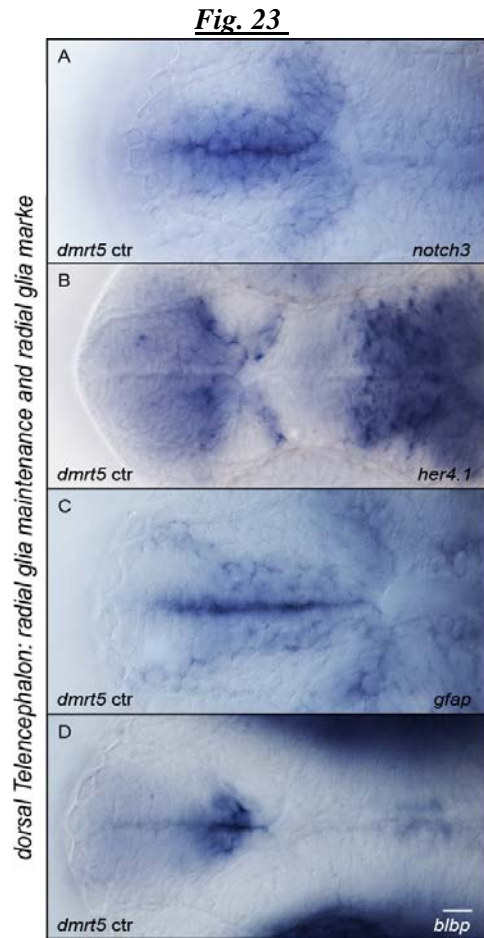
A.1 Chapter: 3.6 Dmrt5 is required for stem cell survival and neuronal differentiation in the olfactory system

Control morpholino experiment to

Fig. 27
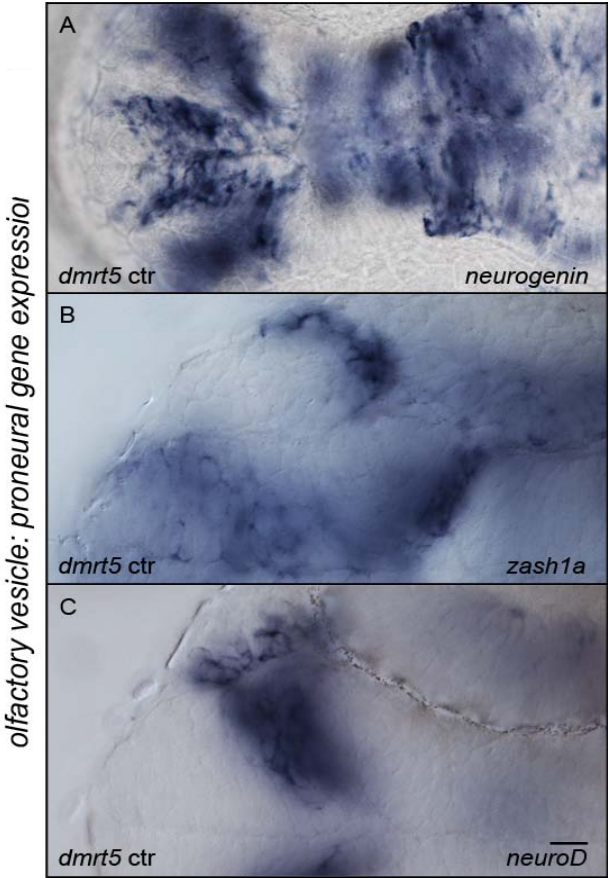
Fig. 30
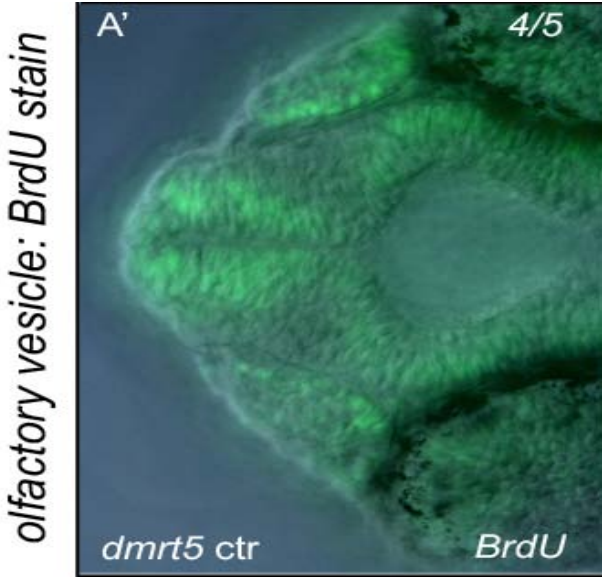
Fig. 33
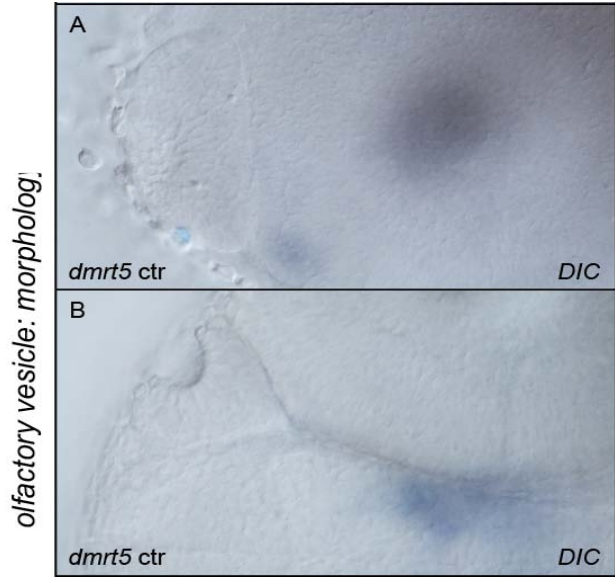
Fig. 30 BrdU Overview images
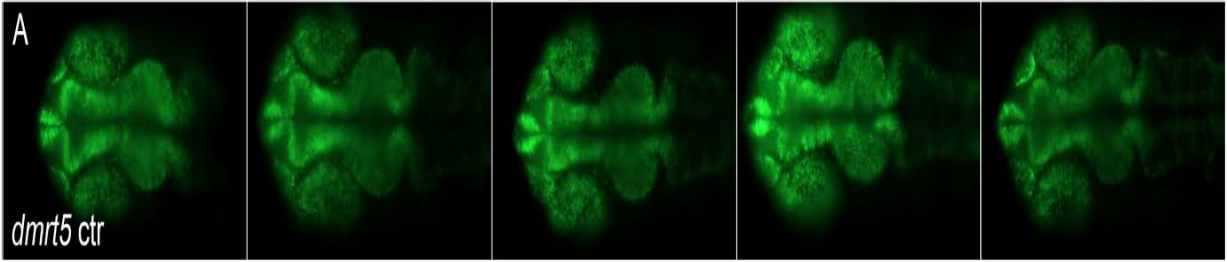
A.1 Chapter 3.7: Pituitary differentiation

Control morpholino experiment to

Fig. 36
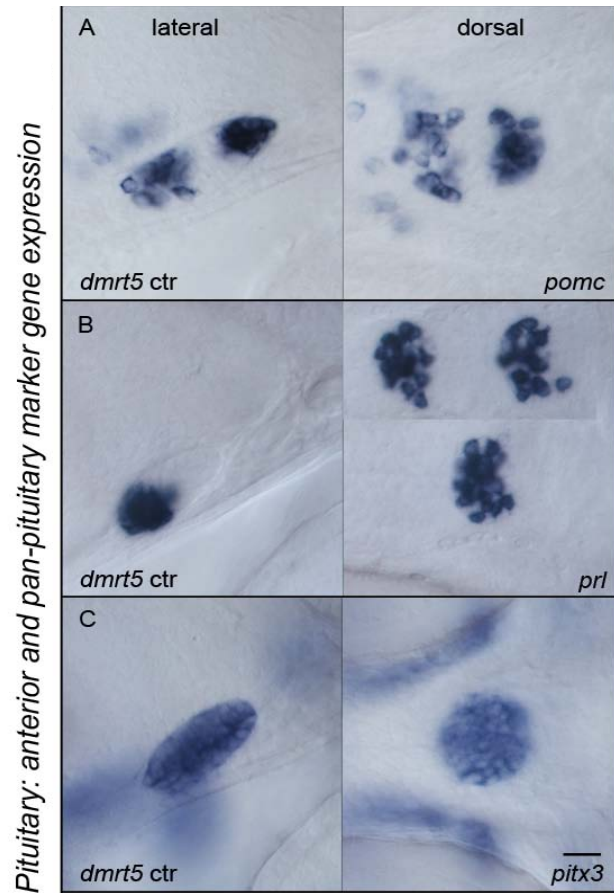
Pituitary: anterior and pan-pituitary marker gene expression

A1 Chapter 3.8: Neurosecretory preoptic area and ventral midbrain differentiation

Control morpholino experiment to

Fig. 37

Neurosecretory preoptic area and ventral midbrain: proneural gene expression

Fig. 38

dorsal Telencephalon: proneural gene expression

v

A1 Chapter 3.8: Neurosecretory preoptic area and ventral midbrain differentiation

Control morpholino experiment to

Fig. 39

Fig. 40

Neurosecretory preoptic area: avpl and oxtl expression

A
dmrt5 ctr — oxtl/avpl

B
dmrt5 ctr — oxtl/avpl

ventral midbraon: sim1a and gnrh2 expression

A
dmrt5 ctr, 31hpf — sim1a

B
dmrt5 ctr, 48hpf — gnrh2

C
dmrt5 ctr. 74hpf — gnrh2

vi
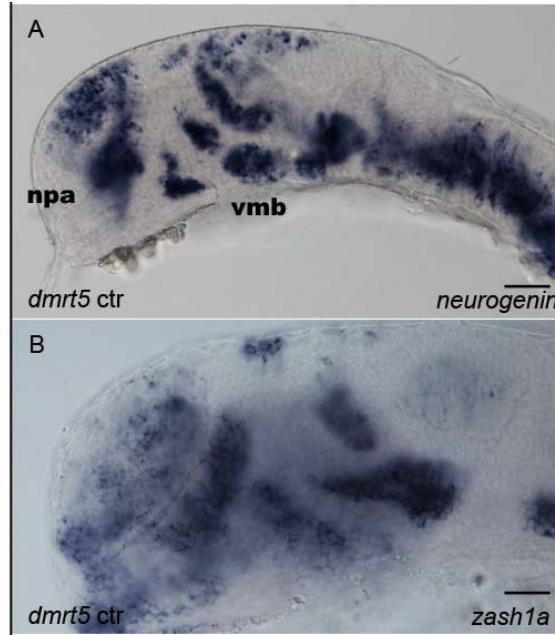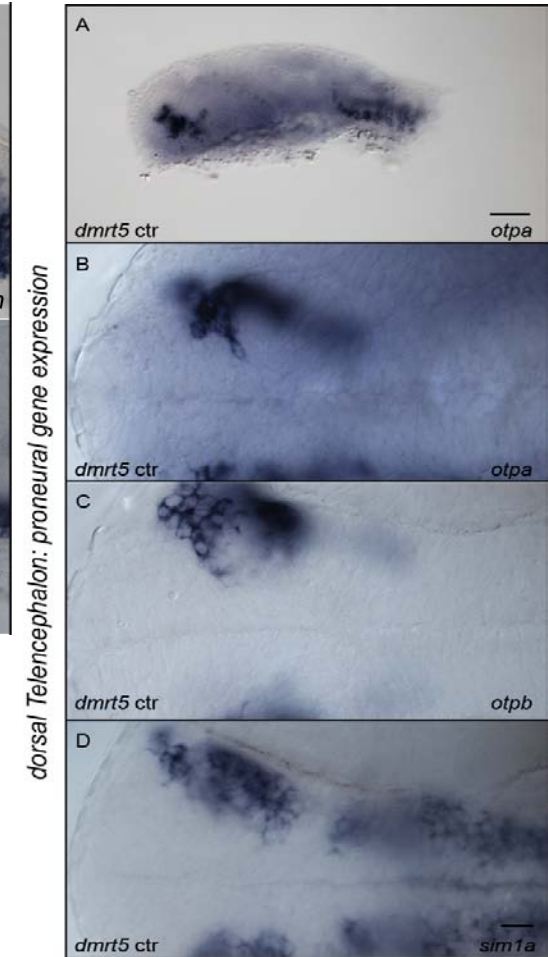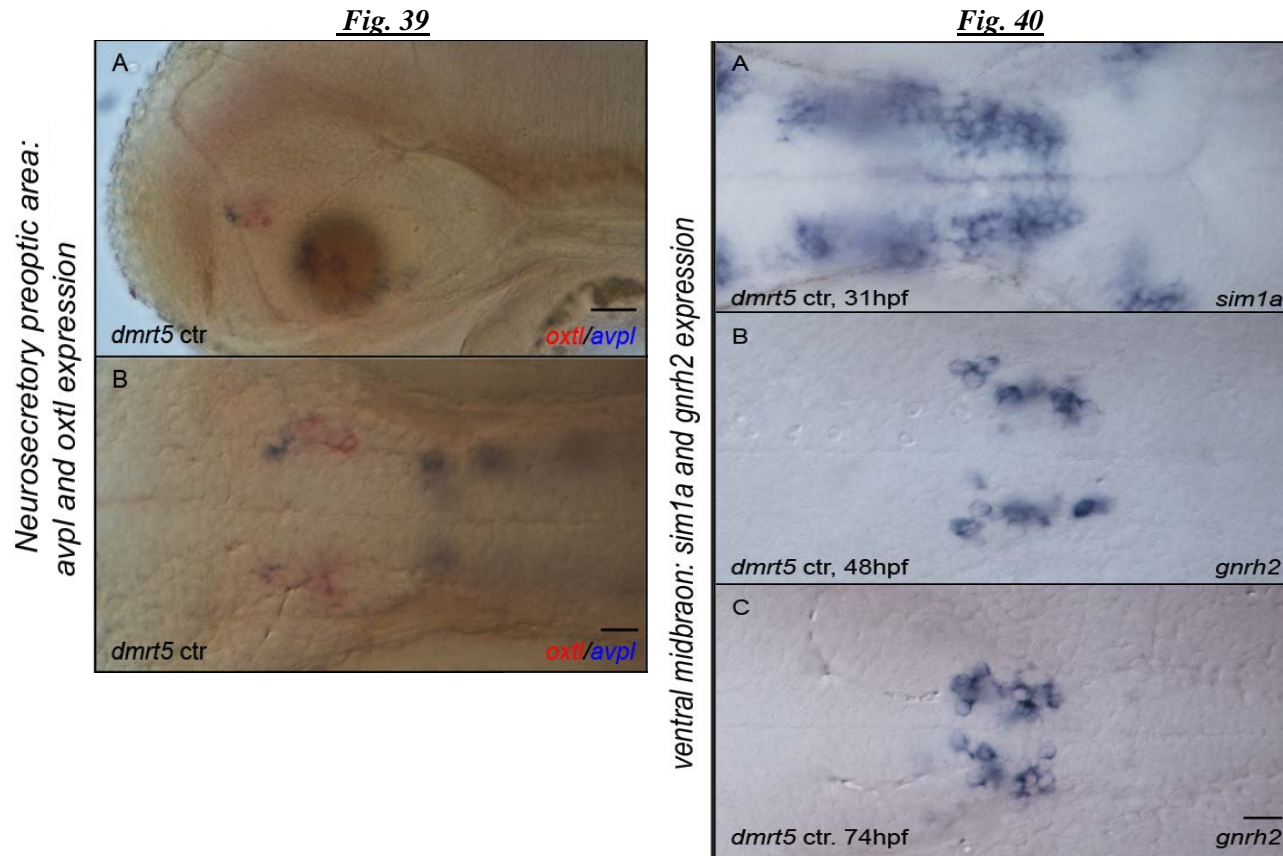
A.2 List of used primers, plasmids and morpholinos

Zinc finger generation		
Degenerated primer for ZFM customization		
Name of primer	5' to 3' sequence	comments
3p_mod1_lib	CCTGTGACCGCCGCTTCAGCVNSV NTVNSCACCTGANKMASCACATCCGGATTCACAC	randomization of the DNA binding zinc finger domains within different zinc finger modules, has to be combined with different set of reverse primers depending on the mode of selection
3p_mod2_lib	CTGCATGAGGAACTTCAGCVNSV NTVNSCACCTGACCCGTCACATCCGCACCCACAC	
3p_mod3_lib	CTGCGGCAGGAAGTTCGCGNNSV NTNNWAACCTGACCCGTCACACCAAGATCCACA	
5p_mod1_lib	CCTGTGACCGCCGCTTCAGCARAV NSNNWRVTCTGACCAMGCACATCCGGATTCACAC	
5p_mod2_lib	CTGCATGAGGAACTTCAGCVNSV NTVNSCACCTGANKGASCACATCCGCACCCACAC	
5p_mod3_lib	CTGCGGCAGGAAGTTCGCGVNSV NTVNSCACCTGACCAMGCACACCAAGATCCACA	
Isolation of dmrt3 target site binding modules		
Oligo 1	GTTCCGGACCGGTTCCAAGACACCCCCCCATGGTA CCCGCCCATATGCTTGCCCTGTCGAGTCCTGCGATCGCCGC	used for completion of the 5' end (incl. KpnI cutting site)
zif268 primer VI	CTCTAGACGTCCTTCTGTC	used for completion of 3' end (spans XbaI site)
Primers used during sequential selection strategy; isolation of specific modules		
varModul1rev (3p_mod1_rev)	CTGAAGTTCCTCATGCAGATTCGACACTGGAAGG	used in combination with oligo1, isolation of module 1, ZF1
varModul1and2Rev (3p_mod2_rev)	CGCGAACTTCCTGCCGCAGATGTCACAGGCAAAAG	used in combination with oligo1, isolation of module 1 and 2, ZF1
5p_mod1_rev	GCTGAAGTTCCTCATGCAGATTCGACACTGGAAGGG	used in combination with oligo1, isolation of module 1, ZF2
5p_mod2_rev	CGCGAACTTCCTGCCGCAGATGTCACAGGCAAAAGG	used in combination with oligo1, isolation of module 1 and 2, ZF2
Primers used during modular assembly strategy, isolation of specific modules		
Module 2 forw	CCCTTCCAGTGTCGAATCTGCATGAGGAACTTCAGC	binds 5' of ZFM2, used during single module isolation during modular assembly method
Module 3 forw.	GCCTTTTGCCTGTGACATCTGCGGCAGGAAGTTCGCG	binds 5' of ZFM3, used during single module isolation during modular assembly method

Primers for subcloning the ZFP encoding sequence into Fok nuclease expression vector		
Primer X	CTAGTTGGGATCC TCTTATGTGGATCTT GGTGTG	introduces a unique BamHI restriction site 3' of the last ZFM encoding sequence
Customization of zif268 target site vector		
sequential selection strategy		
pH3U3-mod1 (3p_TS1)	GCGTGGAGCGGACGAAT	
3p_TS3forw2:	CGCGTGTACACCCGGGCGGCCGCTGATGGCAGCGG ACGAATTCTTTACACTTTATGCTTCCGG	
3p_TS3rev2:	CCGGAAGCATAAAGTGTAAAGAATTCGTCCGCTGC CATCAGCGGCCGCCCGGGTGTACACGCG	
5p_TS1forw:	GTACACCCGGGCGGCCGCTGCGTGGTCGGGACGAATTCTTTACAC	
5p_TS1rev:	GTGTAAAGAATTCGTCCCGACCACGCAGCGGCCGCCCGGGTGTAC	
5p_TS2forw:	GTACACCCGGGCGGCCGCTGCGCGCTCGGGACGAATTCTTTACAC	
5p_TS2rev:	GTGTAAAGAA TTCGTCCCGAGCGCGCAGCG GCCGCCCGGG TGTAC	
5p_TS3forw:	GTACACCCGGGCGGCCGCTTGCCGCTCGGGACGAATTCTTTACAC	
5p_TS3rev:	GTGTAAAGAA TTCGTCCCGAGCGGCAAGCG GCCGCCCGGG TGTAC	
Modular assembly strategy		
5p_TS2forw2:	GTACACCCGGGCGGCCGCTGCGCGCGCGGGACGAATTCTTTACAC	
5p_TS2rev2:	GTGTAAAGAA TTCGTCCCGCGCGCGCAGCG GCCGCCCGGG TGTAC	
5p_TS3forw2:	GTACACCCGGGCGGCCGCTTGCTGGGCGGGACGAATTCTTTACAC	
5p_TS3rev2:	GTGTAAAGAA TTCGTCCCGCCCAGCAAGCG GCCGCCCGGG TGTAC	
pH3u3_MCS_prim_rev	CCTCTAGGTTCCTTTGTTACTTCTTCCGCCGCC	used with TS forward primers to generate target site fragments
pH3U3_MCS_prim_forw	CCGGCGGCAACCGAGCGTTCTGAACAAATCC	used with TS reverse primers to generate target site fragments
Primers to screen self-made ZFN injected zebrafish		
dmrt3HindIIIup-4	CATGGAAGCTTCCACCATGAATGGCTACGGATCGC	amplification of a 382bp long fragment that flanks the self-made ZFN target site, used to amplify fragments for RFLP, T7 endonuclease assay and sequencing
Zfdmrt3Exon1downn0	CTTGCGGTGTTTTGGGGGTCCC	
Primers to screen company made ZFN injected zebrafish		
DMRT3inside1rev	GCATATCGGCAAGATCCCTA	amplification of a 690bp long fragment that flanks the company-made ZFN target site, used to amplify fragments for RFLP and sequencing
Zfdmrt3Exon1downn0	CTTGCGGTGTTTTGGGGGTCCC	
Plasmids and bacterial strains used during ZFN generation		

Plasmids			
Name	Comments	Antibiotic resistance	Addgene No
Ph3U3-zif268Ω	Target site backbone vector	Kanamycin	18046
pB1H2Ω-zif268	Zinc finger expression vector backbone	Ampicillin	18045
pCS2-HA-GAAZFP-FokI-RR	Fok-endonuclease backbone I	Ampicillin	18754
pCS2-Flag-TTGZFP-FokI-DD	Fok- endonuclease backbone II	Ampicillin	18755
Dmrt3-ZFN2_pair2 left	ToolGene ZFN	Ampicillin	/
Dmrt3-ZFN_pair2 right	ToolGene ZFN	Ampicillin	/
Bacteria			
USO hisB- pyrF- rpoZ-	omega knockout Bacteria hybrid selection strain, lacks Histidine synthesizing enzyme	Tetracyclin	18049

Functional analysis of *dmrt3* and *dmrt5*

Probe production				
gene name	Name of primer	5' to 3' sequence	cloned into	ZFIN ID/ Ensembl ID
dmrt5	zfDMRT5 forw	TTCGCGCTACGGAGAAGTAT	TOPO-BluntII	ZDB-GENE-041116-2/ ENSDARG00000039412
	zfDMRT5 rev	TCTATTGCTGAGCGTCATGG		
Brain patterning genes				
Fezf2	zfFez2forw	CAGGGGAGCATTATGCACTT	pDrive	ZDB-GENE-001103-3/ ENSDARG00000070677
	zfFez2rev	TCCGCCGGATAAACAATTAG		
pou50f	zfPou50forw	ATGGCGACAACAGCTCAGTATA	pDrive	ZDB-GENE-980526-372/ ENSDARG00000009823
	zfPou50rev	TCAGCGAACTCTTCCCAAAC		
neural stem cell marker				
her6	zfher6forw	GGTTAACACCGAGGTCAGGA	TOPO-BluntII	ZDB-GENE-980526-144/ ENSDARG00000006514
	zfHer6rev	GCATCACAACGTGGAAAAGA		
sox2	zfSox2forw	CTCGGGAAACAACCAGAAAA	TOPO-BluntII	ZDB-GENE-030909-1/ ENSDARG00000070913
	zfSox2rev	TTCATATGCGCGTAGCTGTC		
radial glia marker				
blbp	zfBLBPforw	GATGCATTTTGTGCCACTTG	TOPO-BluntII	ZDB-GENE-000627-1/

	zfBLBPrev	CGTCAAGTTGCCAGGGTAAT		ENSDARG00000007697
gfap	zfGFAPforw	TTCTCCTCCACCATGGAGTC	TOPO-BluntII	ZDB-GENE-990914-3/
	zfGFAPrev	TGAGTCCATCCACCTGTCTG		ENSDARG00000025301
notch signalling and proneural genes
her15	zfHer15for	TCGCTCTGCTCAGAGAAACA	TOPO-BluntII	ZDB-GENE-030707-2/
	zfHer15rev	CGTGCTCTTTCAAAAGAAATGAC		ENSDARG00000054562
neurogenin1	Neurog1forwHindIII	CCCAAGCTTATGGAGATCGTATACTCCGATATGG	TOPO-BluntII	ZDB-GENE-990415-174/
	Neurog1revXbaI	CTAGTCTAGATTAATAGATGCTAGGCACGAAGTTGC		ENSDARG00000056130
zash1a	zfZash1aforw	CTGGGCAGTCCAAAGAAAAC	TOPO-BluntII	ZDB-GENE-980526-90/
	zfZash1arev	TTTACGAACGCTCAAAACCA		ENSDARG00000038386
nose specific markers
gnrh3	zfGnrh3forw	GAACAAACACAGCAGTTTTAGCA	TOPO-BluntII	ZDB-GENE-030724-4/
	zfGnrh3rev	ACAGCCCATCTGTTCCTTCA		ENSDARG00000056214
pituitary markers
gh	zfGH_forw	TAGAGCATTGGTGCTGTTGC	TOPO-BluntII	ZDB-GENE-030725-2/
	zfGH_rev	ATTTGGCTGTCCATCGAGAC		ENSDARG00000038185
gnrh2	zfGnRH2forw	TGATTTCACTCAACCGCTCA	TOPO-BluntII	ZDB-GENE-030516-1/
	zfGnRH2rev	ATTGTAGGAACTGCTGCAAATG		ENSDARG00000044754
gsu-a	zfGsu-aforw	TGGATGTGAAGAGTGCAAAC	pJet	ZDB-GENE-040715-2/
	zfGsu-arev	TTTACAATAATTATGCCAACCATTTT		ENSDARG00000040479
pitx3	zfPitx3forw	TCCCATCAGAACCACACAGA	TOPO-BluntII	ZDB-GENE-041229-4/
	zfPitx3rev	GCTGGCCAGACTGGAGTTAC		ENSDARG00000070069
prl	zfPrl1forw	CTCAGCACCTCACTCACCAA	TOPO-BluntII	ZDB-GENE-030513-1/
	zfPrl1rev	ACAGCGGAGGACTTTGAGAA		ENSDARG00000037946
tsh-beta	zfTSHb_forw	GTTATTGGCATGCTGGGACT	TOPO-BluntII	ZDB-GENE-030513-3/
	zfTSHb_rev	CCAATATGCTTGGGCGTAGT		ENSDARG00000033726
pre-optic area and hypothalamus
avpl	zfAVPLforw	TCTGCTGTCTGTGTGTGTGC	TOPO-BluntII	ZDB-GENE-030407-2/

	zfAVPLrev3	AGACGCAGCAGAGTTTCTCC		ENSDARG00000058567
crh	zfCRH-2f	CTCGCCACTTTTTGACATGA	TOPO-BluntII	ZDB-GENE-041114-75/ ENSDARG00000027657
	zfCRH-2r	ATTTTGCGGTTGCTGTGAG		
oxtl	zfOxtl1forw	ACATCTCAAACTGCCCCATC	TOPO-BluntII	ZDB-GENE-030407-1/ ENSDARG00000042845
	zfOxtl1rev	GCGTTTCATTGGTGGATTCT		
otpa	zfOpta_forw	CAAACCGAATTTGCTTTCATT	TOPO-BluntII	ZDB-GENE-070216-1/ ENSDARG00000014201
	zfOpta_rev	AGAAATGATGGGTGGACGAG		
otpb	zfOptbforw	GCACTGACGACTTTGCTTCA	TOPO-BluntII	ZDB-GENE-990708-7/ ENSDARG00000058379
	zfOptbrev	TCCTGAGTGCTCCATGACTG		
sim1a	zfSim1aForw	CACCTGAGAATGGGGACAGT	TOPO-BluntII	ZDB-GENE-020829-1/ ENSDARG00000023316
	zfSim1aRev	GTCCGCCTCATACAGGTGTT		
sst1.1	zfSST1.1f1	CGCCGTCAGCAGCGTCTCAG	TOPO-BluntII	ZDB-GENE-030131-4743/ ENSDARG00000040799
	zfSST1.1r1	CCTCGGTGAGAGCTACCATCGTT		
trh	zfTRH1f	GAGGAGCTGTTCCAGCGGGC	TOPO-BluntII	ZDB-GENE-020930-1/ ENSDARG00000006868
	zfTRH1r	GGGCTCCGCTCGTGTCCAGG		
Splice test primers				
dmrt5	zfDMRT5spliceForw1	TAAGCGCTACTGCAGATGGA	Both primers are binding into intron flanking exons, allowing the amplification of corresponding cDNA templates to spliced and unspliced mRNA.	
	zfDMRT5spliceRev1	TCTGCTGTGAGCCGAGTATG		
fezf2	zfFezf2forw.	GCTCCTCTTGTTGGAGAACG		
	zfFezf2rev	CAGGTGAAGGGCTTCTTGTC		
Standard Primer				
zfGapdh-Ex11FOR		GATTGCCGTTCATCCATCTT		
zfGapdh-Ex12REV		TCCATTTCTCACAAACAGAGGA		
M13 Forward (−20)		GTAAAACGACGGCCAG		
M13 Reverse		CAGGAAACAGCTATGAC		
Sp6		ATTTAGGTGACACTATAG		
T7		TAATACGACTCACTATAGGG		
Used plasmids and probes from other resources				

Riboprobes against		
Gene	Resource	ZFIN ID/ Ensembl ID
dbx1a	Flora Rajaei	ZDB-GENE-000128-8/ ENSDARG00000086393
dmrt3	Flora Rajaei	ZDB-GENE-021220-3/ ENSDARG00000035290
her6	Ram Vinod Roy	ZDB-GENE-980526-144/ ENSDARG00000006514
krox20	Yao Sheng	ZDB-GENE-980526-283/ ENSDARG00000042826
NeuroD	Yao Sheng	ZDB-GENE-990415-172/ ENSDARG00000019566
th	Ram Vinod Roy	ZDB-GENE-990621-5/ ENSDARG00000030621
shh	Yao Sheng	ZDB-GENE-980526-166/ ENSDARG00000068567
Zash1b	Yao Sheng	ZDB-GENE-980526-174/ ENSDARG00000094379

Plasmids for riboprobe production			
Gene	Vector backbone	Resource	ZFIN ID/ Ensembl ID
delta-A	pDrive	Winkler lab (Jan Brocher)	ZDB-GENE-980526-29/ ENSDARG00000010791
notch3	pDrive	Winkler lab (Jan Brocher)	ZDB-GENE-000329-5/ ENSDARG00000052139
pax6a	pBluescriptIISK	Veladimir Korzh	ZDB-GENE-990415-200/ ENSDARG00000045045
POMC	pCRII-TOPO vector	Winkler lab (Thuy Than To)	ZDB-GENE-030513-2/ ENSDARG00000043135
wnt1	pGEM1	Winkler lab	ZDB-GENE-980526-526/ ENSDARG00000055554

Used antibodies and antibody fragments for staining protocols			
Name of antibody	species	Working dilution	Company
Anti- acetylated Tubulin	mouse	1:1000	Sigma
Anti- BrdU-G3G4	mouse	1:1000	Developmental Studies Hybridoma Bank
Anti-digioxigenin AB fragments	sheep	1:2000	Roche
Anti-Fluorescein AB fragments	sheep	1:2000	Roche
Anti-HuC/HuD	mouse	1:1000	Molecular probes
Anti-mouse Alexa flour 488	goat	1:1000	Invitrogen
Anti- phospho Histone 3 (pH3)	rabbit	1:1000	Millipore
Anti-rabbit Alexa flour 488	goat	1:1000	Invitrogen

A.3. List of used Materials and Reagents

A.3.1 Equipment:

Company	Name	Comments
Balance		
Mettler Toledo	EL303	
Centrifuges		
Beckman Coulter	Avanti J-26 xp	
Labnet	Spectrafuge 16M	Phenol-Chloroform clean up
Sorvall	Legend Micro21	
Sorvall	Legend Micro21R	Thermofuge
Sprout	Microcentrifuge	
Chillers and Freezers		
ARDO	NVE1810	
Liebherr	Medline chiller	
Sanyo	Biomedical freezer	at -20/ -80°c
WISD	Wise Cryo freezer	
Gel electrophoresis		
Bio Rad	Gel trays and combs	
Bio Rad	Power pac basic	
Bio Rad	Wide Mini Sub Cell GT	
Syngene	G:Box gel documentation system	
WISD	WUV-M10 UV table	
Heat blocks and Incubators		
Contherm	Digital Series incubator	at 37°c, bacteria
Eppendorf	Thermomixer compact	
Infors	Multitron shaking incubator	at 37°c, overnight cultures
MRC	Dry bath incubator	
Sanyo	CO_2 incubator	at 28/ 30°c, zebrafish
Light sources for microscopy/ microinjection		
Dolan-Jenner	Fiber Lite Mi-150	
Microinjection		
Eppendorf	Femtojet microinjector	
Harvard Apparatus	GC100F-10 glass capillaries	
Narishige	Needle puller PC-10	
Microscopy		
Leica	S8APO	
Nikon	Digital Sight camera system	
Nikon	Eclipse 90i	High magnification and DIC pictures
Nikon	Intensilight C-HGFI UV source	
Nikon	SMZ1000	For microinjections and general overview pictures
Zeiss	LSM510 Meta	High resolution confocal microscopy

PCR machines/ Sequencing machines		
Applied Biosciences	Veriti 96 Well Thermal cycler	
Applied Biosystem	Abi3130x1 sequencer	
Biometra	T-personal PCR machine	
Stirring hot plates and pH meter		
Favorit	Stirring hot plate	
Schott	pH meter	
WISH vessel shaker and Vortex machines		
Chiltern	MT19 vortex	
Grant Bio	POS-300 vessel shaker	
Scientific Industries	Vortex Genie 2	
Stovall Life Sciences	Vessel shaker	
Water bath for in-situ technique		
GFL	Type 1003 water bath	

A.3.2 Used Enzymes and Kits:

Company	Name	Comments
Enzymes (other than restriction enzymes)		
Fermentas	PNK	phosphorylation reactions
	Proteinase K solution	*in-situ* protocol
	RiboLock RNAse inhibitor	RNA protocols
	SAP	dephosphorylation reactions
	SP6 RNA polymerase	probe production
	Taq Polymerase	clone test PCR's
	T7 RNA polymerase	probe production
Finnzymes	Phusion	high fidelity PCR reactions
NEB	T4 ligase	Ligation reactions
	T7 Endonuclease	ZFN mutant screens
Roche	T4 ligase	Ligation reactions
Restriction enzymes		
Fermentas	ApaI, BamHI, EcoRI, EcoRV, HindIII, KpnI, NotI, RsrII, SmaI, SalI, XbaI, XhoI	
NEB	BsmI, CviAII, KpnI, MspA1I, XbaI	
Enzyme Kits		
Ambion	mMessage mMachine Kit SP6/ T7	
	Poly (A) tailing kit	
Applied Biosystems	Big Dye Terminator v3.1 cycle sequencing kit	
Fermentas	RevertAid first strand cDNA kit	
Invitrogen	Zero-Blunt TOPO PCR cloning kit (pCR Blunt II TOPO vector)	
Millipore	AopoTag peroxidase *in-situ* apoptosis detection kit	
Roche	Rapid DNA ligation kit	

Other used Kits		
Promega	Wizard plus SV Miniprep DNA purification system	
	Wizard SV Gel and PCR clean-up system	
Qiagen	RNEasy Mini Kit	

A.3.3 Chemicals and consumables

Company	Name	Comments
1st Base	20x SST, Agarose, Tris	
AppliChem	Albumin fraction V, Glycerin	
Amresco	Phenol-Chloroform, pH 4.7	RNA isolation
Becton- Dickinson	Difco LB agar, LB broth	
Bio Rad	Agarose, beta-Mercaptoethanol	
Calbiochem	Ammonium chloride (NH_4Cl)	
Fermentas	IPTG	
Gadot	Ethanol	
Gibco	Kanamycin	
J.T. Baker	Methanol	
Kanako Kaguka	Isopropanol	
Merck	Calcium chloride ($CaCl_2$), Chloroform, di Sodium hydrogen phosphate (Na_2HPO_4), Glycine, Magnesium chloride hexahydrate ($MgCl_2 * 6H_2O$), Phenol, Potassium chloride (KCl), Potassium dihydrogen phosphate (KH_2PO_4), Potassium hydroxide (KOH), Sodium chloride ($NaCl$), Sodium hydroxide ($NaOH$), Sodium sulphide (Na_2SO_3), Zinc sulphate heptahydrate ($ZnSO_4$)	
Roche	Anti-DIG/ Fluorescein AP Fab fragment, BCIP/ NBT solution, Blocking reagent, Fast Red tablets	
Sigma	3-amino 1,2,4 triazole, Agar, Adenine hydrochloride, Amino acids (L-Amino acid Kit), citric acid, D- glucose, Dimethylsulphoxide (DMSO), Ethyl-3-aminobenzoate methyl sulfonate salt (Tricaine), Formamide, Isoamylalcohol, Phenol-Chloroform-Isoamylalcohol (25:24:1, pH 8), Torula yeast RNA, Sheep serum, Sodium acetat, Tetracycline hydrochloride, Thiamine hydrochloride, Triton-X 100, Uracil	
SCRS	Tween 20	
US Biological	Ampicillin sodium salt	
Consumables		
Axygen Scientific	0.2 and 1.5 ml microtubes ("Eppendorf tubes"), 10 µl pipette tips	
Becton Dickinson	Syringes (3 ml to 10 ml)	
Continental lab products	Sterile/ non-sterile pipettes	
Eppendorf	Microloeader	
Greiner Bio one	0.2 and 1 ml pipette tips, 2 ml, 15 ml and 50 ml tubes	
Nalgene	Bottle top filter (250/ 500 ml)	
Nipro	Syringe needles (various sizes)	
Sartorius stedim	Syringe filter	